

UNCLASSIFIED

AD 400 237

*Reproduced
by the*

ARMED SERVICES TECHNICAL INFORMATION AGENCY
ARLINGTON HALL STATION
ARLINGTON 12, VIRGINIA



UNCLASSIFIED

NOTICE: When government or other drawings, specifications or other data are used for any purpose other than in connection with a definitely related government procurement operation, the U. S. Government thereby incurs no responsibility, nor any obligation whatsoever; and the fact that the Government may have formulated, furnished, or in any way supplied the said drawings, specifications, or other data is not to be regarded by implication or otherwise as in any manner licensing the holder or any other person or corporation, or conveying any rights or permission to manufacture, use or sell any patented invention that may in any way be related thereto.

CATALOGED BY ASTIA
AS AD N~~4~~00237

400 237

N-63-3-1

⑩ ⑨

GLASS FIBER REINFORCED PLASTICS

Qualified requesters may
obtain copies of this
report from ASTIA.

Final Report
November 30, 1962

Contract NOw 61-0613-d

Prepared for U. S. Navy
Bureau of Naval Weapons
Washington, D. C.

Prepared by: B. Walter Rosen and A. E. Ketler, Jr.
with Appendix by Prof. Z. Hashin (Consultant)

Space Sciences Laboratory
GENERAL ELECTRIC COMPANY
Philadelphia, Pa.

ASTIA
APR 5 1963
A

FOR ERRATA

AD _____

400 237

THE FOLLOWING PAGES ARE CHANGES

TO BASIC DOCUMENT

GENERAL ELECTRIC
COMPANY

VALLEY FORGE SPACE TECHNOLOGY CENTER (MAIL P. O. BOX 8555, PHILA. 1, PA.) . . . TEL. 969-2000

**MISSILE AND
SPACE DIVISION**

**SPACE SCIENCES
LABORATORY**

AD 400 237

April 3, 1963

**SUBJECT: Contract NOW 61-0613-d
Final Report**

Under date of March 27, you were sent the final report for the subject contract. Some of the photographs in that report did not reproduce clearly. These have been reprinted and are enclosed.

Very truly yours,

J. H. Wood

J. H. Wood
Senior Technical Editor
Space Sciences Laboratory

 **ACCENT**
ON **VALUE**

DDG
OCT 18 1963
TISIA C

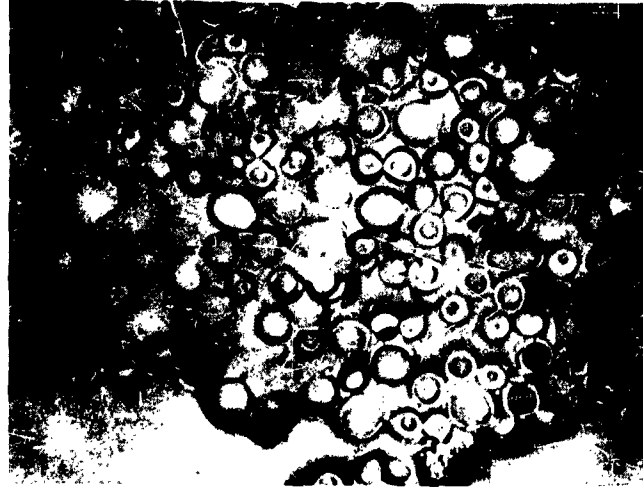


Fig. II-1 Typical Initial Multiple Hollow Fibers. (100X)

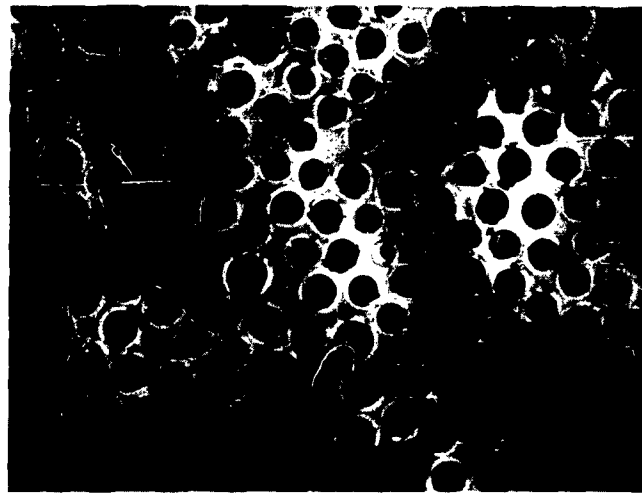


Fig. II-2 Typical Hollow Fibers Made Individually. (154X)



Fig. II-3 Bundles of Fibers Ready for Impregnation.



Fig. II-4 Expansion Device Used in an Attempt to Make Oval Shapes Out of Rings.

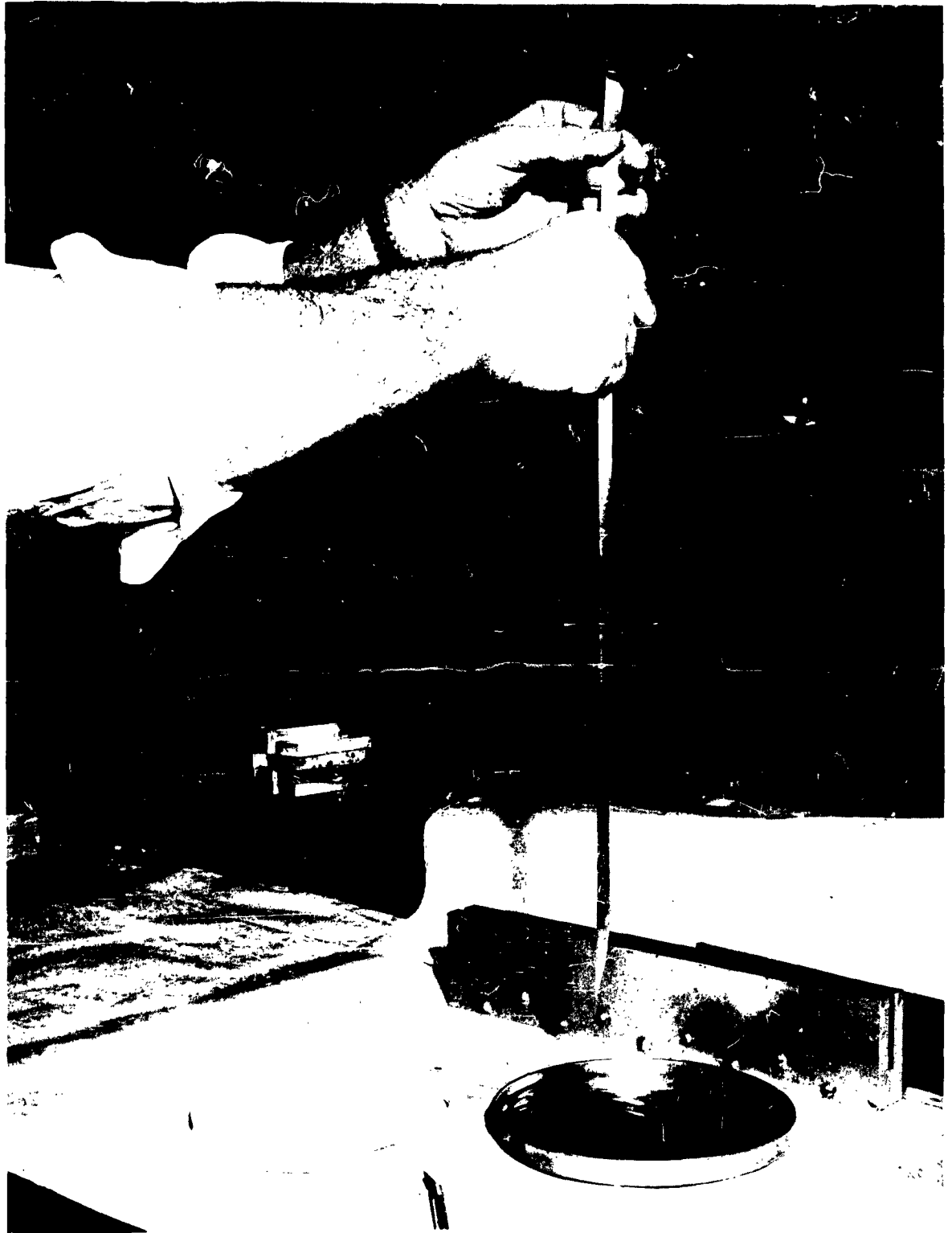


Fig. II-6 Straightening Wet Fiber Hank.

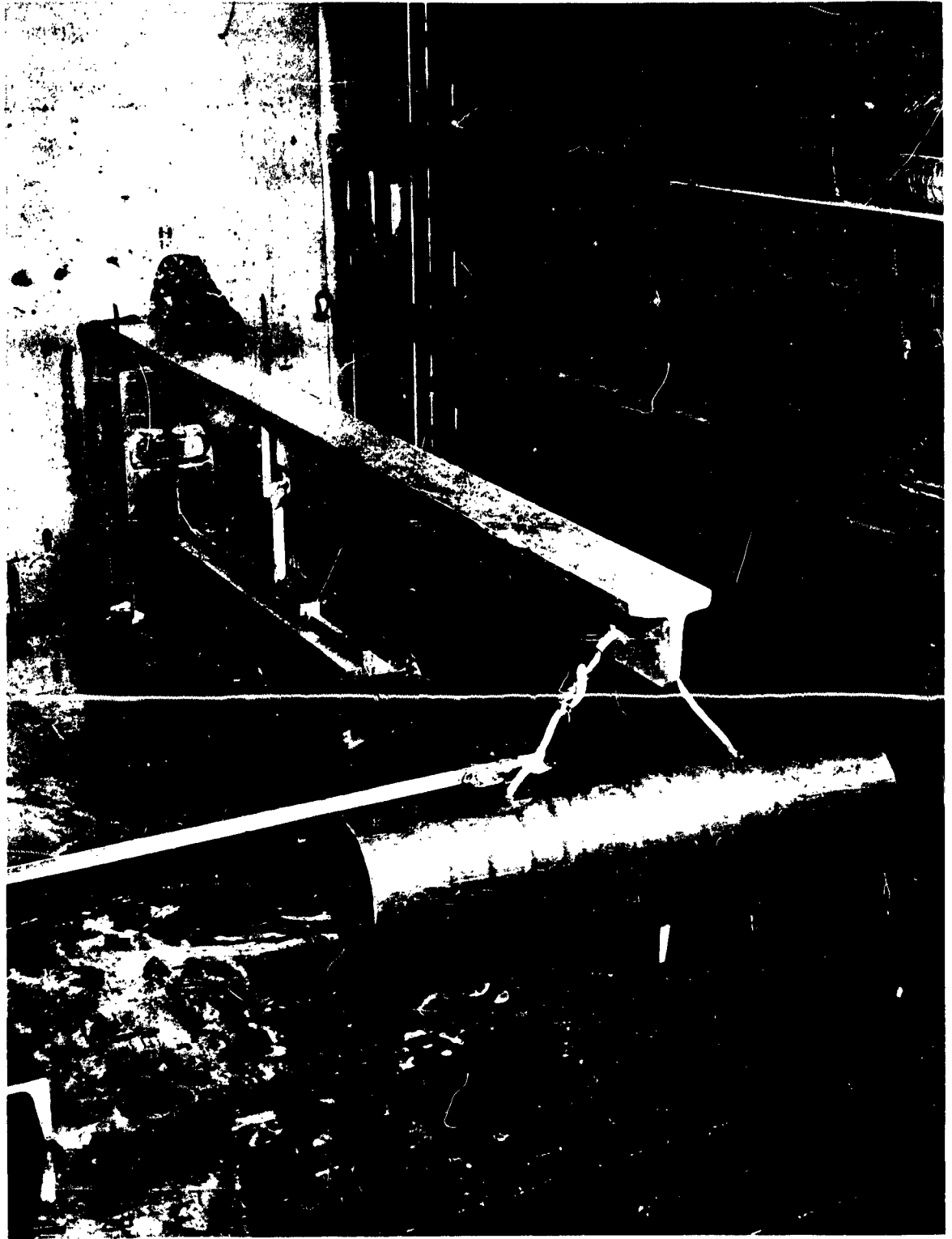


Fig. II-7 One Side of the Tandem Pressure Molding Press.

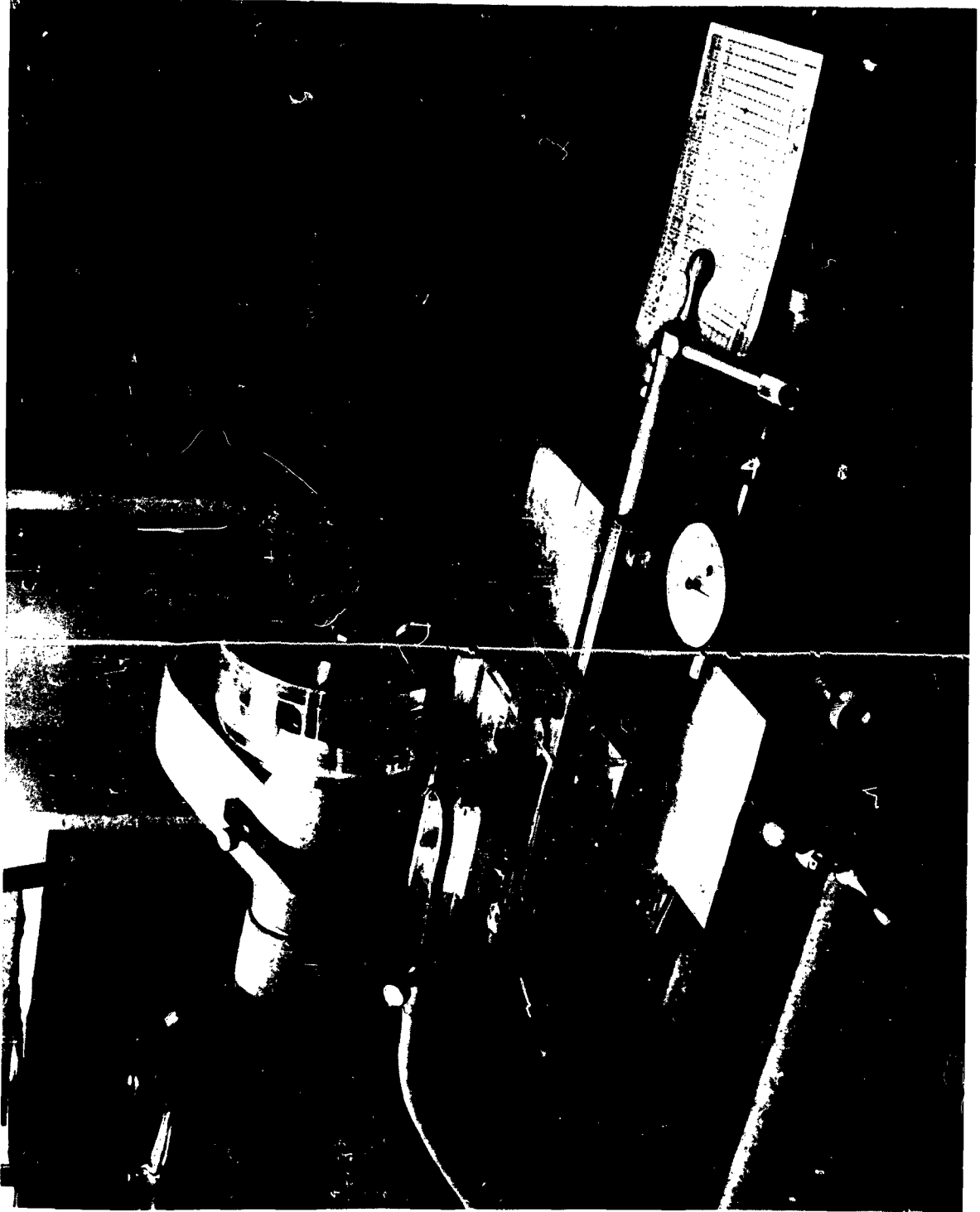
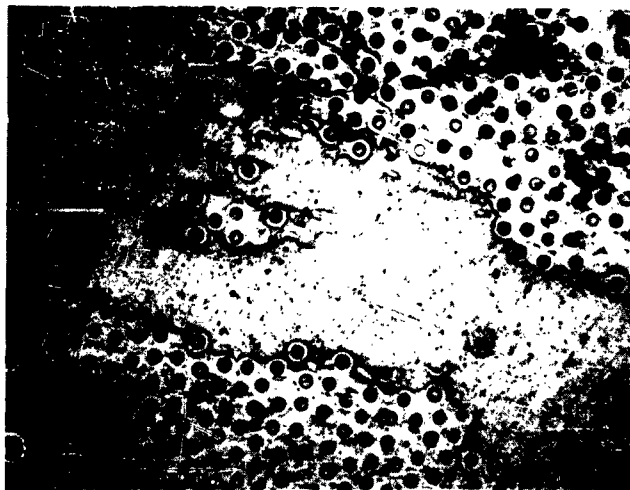


Fig. III-3 Cut-off Fixture Used to Square Ends of Axial Compression Specimens.



Solid Fiber Composite



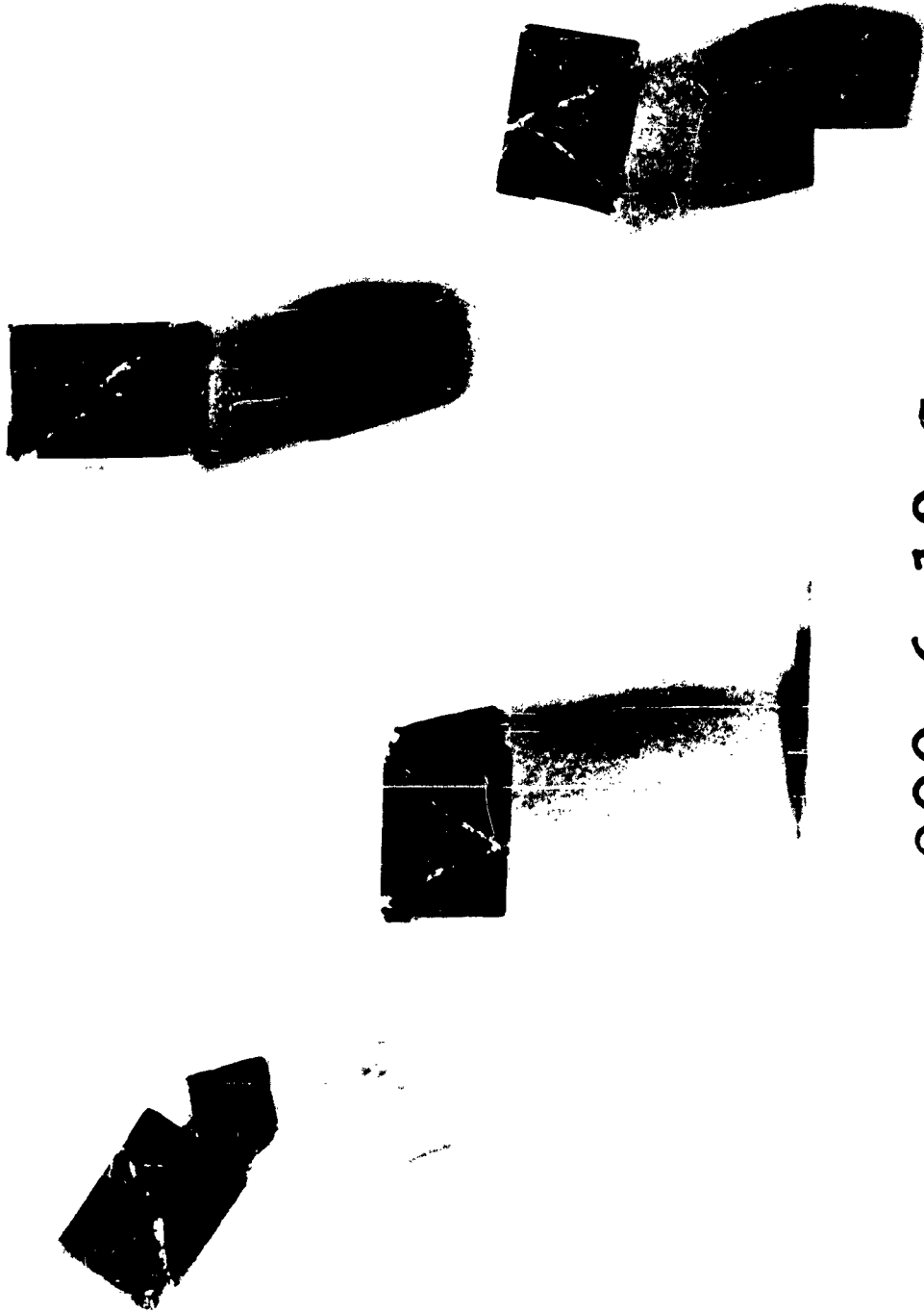
Hollow Fiber Composite

Fig. III-7 Shear Failure Mode of Solid and Hollow Fiber Specimens (154 X).



100-2-12-G

Fig. III-8 Typical Transverse Compression Failures of Solid Fiber Reinforced Composites.



200-6-13-G

Fig. III-9 Typical Transverse Compressive Failures of Hollow Fiber Reinforced Composites.

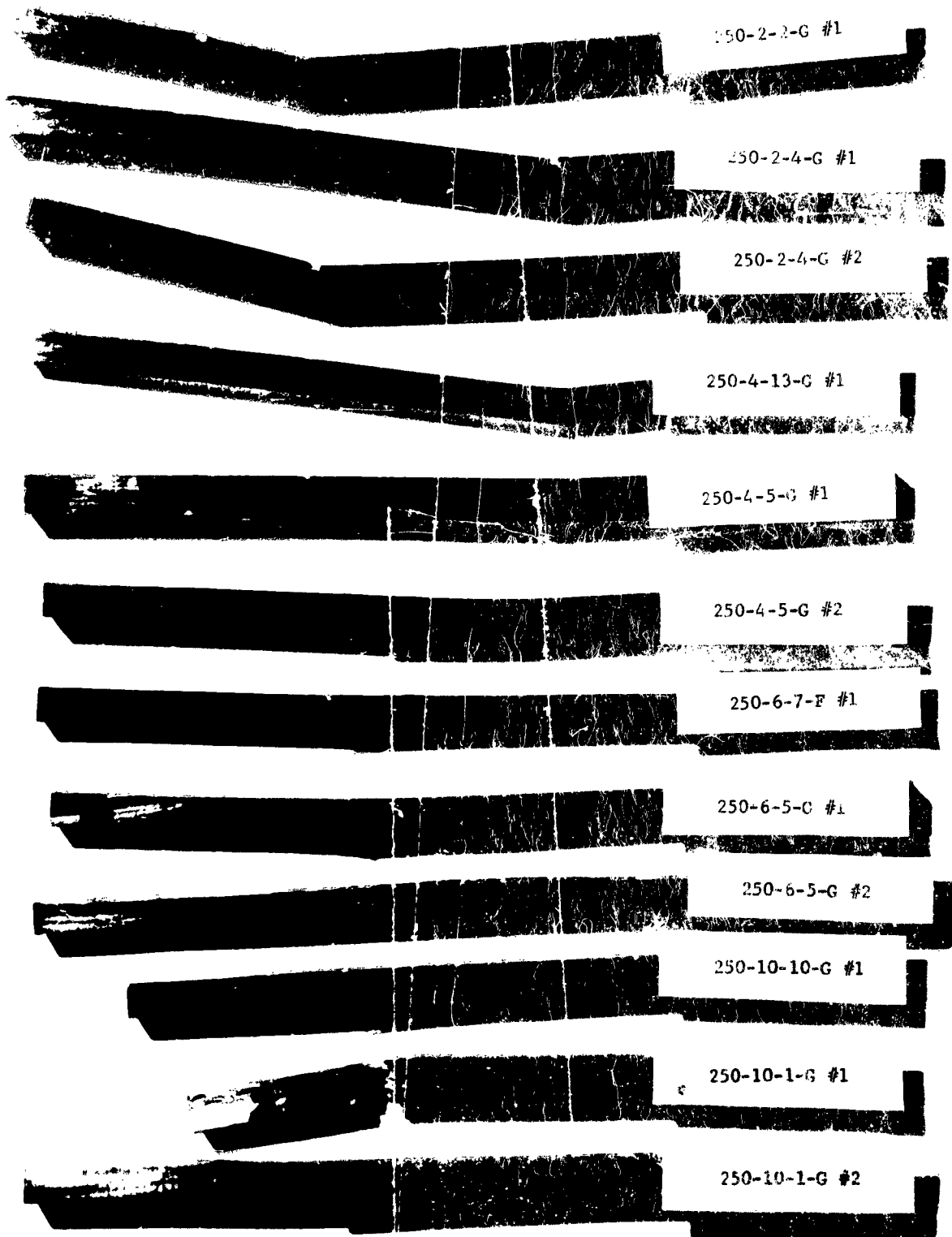


Fig. III-11 Typical Bend Test Failures.

HOLLOW GLASS FIBER REINFORCED PLASTICS

**Final Report
November 30, 1962**

Contract NOw 61-0613-d

**Prepared for U. S. Navy
Bureau of Naval Weapons
Washington, D. C.**

**Prepared by: B. Walter Rosen and A. E. Ketler, Jr.
with Appendix by Prof. Z. Hashin (Consultant)**

**Space Sciences Laboratory
GENERAL ELECTRIC COMPANY
Philadelphia, Pa.**

Abstract

A program to evaluate the improvement in bulk properties obtained by utilizing hollow glass fibers as the reinforcing material for glass-plastic composites was conducted. Controlled fabrication of fibers and uniaxially stiffened composites was demonstrated. Mechanical, electrical and physical properties were determined experimentally. Mechanical performance was defined analytically. The hollow glass fiber composites were shown to have improved structural efficiency for applications where stiffness or compressive strength is the governing structural criterion.

Acknowledgements

The program described herein was supported by the U. S. Navy, Bureau of Naval Weapons under Contract NOW 61-0613-d ("Improvement of Reinforced Plastics") with Mr. P. Goodwin as the cognizant contract officer.

The authors are pleased to acknowledge the significant contributions denoted by name in the table of contents as well as the advice and encouragement provided by Drs. F. W. Wendt, and H. G. Lorsch.

TABLE OF CONTENTS

	<u>Page</u>
I. Summary and Conclusions	1
II. Fabrication	3
A. Fiber Fabrication	3
B. Composite Fabrication (<u>by C. W. Wilson</u>)	10
III. Test	19
A. Physical Property Measurements	19
B. Mechanical Property Measurements	20
1. Fibers	20
2. Composites	26
C. Electrical Property Measurements (<u>by H. T. McLean</u>)	48
1. Identification of samples	48
2. Fabrication of electrical test specimen	50
3. Instrumentation	60
4. Test procedure	60
5. Results	61
IV. Analysis	81
A. Material Analysis	82
1. Longitudinal elastic constants	83
2. Transverse elastic constants	95
3. Elastic constants for biaxially stiffened material	96
B. Structural Analysis	100
1. Structural efficiency analysis	100
2. Stability analysis	119
C. Acoustic Behavior (<u>by G. DiLeonardo</u>)	124
1. Acoustic parameters	124
2. Velocity of sound in composites	124

	<u>Page</u>
3. Acoustic impedance	133
Appendix A - Transverse Elastic Moduli of Tube Reinforced Materials (by <u>Z. Hashin</u>)	136
1. Introduction	136
2. General method	136
3. Effective transverse bulk modulus, \bar{K}^*	144
4. Bounds for the effective shear modulus G^*	148
5. Problem of sheared composite cylinder	150
References	155
Key to Nomenclature	157

I. Summary and Conclusions

The program described in this report was directed at a quantitative evaluation of the bulk properties of hollow glass fiber reinforced plastic composites, and a comparison of these properties with those of solid glass-plastic composites. The program included the development and standardization of fabrication and test techniques and an experimental and analytical determination of composite material properties. The program resulted in the definition of mechanical, acoustical, electrical and physical properties of this material as a function of fiber geometry, and in the demonstration of improved structural efficiency for the hollow fiber composites.

In particular the techniques for drawing single hollow glass filaments were improved to yield a product of controlled geometry suitable for material evaluation. Toward the close of the contract period, a new source of hollow glass fibers became available. The Pittsburgh Plate Glass Company supplied multiple filament rovings for evaluation under this program. A technique for fabricating uniaxially stiffened composite test specimens, utilizing the available fibers, was developed and utilized to prepare mechanical and electrical property test specimens. Testing techniques were standardized and applied to the determination of static compression and bending properties, dynamic bending properties and electrical properties including evaluation of dielectric constant and strength, dissipation factor and D-C insulation resistance. Analytical programs were performed to evaluate elastic constants, acoustical properties and structural efficiency of the hollow glass fibers.

The principal results and conclusions of the study are:

1. Hollow fiber composites demonstrate improved structural efficiency for applications where stiffness or compressive strength is the governing structural criterion.
2. Specimens lighter than water (0.82 g/cc) have demonstrated axial compression strength to density ratios as high as 2.6×10^6 inches (average of 13 tests was 2.3×10^6 inches).
3. Hollow glass fibers can be successfully manufactured in diameters as low as .0010" and with ratios of inside radius to outside radius as high as 0.88.
4. Compressive strength of hollow fiber composites transverse to the fiber direction are lower than the strength of solid fiber composites for ratios of fiber inside to outside radius greater than 0.5.
5. Tensile strength of individual fibers is very sensitive to the fiber geometry in the range tested. Strength decreases as fiber diameter increases and increases as fiber hollowness increases.

6. Electrical properties of the material are highly anisotropic and are relatively insensitive to humidity.

7. Dielectric constant decreases considerably with increasing ratio of inner to outer fiber radii.

8. Four of the five elastic constants necessary to describe the material have been evaluated analytically.

9. The longitudinal modulus of elasticity of hollow glass fiber composites is essentially the weighted average of the constituent moduli.

10. Wave velocities for large wavelength disturbances have been determined analytically.

II. Fabrication

The methods used in fabricating the hollow fiber composites are described below along with a summary of the fiber fabrication program.

A. Fiber fabrication

The fibers used in this program varied from the initial single filament drawn from a tube by General Electric's Lamp Glass Department to the current multiple filament strands produced by the Pittsburgh Plate Glass Co.

General Electric's Lamp Glass Department's first fibers were made nearly three years ago by attenuating a single hollow tube to a diameter of about .0035". Attempts at manufacturing multiple fibers by this method proved more difficult than expected. Although a small quantity of 35 fiber rovings was drawn, the individual fibers proved to be non-uniform in size and hollowness and generally inferior to those drawn individually.

Process improvements were made, however, resulting in smaller diameter fibers with extremely thin walls by the single fiber process. This process was used during the past year to produce a large quantity of fibers in a range of fiber sizes with varying degrees of hollowness for this program. The fibers were of exceptional quality and provided a means for experimental correlation with theoretical predictions.

A new process developed by the Pittsburgh Plate Glass Co. has made available a filament windable hollow fiber roving containing up to 1000 fibers. This new material makes possible for the first time, the fabrication of large shapes from hollow fibers.

1. Process development

Prior to this present contract, hollow fibers made of E-glass and quartz having outside diameters of 6 and 9 mils and having wall thicknesses of 1 to 2 mils had been drawn successfully by the Lamp Glass Department of the General Electric Company. Since the initial attempt at making hollow fibers had been so successful, it was believed that the simultaneous drawing of a great number of hollow fibers, say 30 to 50, would be relatively simple.

It was therefore planned initially to draw 35 fibers at a time. These fibers were to have outside diameters of .006", .002" and .0007" with wall thicknesses varying from .0015" to .0002". By varying the outside diameter, the overall size effect was to be evaluated. The effect of varying the wall thickness for a given constant outside diameter was to be evaluated on fibers

of intermediate size: say .002" O. D. In order to be able to compare hollow fibers with solid fibers, the use of standard, high-strength E-glass was felt to be desirable. The versatility of the process would be demonstrated by also making a limited number of quartz fibers, both hollow and solid.

The question of finish was to be evaluated during the course of the program. Since the hollow fibers are extremely delicate, a minimum amount of handling is desirable. The application to the fibers of a standard finish, such as A-1100, at the end of the manufacturing process prior to collection on a spool did not appear feasible at the time of initiation of the program. It was therefore decided to coat the fibers initially with starch and oil, because a finish of some kind is required both for protection of the fiber surface and for making a bundle of fibers stick together during winding into a roving. This starch-oil would be burnt off and A-1100 sizing applied before the actual filament winding operation.

In order to check out the process of drawing 35 fibers simultaneously which had not been previously tried by the Lamp Glass Department, solid fibers were used initially. After some minor difficulties, 35 solid fibers of .0009 in. O. D. were successfully drawn simultaneously and wound on a drum. Three of these 35 fiber bundles were then re-wound on a drum. These three bundles were then re-wound into a single end, 105-filament roving. These rovings were wound on 4" diameter drums and shipped from the Lamp Glass Department to the Missile and Space Division for filament winding.

Having somewhat perfected the manufacturing process of simultaneously drawing multiple fibers, 35 hollow fibers were then drawn. These fibers had an outside diameter of .002" and an inside diameter of .0015" or less. A considerable number of the multiple fibers was broken, either during the initial drawing process or during the subsequent winding of three bundles of 35 fibers each into a single roving. This breakage did not seem to decrease the strength of the composite end product, but the presence of many loose filament ends complicated the winding process. For example, it was necessary to unwind from the inside of the spool in order to avoid having the loose ends break the roving being wound.

The drawing process was modified several times in order to achieve better uniformity and smaller fiber diameters. Bundles of 35 hollow fibers having .0009" O. D. and having a nominal wall thickness of .0002" were then manufactured, and 3 of these combined into a single roving. Six pounds of these hollow fibers and 6 pounds of the same O. D. solid fibers were manufactured and shipped. Aluminum spools were substituted for the cardboard spools used in the initial shipment. This eliminated the necessity of rewinding

the rovings before burning off the starch and oil finish which was applied to all the fibers at manufacturing.

A typical photomicrograph of these hollow fibers is shown in Fig. II-1. This figure shows a single roving, nominally consisting of 105 filaments. It should be pointed out that the actual number of filaments in this roving was higher than the number indicated by actual count of the fibers in the pictures. These micrographs were made by imbedding the roving in a plastic matrix, then cutting it and polishing it to an extremely high finish. If, during the cutting process, a fiber broke below the surface, it would never be touched by the polishing wheel and thus would not show up in the micrograph. The large, vacant spaces in some of the fiber bundles of Fig. II-1 are probably filled by such fibers which were cut below the surface. It is apparent that good control was maintained on the O. D. of the hollow fibers, but that the wall thickness varied a great deal. As a matter of fact, some of the fibers are actually solid.

The variation in wall thickness of the hollow fibers may have been due in part to the non-uniformity of the heating and drawing process of the non-uniformity of the raw material. The raw material of the fibers, both hollow and solid, was E-glass supplied by Owens-Corning Fiberglas Corp. Careful testing of the raw material supplied uncovered a tendency of this glass to boil.

The boiling problem was solved by the use of special, high purity E-glass manufactured by the Bridgeville Glass Works, Bridgeville, Pa. (designated type 172). It has the following composition:

SiO ₂	60%
Al ₂ O ₃	20%
CaO	7%
MgO	8%
NaO	1%
B ₂ O ₃	4%

Its general properties are

Modulus of elasticity:	10.7 x 10 ⁶ psi
Specific gravity:	2.43
Thermal expansion:	4.2 x 10 ⁻⁶ per °C, (0-300°C) 2.33 x 10 ⁻⁶ per °F, (32-482°F)
Softening point:	914°C

A part of the difficulty encountered in pulling 35 fibers simultaneously may also have been due to the slight fluctuations in drawing speed and tension, inherent in the process. Prior to the commencement of the present contract, such difficulties were minor because only single hollow fibers had been drawn.

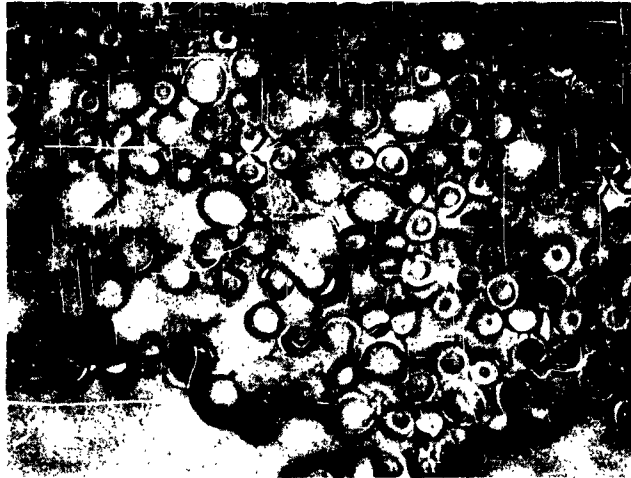


Fig. II-1 Typical Initial Multiple Hollow Fibers. (100X)

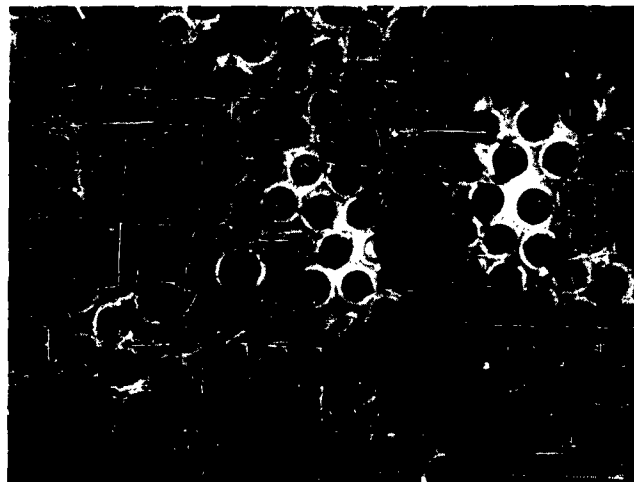


Fig. II-2 Typical Hollow Fibers Made Individually. (154X)

(It is now known that greater uniformity can be achieved by drawing a single fiber at a time.) In order to avoid the difficulties encountered with multiple fibers, it was therefore decided to revert back to drawing individual hollow fibers. Less breakage was encountered than with the multiple drawing process, and the uniformity of the fibers improved considerably.

Another advantage of drawing single fibers is that the process can be stopped when the fiber breaks without adversely affecting other fibers. If a fiber breaks during the simultaneous drawing of 35 fibers, the process could not be stopped because the remaining 34 fibers would also break. Therefore, it was the practice not to stop when individual fibers broke but to let the bundle of 35 fibers come down to a pre-determined number, say 25 to 30, before stopping the drawing process and re-gathering all 35 fibers. This change in the program thus permitted the production of improved fibers for test purposes and provided the opportunity for better understanding of the new techniques before drawing multiple hollow fibers.

The photomicrograph of Fig. II-2 is indicative of the uniformity of fiber dimensions produced by drawing one filament at a time. The single filaments were wound on 6" diameter Teflon bobbins with 1/4" x 1/4" cross-sections. Other winding techniques were studied along with alternate schemes for shipping. Deionized water was used to wet the glass fibers after drawing, and specimens were subsequently shipped wet from Cleveland, Ohio, to Philadelphia, Pa. This water acted as a lubricant and protected the delicate fibers during handling and shipping. After removal from the filament forming machine the glass-filled bobbins were sealed with a plastic film to retain this water until processed into samples in this laboratory. (See Fig. II-3)

Plans were made to produce a series of fiber sizes and geometries that would isolate the two variables, outside diameter d_f and ratio of inside diameter to outside diameter, α . This group is shown below, along with the sequence of production. A total of 150 bundles was to be produced: 15 in each of the 10 types. Planned production rate was about 15 bundles per week.

Table of Quantities of Fiber Bundles
Produced in the Various Geometries

		α			
		.80	0.67	0.50	0
(Size)	d_f				
	.0025	15	15	15	15
	.0020		15		15
	.0015		15		15
	.0010		15		15

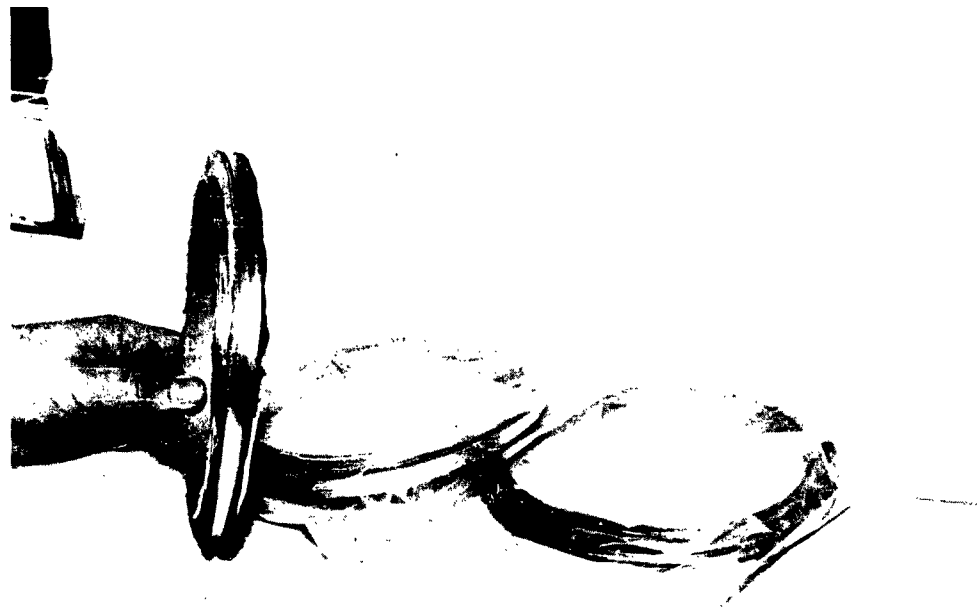


Fig. II-3 Bundles of Fibers Ready for Impregnation

Water was employed as a lubricant on some of the earlier glass fibers. It was removed by drying at 250°F overnight (15-18 hours) prior to resin impregnation. It was thought that the water could deteriorate the glass fibers, dissolving some of the alkali from the surface of the glass. Also, after the water had evaporated from the glass, the resulting surface was thought not to provide as good a coupling boundary between the glass and the resin as could be obtained using other treatments. In order to evaluate glass fiber surface finishes and the resultant effects on strength, the following treatments were evaluated:

- a. A-1100 treatment applied to the glass immediately after forming was used as a lubricant during molding.
- b. Uncoated virgin glass with resin free of coupling agent. Water was used as a lubricant during molding.
- c. Uncoated virgin glass molded with resin containing 2% Syl Chem 90 as the coupling agent. Water was used as a lubricant during molding.
- d. Single specimen of each (a, b, and c) was also prepared using n-heptane as a lubricant.

Tests with these sizing agents showed only slightly higher compressive composite strengths over un-sized or untreated fibers. It was therefore concluded that, for the purpose of this contract which was to evaluate improvements of hollow fibers over solid ones, dry fibers would be used throughout. This eliminated the additional process control variables, namely quality and quantity of sizing, and therefore improved the reliability of the conclusions drawn from the test program. The fibers, wound wet with deionized water, were dried thoroughly prior to shipment in sealed plastic bags. Time in shipping or storage was of no consideration since no moisture was present.

A great deal of difficulty was experienced in making both small diameter ($d_f = .001''$) and thin walled ($\alpha = .8$) fibers. A large number of trial runs had to be made, rejecting many fiber bundles, before the required quantities of good fibers were produced. Solid fibers presented no particular manufacturing or handling problems in the diameters considered.

Classifying a 15 bundle lot, the expected quality (based on visual inspection of fiber sizes and uniformity throughout the bundle) is 62% good, 27% fair, and 11% poor. The one or two poor bundles were used first to check out the impregnation process. The fair ones were impregnated and used to check out the testing procedures. Then final measurements were made on the remaining (9 or 10) good bundles.

Toward the completion of this program, a source was found which could supply a filament-windable hollow glass fiber roving. The Pittsburgh Plate Glass Co. manufactured several pounds of fibers .0005" and .00065" diameter with a ratio of inside diameter to outside diameter of approximately 0.67. Solid control fibers were also supplied in the same outside diameters.

The fibers were drawn 50 at a time and then rewound into rovings. The first shipment, .0005" diameter, was comprised of 8 ends per roving for a total of 400 fibers. Only a light sizing was applied and hence the roving was quite easily abraded. A later shipment of .00065" diameter fibers, wound with 20 end (1000 fibers) rovings, was treated with both sizing and an epoxy-compatible resin. Consequently, these rovings were easier to handle and much less susceptible to abrasion and handling damage.

B. Composite fabrication

A technique which could use the available spools of very delicate singly wound hollow fibers was developed for the fabrication of long thin rods suitable for mechanical and electrical testing. The rods were quite uniform and proved to be a reliable test medium, free from major uncontrolled fabrication variables.

1. Process development

In an attempt to obtain initial composite test specimens expeditiously, it was planned to wet a package of glass fibers while wound on a drum and then transfer it to a fixture which deformed it into an oval shape. The fibers in this oval mold were then to be impregnated with epoxy resin, the resin cured, and the straight parts of the oval shape cut out and used as compression test specimens.

Fig. II-4 shows the expansion device designed to mechanically deform the circular Teflon bobbins wound with hollow fibers (ref. 4) into the oblong shape. This was tried with both hollow and solid fibers, but the results were very poor. Catenary action due to slack in the tightly wound fibers caused the supposedly straight sides to bow outward and destroy the collimation of the fibers. It was impossible to maintain a uniform shape and fiber density throughout the "straight" portions of the oblong shape. A better technique which produces an excellent, straight specimen up to 15" long was devised. This technique utilized the mold shown in Fig. II-5. The process consisted of immersion of a glass fiber filled

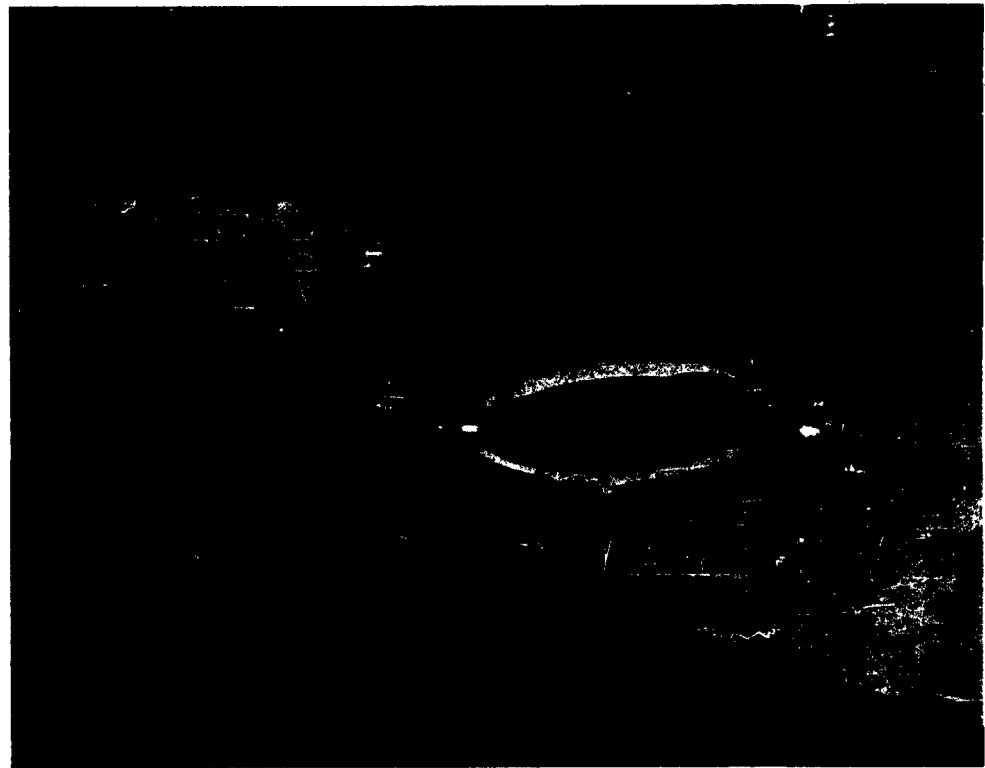


Fig. II-4 Expansion Device Used in an Attempt to Make
Oval Shapes Out of Rings

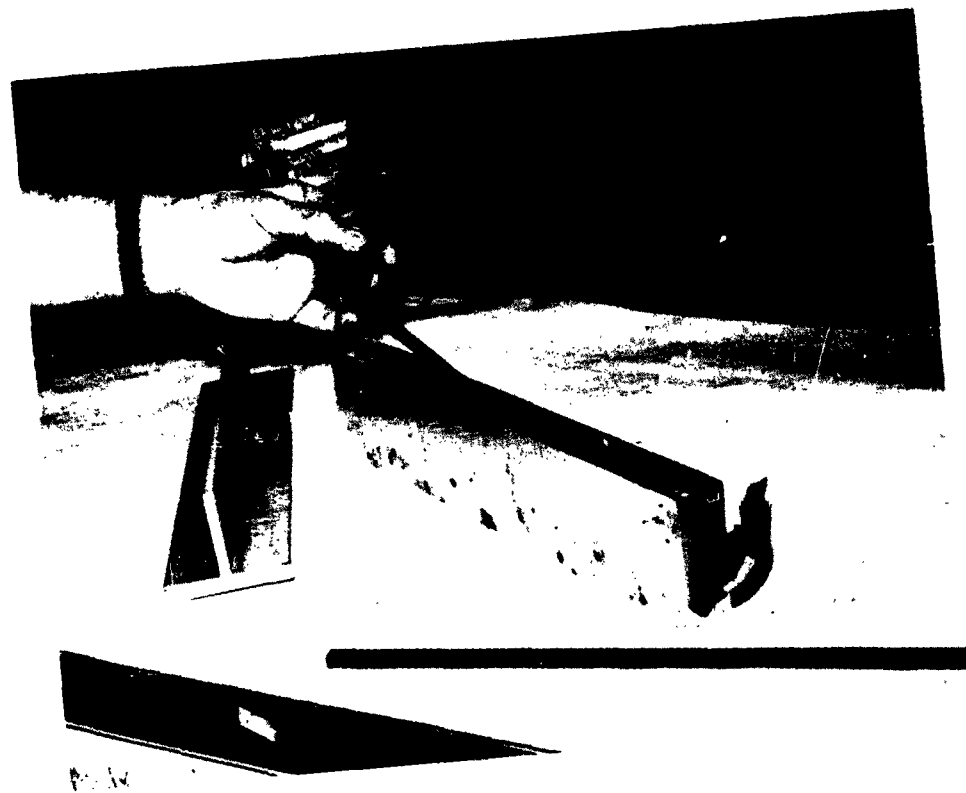


Fig. II-5 Molding Fixture, and Finished Specimen

Teflon ring in water. Then a cut was made through the fibers and ring at one point in the circumference. Stripping the wet hank of fibers from the ring was quite simple. By gently wiping the hank between the fingers, the cantenary effects caused by the initial winding diameter differences among the fibers were eliminated. This procedure achieved good collimation of the filaments (Fig. II-6) and resulted in no measurable fiber damage. The wet hank of fibers was then inserted into the channel-shaped section of an open end 15" long x 1/4" wide mold. A male plunger was inserted into the mold and the fibers dried overnight at 200°F. Removal of the part from the mold after curing was assured by the application of a mold release compound during the initial mold assembly. The resulting dried bundle of glass was tightly bonded (conherent). This inter fiber bonding was caused by the polarity of the water molecules which, upon removal from the glass fibers, left behind an electrical surface charge causing the fibers to attract one another. There also appeared to be a small degree of permanent bonding between the raw, dry fibers. The resulting stiff structure prevented uniform resin impregnation. Also, due to lack of resilience of the stiff fibers, it was impossible to accurately control the fiber density and resin content.

Various volatile organic liquids of low dielectric constant were evaluated to find one which would provide lubrication during the wiping process but which would evaporate, leaving a soft, clean resilient fiber bundle (as cotton yarn) which would completely occupy the mold cavity over wide ranges of resin content. The solvent which appeared best in this respect and which was accepted for this program was n-heptane. This compound has a dielectric constant of 4.3 compared to water of 81.07, is non-toxic, readily available and leaves no residue after drying. Processing the hank of fibers was accomplished using the same technique as outlined above, except that n-heptane was used in place of water as the solvent. A bundle of fibers, after evaporation of the n-heptane solvent, displayed almost no interfiber bonding and permitted thorough and uniform resin impregnation. There were, however, still a few thin, isolated stiff areas which did not respond to this de-bonding treatment. This procedure did permit, however, accurate control of resin content in the finished composite, since the excess resin was squeezed out in proportion to the plunger pressure exerted.

The lack of cohesive forces among the dried fibers when using a non-polar solvent introduced a new problem. These dry, highly mobile fibers behaved badly during molding and displayed a tendency to float to the top of the mold cavity. A few stray fibers wedged into the clearance provided for the male plunger and caused binding between the mold parts, especially at the ends of the mold where the fibers were bent upward to maintain their open ends above the fluid level. A number of specimens was destroyed before the problem was resolved and steps could be taken to correct it. The ends of the fiber were taped and tied into position with string, thereby constraining the scraggly ends of the fiber bundles and preventing flotation



Fig. II-6 Straightening Wet Fiber Fluff.

and binding. Care was taken not to constrict the axial flow passages around the fibers by binding the ends too tightly.

Preparation of the samples was accomplished by placing the pre-dried fibers and mold, at a temperature of 165°F, into a metal tray-like container. This in turn was placed on a hot plate at 165°F in a vacuum tank. The male plunger was shimmed up approximately 1/8" above the dried glass bundle, and resin at 165°F was poured into the container to a level above the dried fibers. Penetration of resin into the centers of the hollow fiber was prevented by maintaining the exposed fiber ends above the resin level. The tank was then sealed and evacuated for one hour. After impregnation was completed, the mold was removed from the vacuum chamber and placed inside a curing oven. Before curing, the mold shims were removed and weights were added to obtain the desired molding pressure. In order to produce specimens having a range of resin contents, the specimens were molded under various pressures. A simple cantilever system was constructed and located inside the temperature-controlled curing and drying oven (Fig. II-7). By applying various weights to the end of the cantilever handle, the effective molding pressure could be varied from about 1 psi to 50 psi. The pressurizing device could accommodate two individual molds. Fig. II-5 shows a typical specimen after curing. The composite then rested for one hour under the plunger pressure at a temperature somewhat below the curing temperature to stabilize the matrix. The curing cycle took place overnight at 200°F.

The resin system used in this work was as follows:

Resin:

100 parts Kopoxite - Koppers Chemical Company
(resorcinal diglycidal ether)

Cross-Linking Agent:

125 parts Methyl Nadic Anhydride

Toughening Agent:

25 parts EM 207 - Thiokol Chemical Company

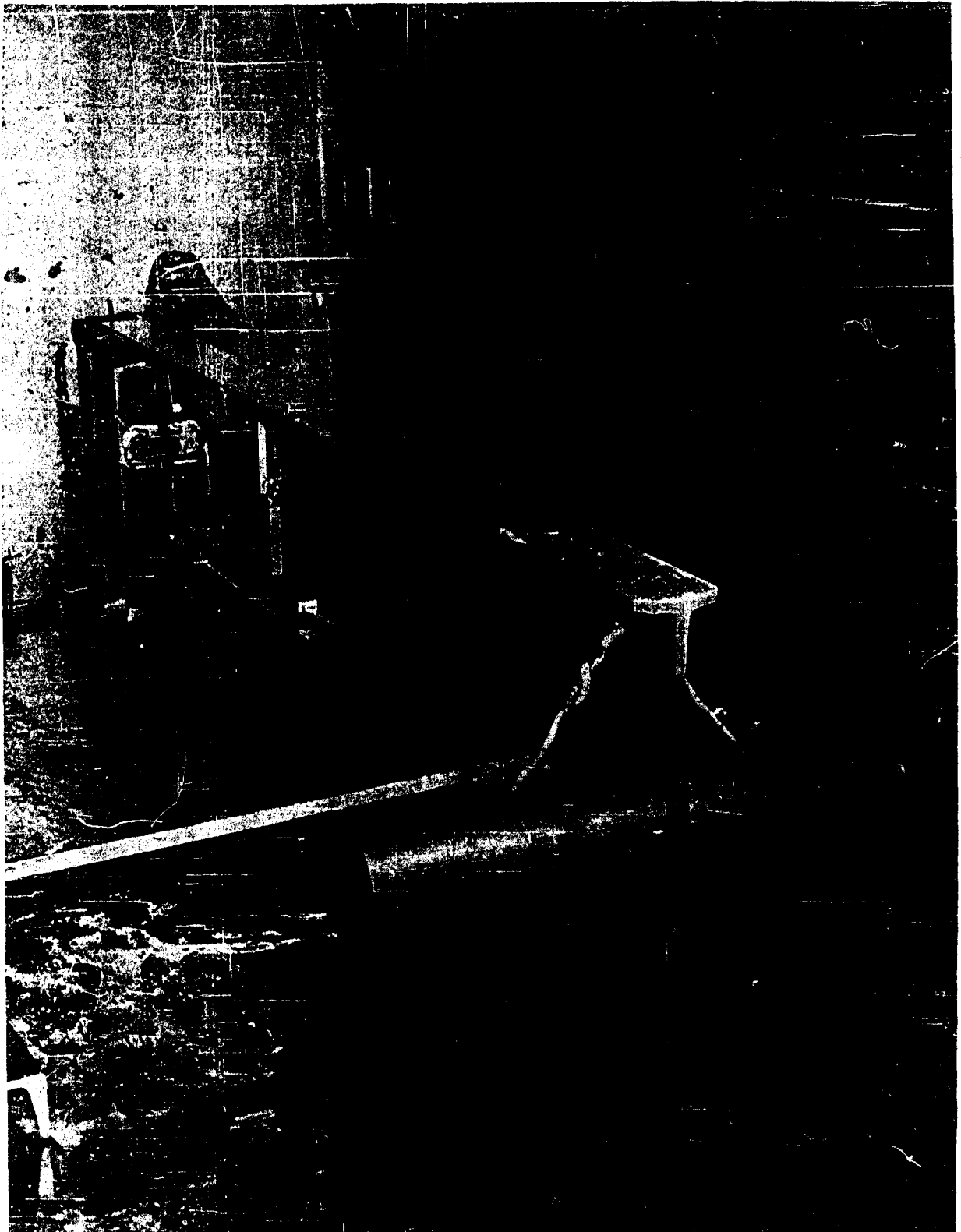


Fig. II-7 One Side of the Tandem Pressure Molding Press.

Catalyst:

1 part BDMA

(Benzyl dimethylamine)

Physical properties of the resin are:

Specific gravity	1.27
Modulus of elasticity	0.5×10^6 psi
Tensile strength	12,500 psi
Compressive strength	17,500 psi

Some of the good features of this resin system are low viscosity, high impact strength, high modulus, good transparency, low shrinkage, and good adhesion to glass.

The following is a summary of the final specimen fabrication procedures listed in order of their occurrence. Minor changes were made to simplify and improve the resulting specimens.

1. The glass fibers were drawn and wound on cardboard spools. A solvent, de-ionized water, was used to lubricate the fibers and prevent abrasion.
2. The fiber bundles were then dried for one hour at 200°F.
3. The dried bundles were packaged in polyethylene bags and shipped in padded cardboard boxes from Cleveland, Ohio, to the Valley Forge, Pennsylvania, site.
4. The fiber bundles were removed from the plastic bags and soaked in a tray containing n-heptane solvent. This softened the fiber bundle and prevented damage from subsequent handling.
5. A cut was made radially through the wet, circular bundle and the resulting hank was removed from the cardboard spool.
6. Fibers were axially oriented by wiping the solvent soaked fibers with the fingers. These fibers then were allowed to dry at room temperature for several hours.
7. Evaporation of the non-polar solvent n-heptane left the fibers free from electric charges and completely unbonded.
8. The hank of dry fiber was dipped into a room temperature bath

of catalyzed resin and hand wiped with soft foam rubber pads to assure complete impregnation and wetting of all the fiber surfaces and improve axial orientation of the fibers.

9. The resin impregnated hank was then placed into the cavity of a stainless steel mold. The fiber ends were tied and the plunger was inserted to prevent floatation of the hollow fibers. Additional liquid resin was poured into the mold to form a reservoir. Ends of the hollow fibers always remained above the liquid level. The entire assembly was evacuated for one hour at room temperature to eliminate any remaining air bubbles.
10. The assembly was then removed from the vacuum chamber and placed into an oven. A load was applied to the plunger for an effective pressure of 10 psi on the glass bundle. There it remained at 165°F until the fibers had adequate time to settle, about one hour. The resin remains a liquid throughout this process.
11. The oven temperature was then raised to 200°F and the composite cured for 16 to 20 hours.
12. The composite rod was finally removed from the mold, dried, and cut into test specimens.

III. Test

A. Physical property measurements

Measurements of density, resin content and fiber geometry were made on the specimen before testing. The resulting values of ρ_c , v_b , v_f and α were used to establish correlations with the experimental results such as strength and modulus of elasticity.

1. Specific gravity

Specific gravity of the composite, ρ_c , was determined from three one-inch long samples removed from the center and approximately one inch away from each end of a long specimen.

2. Resin content

This was determined from the weight reduction of specimens after firing in a muffle furnace at 1000°F for three hours. The resin was quickly volatilized, however, there was no significant glass loss in the time allowed.

The equations used to transform the weight fractions, w , to volume fractions, v , are

$$v_b = w_b \frac{\rho_c}{\rho_b} ; \quad v_f = w_f \frac{\rho_c}{\rho_f} \quad (1)$$

The average ratio of inside to outside fiber diameter is given by

$$\alpha = \sqrt{\frac{v_b}{1-v_b}} = \sqrt{\frac{1-v_b-v_f}{1-v_b}} \quad (2)$$

3. Photomicrographs

Samples approximately 1/8" long were removed from near the center of each molded specimen and imbedded in resin. After polishing, all samples were scanned optically. Photomicrographs were taken of typical areas at various magnifications.

B. Mechanical Properties

1. Fibers

A total of 489 hollow and solid fibers was tested in tension and the corresponding tensile strengths calculated. A regression analysis of the test results showed considerable increases in strength with decreasing fiber diameter and increasing hollowness.

Because of the specialized equipment needed for testing and optically measuring hollow glass fibers, it was decided to utilize the service of the nearby Philadelphia College of Textiles and Science. The tests were performed under the direction of Dr. Percival Thiel and W. Wolfgang.

The following testing procedure was shown to produce good tensile tests of the fibers.

1. Select fibers for tests randomly from each spool of different geometry and size fibers.
2. Cut each fiber into 1.25" lengths.
3. Cement* each fiber onto two 3/4" metal tabs, using fine combs to maintain alignment. Each end of the fiber extended 3/8" onto each tab, leaving 1/2" of fiber exposed between the edges of the tabs. Care was taken to prevent cement from entering the open ends of the hollow fibers.
4. Dry specimens overnight before testing.
5. Pull fibers on a Scott IP-2 constant load rate, inclined plane tensile testing machine.
6. Examine broken fibers and reject those tests having failures near the tabs.
7. Measure cross-sectional area optically at failure ends of the fibers. This is done directly on a Spencer objective microscope.

Table III-1 presents the results of 281 hollow fiber tests and Table III-2 presents similar results for 208 solid fiber tests. Each fiber test is listed according to its outside diameter, d_f , and the ratio α . The corresponding net fiber stresses at failure are given in ksi. The results were normally distributed as shown in Fig. III-1.

* Cement is cellulose nitrate in acetone or ether solvent.

TABLE III-1

Hollow Fiber Tensile Test Data

d_f	α	σ_f									
.00098	.643	149	.00105	.733	244	.00126	.777	214	.00189	.852	81
		179			245			214			107
	.715	136			258			227			129
		174		.770	192			254			156
		201			236			272			179
		207			236			277			193
		223		.800	293			278	.00192	.855	124
		228	.00108	.712	203			334			148
		245		.725	149	.00130	.785	247			218
		245		.765	118			275			232
		250			158	.00133	.790	244		.865	98
		269			200			244	.00196	.857	137
	.770	160		.806	225			252			137
.00094	.702	78	.00119	.765	248	.00136	.795	62			170
		190			250			191			179
		453			274			197			186
.00102	.686	199	.00122	.746	259			226	.00200	.860	84
	.725	167		.770	93	.00140	.800	183			129
		178			125			228			159
		189			132			250			204
		209			190			306			219
		231			197	.00150	.813	212			228
		251			208	.00161	.826	94			252
		273			227	.00164	.829	205	.00203	.863	73
		276			232	.00172	.837	158			103
		281			243	.00175	.840	246			111
	.754	300			246			287			151
.00105	.629	179			250	.00178	.842	180			156
	.705	101			271	.00182	.846	125			173
		253			273			223			191
		205			273	.00186	.849	116			205
	.725	208	.00126	.777	78			180	.00206	.864	89
	.733	228			156			180			90
		236			191	.00189	.849	189			96

Stresses in ksi

TABLE III-1 (Continued)
Hollow Fiber Tensile Test Data

d_f	α	σ_f												
.00206	.864	135	.00217	.871	121	.00228	.877	37	.00238	.735	126	.00245	.829	90
		144			122			84			134			172
		166			123			86			137		.886	89
		172			165			96			145	.00248	.750	102
		196			256			109		.812	63			115
		210	.00220	.668	102			117		.882	94			137
		216			104			158			112			166
.00210	.866	41		.682	63	.00231	.659	129			126		.759	102
		63			85		.667	121	.00242	.736	83		.790	120
		77			136		.728	106			94			
		92		.692	201			129			102			
		115		.873	90			130			133			
		116			103			147			138			
		135	.00224	.656	127			159			147			
		148		.688	62		.877	126		.752	117			
		184			72			135		.885	83			
.00214	.607	62			86			195			120			
	.654	59			119	.00234	.718	103	.00245	.715	144			
		139		.705	136		.735	61		.727	97			
	.869	143		.768	138			109		.743	76			
		186		.788	55			111			76			
		213		.875	106			140			83			
	.873	70			82			141			85			
		101	.00228	.658	112			146			85			
		158			114		.762	106			102			
		161		.676	122		.880	118			107			
.217	.598	56			122			126			118			
	.612	69		.693	85			136			120			
	.664	160		.720	151			182			127			
	.678	66		.737	82	.00238	.735	67			137			
		74			118			85			159			
		118		.780	90			92			177			
		138			252			102			195			
	.871	62		.815	136			107		.759	102			

TABLE III-2

Solid Fiber Tensile Test Data

d_f	σ_f										
.00088"	83	.00116"	129	.00136"	115	.00150"	56	.00178"	123	.00242"	90
.00098	57		137		125		80	.00182	61	.00245	42
	284		141		138	.00154	70		65		47
.00102	116		141		159		110		116		52
	135		151		179		116		133		63
.00105	138		169		213		119	.00186	50		66
	143		201	.00138	49	.00156	42		60		68
	172	.00117	85		53	.00168	159		84		71
	176	.00119	131	.00140	57	.00172	114		88		76
	181		159		58	.00175	61		91		76
	186		163		60		64		103		106
	190	.00120	80		75		66	.00189	59	.00248	58
.00108	75	.00122	122		82		68		64		64
	147		132		92		69		77		68
	157		137		96		71		83		70
	159		142		96		71		110		81
	160		157		100		72	.00192	100		81
	175	.00126	85		102		76	.00196	53	.00252	49
	181		97		108		77		54		60
.00109	128		133		109		78	.00200	64		65
	130		142		122		80	.00210	56		71
.00112	74	.00130	73		150		83	.00228	51		77
	115		112	.00142	56		84		59		78
	129	.00132	78		70		109	.00234	53		85
	134		98	.00144	54		119		72		86
	139		106		65		127		91		92
	141		113		78	.00178	65	.00238	65	.00256	59
	150		121		100		70	.00242	57		61
	161		126		106		78		57		73
	162		135	.00148	87		84		57	.00259	32
	185		145		99		87		61		84
	231		148		101		95		63	.00262	44
.00116	113	.00136	73		103		97		69	.00270	53
	115		102		122		100		77	.00284	38
					157		104		84	.00287	48

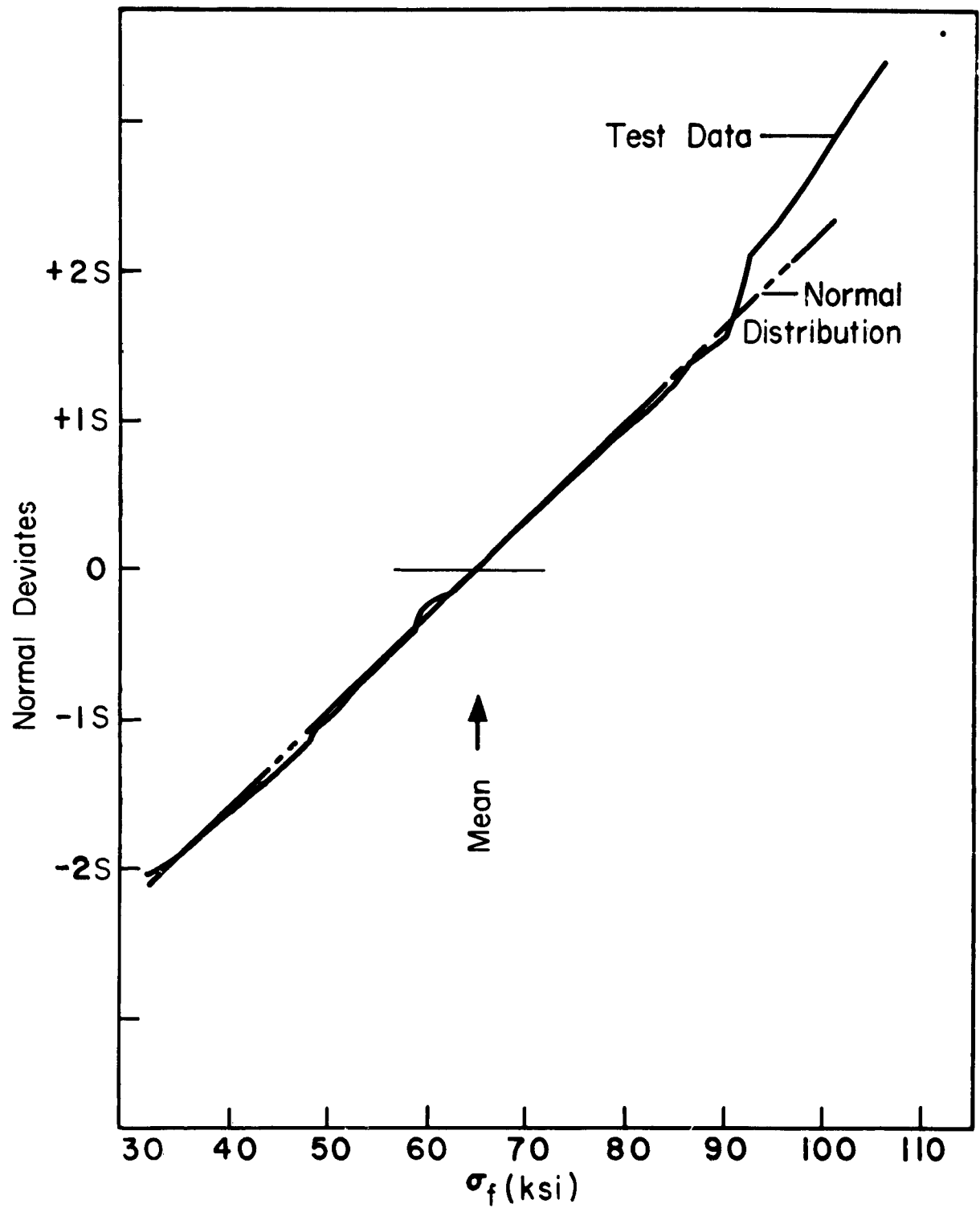


Fig. III-1 Cumulative Distribution of a Typical Group of 100 Solid Fiber Tensile Tests.

A number of regression analyses were made using an IBM 1620 computer and introducing various types of functions.

First, only solid fibers were considered to eliminate the variable α . The constants were found for the equation

$$\ln \sigma_f = A_0 + A_1 \ln d_f$$

The resulting best-fit of the solid fiber tests was the relationship

$$\sigma_f = \frac{0.246}{d_f^{0.92152}}$$

Next, both hollow and solid fiber test data and the previously deleted variable α were introduced in the form

$$\sigma_f = A_0 + \frac{A_1}{d_f^{0.92}} \left[1 + \frac{A_2}{A_1} \alpha + \frac{A_3}{A_1} \alpha^2 \right]$$

The exponent of d_f was rounded off to two significant figures to somewhat simplify the function. The results of this attempt to fit all the data points with a least-root-mean-square-error curve yielded the relationship

$$\sigma_f = 1.8827 + \frac{0.26341}{d_f^{0.92}} \left[1 - 0.66285\alpha + 1.96824\alpha^2 \right]$$

The residual sum of squares of deviation was 788,900.

Introducing α^3 into the function resulted in the equation

$$\sigma_f = 0.6555 + \frac{0.2761}{d_f^{0.92}} \left[1 - 1.196\alpha + 3.1267\alpha^2 - 0.7432\alpha^3 \right]$$

The corresponding residual sum of squares of deviations of 789,300 was slightly more than that for the 2nd order equation.

A better fit was obtained using the absolute value of d_0 rather than the ratio $\alpha = d_0/d_f$. This resulted in

$$\sigma_f = 2.0746 + \frac{0.2176}{d_i^{0.42}} \left[1 + 1560d_o - 498,000d_o^2 \right]$$

with a residual sum of squares of deviations of 778,060. This equation is plotted in Fig. III-2 vs. α for various values of d_o . It is apparent that the net fiber strength increases with decreasing outside fiber diameter and with increasing inside fiber diameter. This is a significant result and indicates that estimates of performance of hollow fiber composites under tensile loads must be revised, and that the outlook appears more promising. The problem remaining is to improve the reliability of hollow fibers so that these higher strengths can be utilized in actual structures.

2. Composites

Philosophy of experiment design was to compare the properties of hollow fiber reinforced plastics with solid fiber ones. Consequently, the testing procedures were simplified as much as possible and then frozen very early in the program so as to eliminate as many extraneous variables as possible. As a result of this philosophy, the test data shows the effects of fiber geometry for comparison with the analytical predictions. Care must be taken, however, in comparing the experimental results reported herein with those obtained by other experimenters, because of possible differences in testing techniques, and in fiber and specimen preparation

a. Longitudinal (axial) compression

Test specimens were cut from a long composite rod, described earlier in this report, in three lengths: 2", 1" and 3/8", using a special cut-off fixture to assure square, non-ragged ends. This fixture containing a diamond cutting wheel is shown in Fig. III-3. Tests were performed on specimens taken from 26 different rods. The results are presented in table III-3. The failure stress is presented in Fig. III-4 in the form of a strength-density ratio as a function of the fiber radius ratio. Each data point is the average value for a given rod and represents a number of points as shown in Table III-3. All data are normalized with respect to the average experimental strength-density ratio for solid fibers. Only those test specimens which fell within 15% of the nominal fiber volume fraction of 0.3 were plotted. This enables comparison with the analytically predicted strength variation as shown by the curve of Fig. III-4.

The net glass fiber stress σ_f at failure was calculated from the total composite stress σ_c at failure from the equation

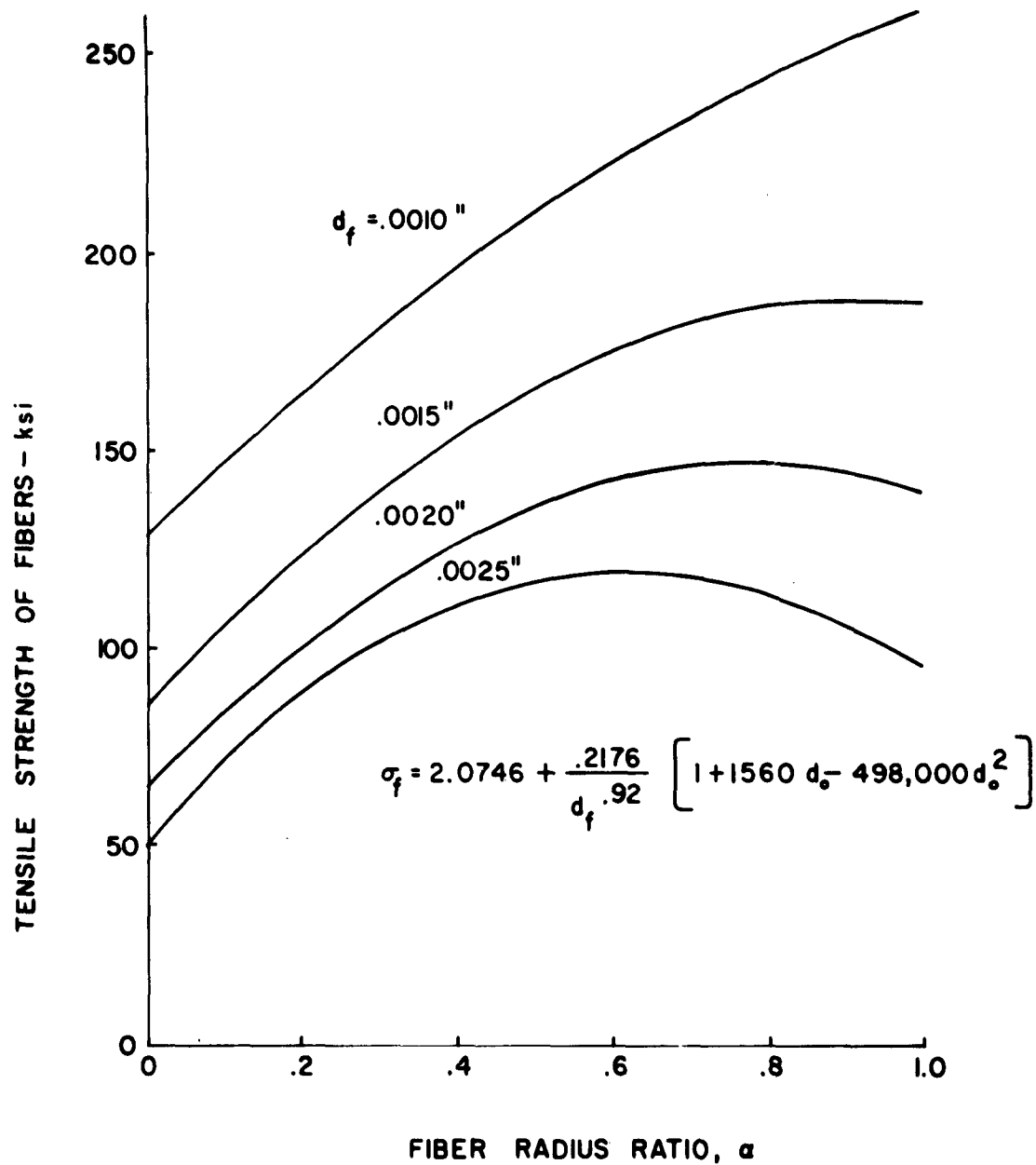


Fig. III-2 Tensile Strength of Glass Fibers-Results of Regression Analysis



Fig. III-3 Cut-off Fixture Used to Square Ends of Axial Compression Specimens

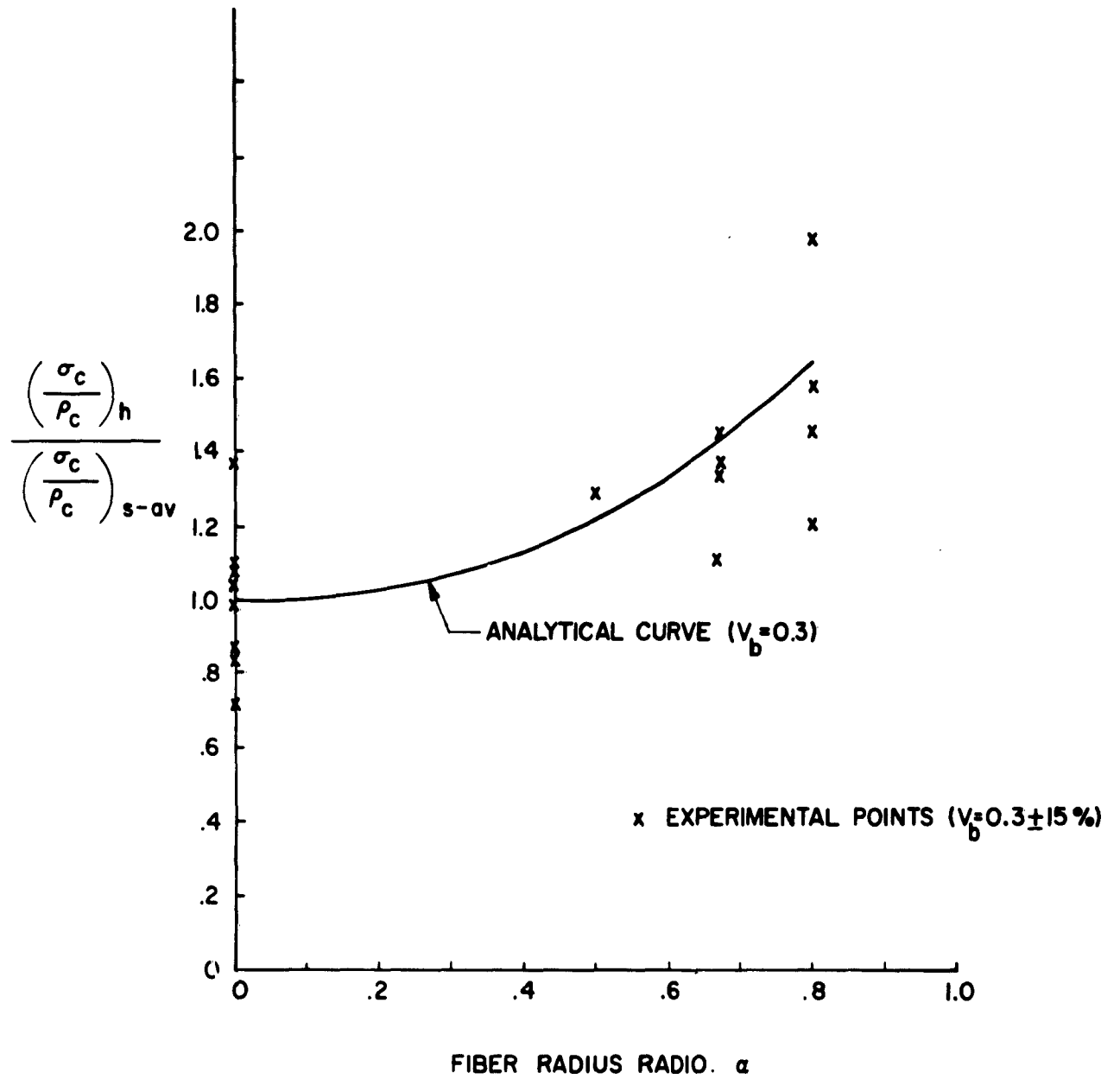


Fig. III-4 Axial Compression Composite Strength Test Data.

TABLE III-3

Axial Compression Test Data

Specimen Designation	V_b	V_f	Ave α	ρ_{Jc} g/cc	σ_c ksi	Ave σ_c ksi	$\frac{Ave \sigma_c}{\rho_{Jc}}$ ksi/in.
250-10-5G	.312	.214	.829	.913	45, 43, 45, 46, 45, 53	46	1.4
250-10-7G	.214	.227	.843	.817	40, 43, 28, 23, 24, 33, 34, 34	32	1.1
250-10-13G	.312	.214	.829	.855	54, 60, 62, 50, 42, 47	52	1.7
250-10-15G	.266	.215	.841	.855	67, 65, 73, 77, 77, 60, <u>81</u> , 68, 71, 71, 64, 78, 72, 71	71	2.3
250-6-6F	.272	.425	.645	1.37	59, 56, 87, 69, 52, 48, 62, 61, 72, 71, 63, 69	64	1.3
250-6-12F	.386	.388	.607	1.42	62, 83, 67, 80, 80, 67, 83, 82, 64, <u>87</u> , 82, 49	74	1.4
250-4-7G	.324	.507	.500	1.63	89, 85, 100, <u>100</u> , 95, 100, 96, 71, 70, 70	88	1.5
250-2-7G	.251	.749	0	2.20	100, 90, 19, 60, <u>109</u> , 69, 90, 104, 94, 43, 54, 71	75	.95
250-2-8G	.258	.742	0	2.10	38, 58, 55, 87, 100, 89, 94, 82, 74, 101, 68	77	1.0
200-6-6G	.340	.325	.712	1.30	66, 55, 50, 75, 87, 81, 75, 99, 88, 78, <u>102</u> , 77, 98	79	1.7
200-6-14G	.363	.390	.622	1.35	68, 82, 86, 69, 84, 84, 83, 77, 70, 74, 88, 53	76	1.6
200-2-1G	.317	.683	0	2.07	94, 97, 120, 102, 82, 86, 74, 104, 88, 92	94	1.3
200-2-2G	.295	.705	0	1.99	70, 82, 98, 62, 108, 86, 99, 58, 77	82	1.1
200-2-14F	.296	.704	0	2.14	120, 121, 117, 122, 122, 122, 120, 120, 128, <u>128</u>	122	1.6
150-6-3G	.328	.355	.687	1.24	55, 69, 65, 81, 68, 74, 91, 80, 44, 72, 86	71	1.6
150-6-15G	.282	.492	.563	1.54	72, 68, 78, 101, 95, 94, <u>108</u> , 88, 90, 78, 92	88	1.6
150-2-13G	.273	.727	0	2.08	61, 74, 78, 92, 82, 78, <u>98</u> , 74, 82, 50, 40	74	1.0
150-2-14G	.275	.725	0	2.03	39, 68, 77, 34, 70, 58, 48, 84, 78, 43, 74	61	.83
100-6-1G	.390	.475	.470	2.12	85, 86, 84, 97, 98, 100, 98, <u>99</u> , 96, 95, 89	93	1.2
100-6-12F	.390	.404	.581	1.47	80, 70, 70, 83, 86, 72, 89, 84, 67, 84, 80, 71	78	1.5
100-2-11G	.284	.716	0	2.09	80, 101, 90, 97, 86, 87, 75, 80, 102, 102, 91, 89, 86	90	1.2
100-2-15G	.272	.728	0	2.06	94, 88, 100, 105, <u>108</u> , 104, 98, 95, 75, 74, 74, 72	91	1.2

TABLE III-3 (Continued)

Axial Compression Test Data

Specimen Designation	v_b	v_f	Ave α	ρ_c g/cc	σ_c ksi	Ave σ_c ksi	$\frac{\text{Ave } \sigma_c}{\rho_c}$ 10 ⁶ in.
1-H	.311	.409	.688	1.43	83, 71, 77, <u>83</u> , 80, 53	70	
2-H	.203	.550	.556	1.70	27, 42, 44, 73, 35	44	
3-H	.370	.350	.665	1.36	81, 78, 106, 98, <u>110</u> , 101	96	
1-S	.370	.630	0	2.06	80, 72, 75, <u>95</u> , 81	81	

$$\sigma_f = \frac{\sigma_c E_f}{v_f E_f + v_b E_b}$$

Values used for the moduli were $E_b = 0.52 \times 10^6$ psi and $E_f = 10.7 \times 10^6$ psi. The other quantities, v_f and v_b , are the volume ratios of fiber and binder respectively, in the total composite and were determined independently for each rod. See nomenclature sheet for a description of the terms.

Maximum values of σ_f are plotted for each test in Fig. III-5. The net glass stress σ_f can be visually interpreted as a measure of structural efficiency for all test specimens without consideration of v_b .

The shape of the "instability-limit" curve for low and intermediate values of α is determined by analytical considerations derived in the Analysis section. The exact vertical location of the curve is determined from the test data, utilizing the criterion that all the composite tests must fall below the micro-buckling envelope. The envelope represents the shape of a theoretical maximum value for fiber instability.

It is not unreasonable to believe that as α is increased to very high values, the failure mode will shift from micro-buckling instability to fiber or resin shear failure. This establishes a horizontal line at the average failure stress of the glass resin system, in this mode.

The compression tests were performed on 2", 1" and 3/8" long specimens, and no significant difference was evident for failure stresses of various length specimens.

There was a considerable number of deviations in the specimens from the theoretically perfect conditions assumed in the determination of the theoretical compressive strength envelope. For example, the ends of the 1/4" x 1/4" cross-section specimens were not perfectly square. The fibers impregnated in the composites were often twisted. Resin-rich areas and voids throughout the cross-sections of the specimens were frequently observed. All these factors contribute significantly to the reduction in compressive strength from the theoretical prediction. This tends to explain the large variations in strength evident in Fig. III-5. It should be noted also that, with improved quality control in the specimen fabrication and testing procedures, more consistent compressive strengths can be expected.

b. Transverse compression

Composites reinforced with hollow fibers, although having improved axial properties, have considerably less strength in the transverse direction.

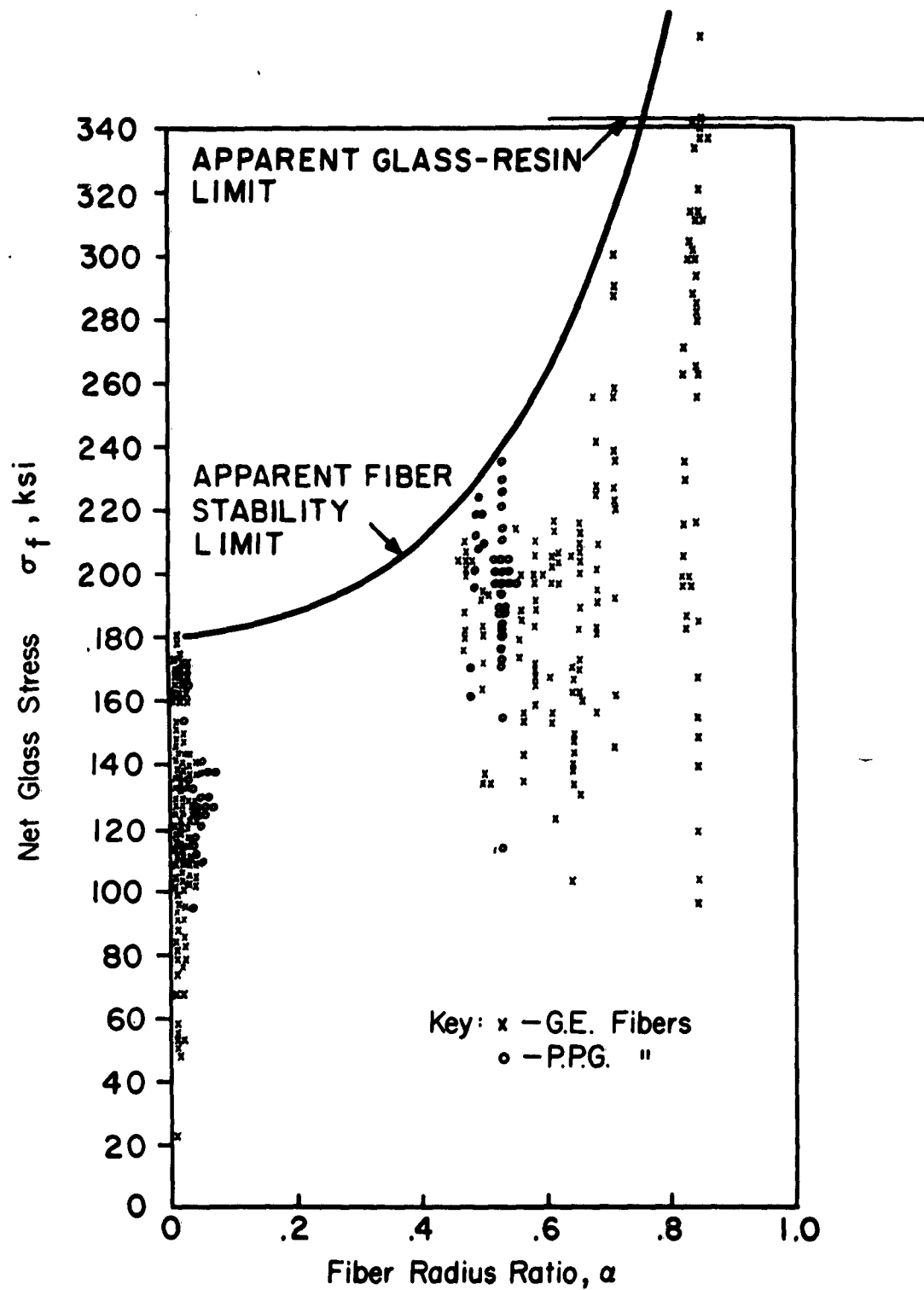


Fig. III-5 Axial Compression Fiber Strength Test Data.

This may be due to the collapse of the thin-walled tubes. Fig. III-6 shows the apparent envelope of failure stress for increasing hollowness of the fibers. For solid fibers and those having only slight hollowness, the horizontal line represents shear failure of the resin between the fibers. The second curve intersecting this horizontal resin failure line represents the model of failure whereby hollow fibers are sheared prior to resin failure. Fig. III-7 shows photomicrographs of these failure modes. Note that solid fibers in the failure area shown in the upper part of the figure remain intact, whereas, many of the hollow fibers in the lower part of the figure have been split longitudinally.

Typical transverse compression failures are illustrated for a very hollow fiber and a solid fiber reinforced specimen in Figs. III-8 and III-9 respectively. Specimens in the photograph are aligned so that the vertical axis approximates the direction of loading.

c. Bending test

A group of 31 rods was tested in 4-point flexure as shown in Fig. III-10. A light load 2P (about 35 pounds) was gradually applied and load-deflection curves were made for points 0 and 1 during both loading and unloading. Each rod was rotated 90° about its longitudinal axis, and the experiment was repeated. After all 4 sides were tested in this manner, each rod was loaded to failure. The maximum loads and failure modes were recorded.

The initial slopes (k) of 496 load-deflection curves (16 per specimen) were obtained from the testing machine strip charts. The k values were averaged for the loading and unloading curves and for the cases in which opposite faces of each rod were loaded. This resulted in 4 k-values for each rod: two for the two bending planes at each of the two measured points 0 and 1.

From the initial dimensions of each rod, the moments of inertia for 2 planes of bending were obtained. One modulus value was calculated for each of the two planes of a rod from the equation

$$E = \frac{0.5}{I_c (k_0 - k_1)_c}$$

for the dimensions shown in Fig. III-10. The subscripts 0 and 1 refer to the location of the measurement and the subscript c refers to the appropriate bending plane. It should be noted at this point that this equation utilizes the relative deflection between the two planes 0 and 1. This portion of the beam is free from shear and therefore not influenced by shear deformations. The

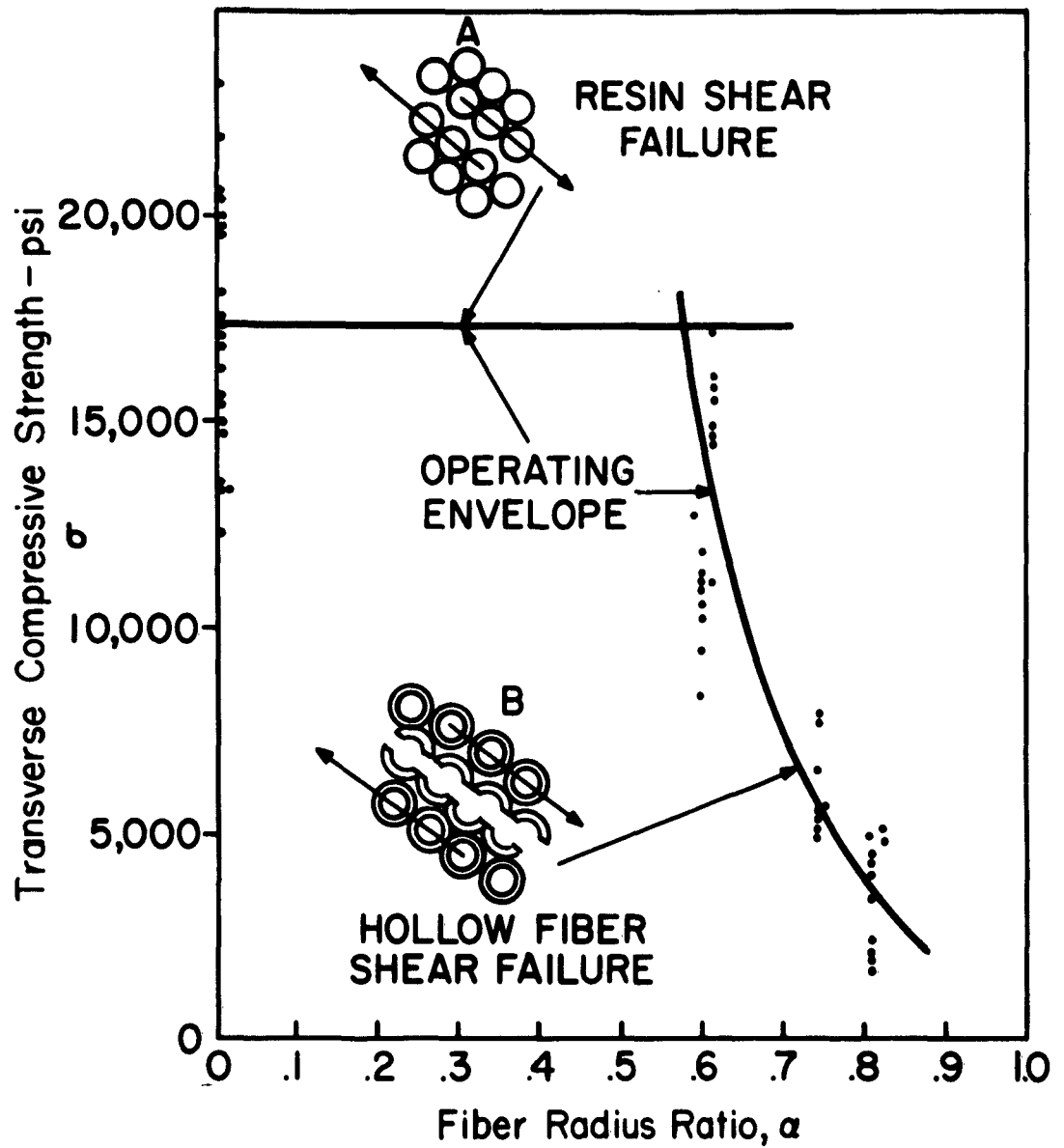


Fig. III-6 Failure Criteria and Experimental Data for Transverse Compression

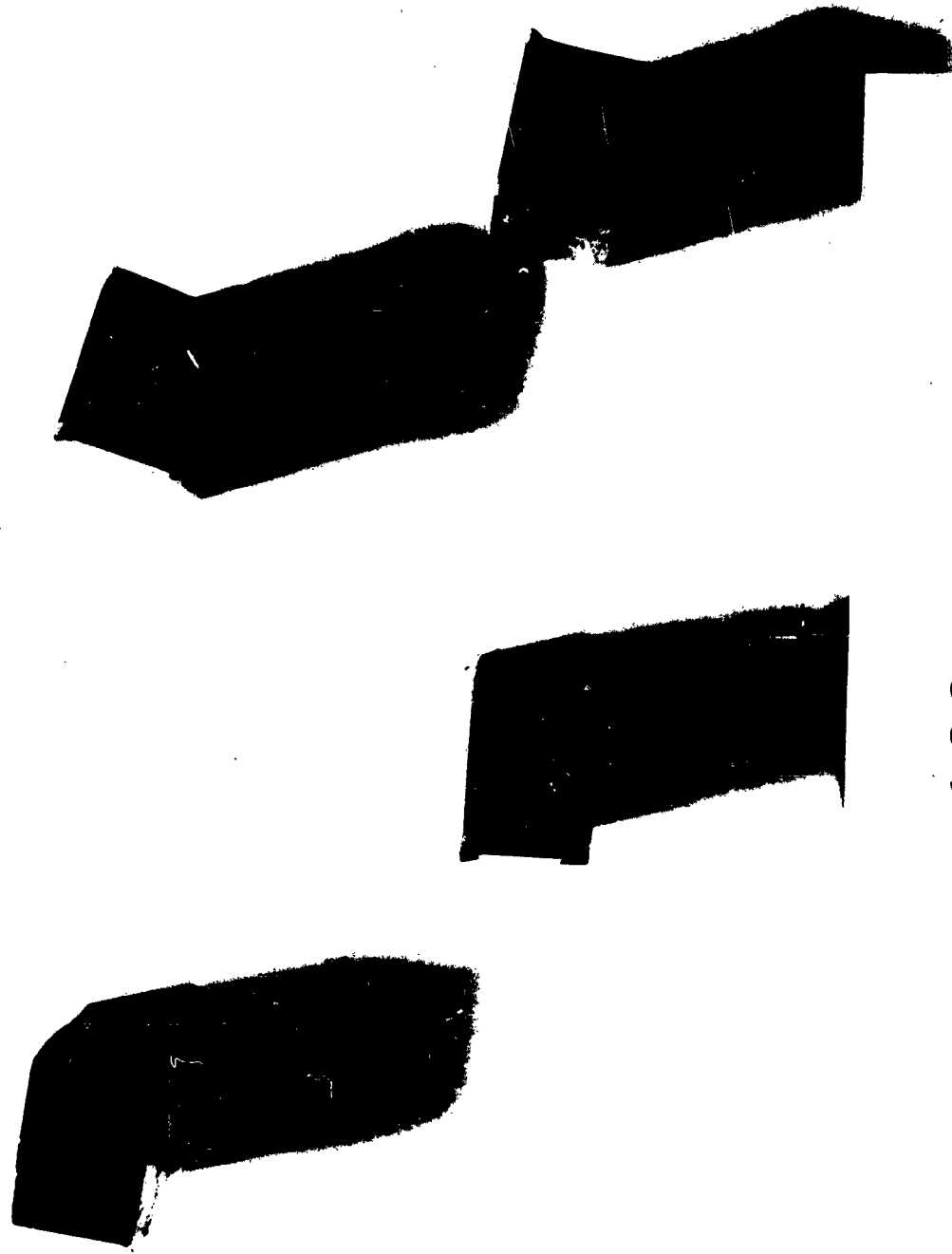


Solid Fiber Composite



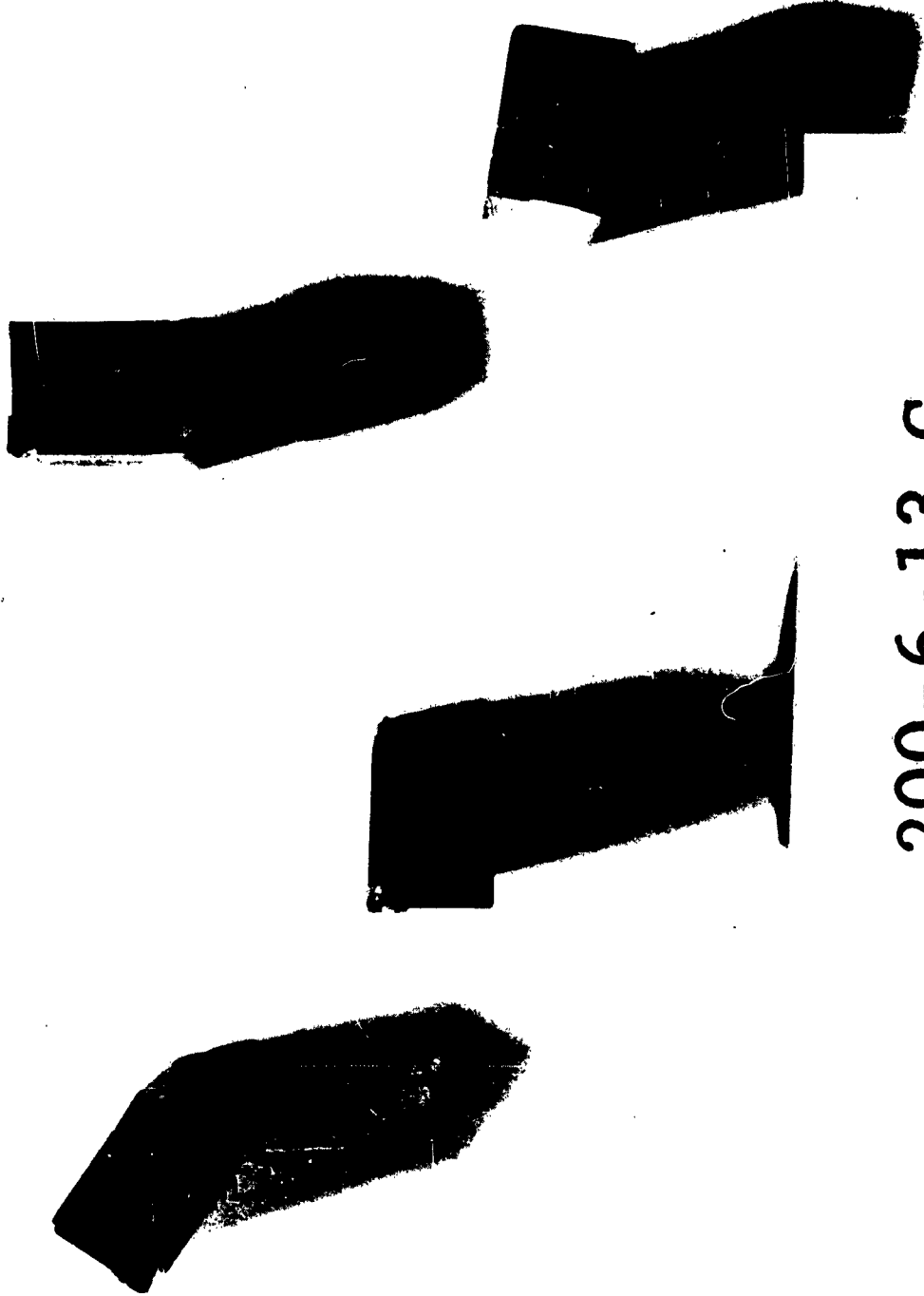
Hollow Fiber Composite

Fig. III-7. Shear Failure Mode of Solid and Hollow Fiber Specimens (154 X)



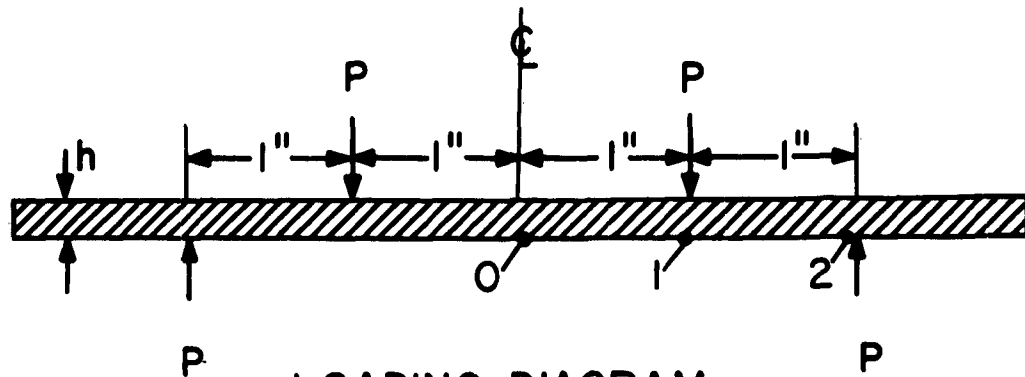
100-2-12-G

Fig. III-8 Typical Transverse Compression Failures of Solid Fiber Reinforced Composites.

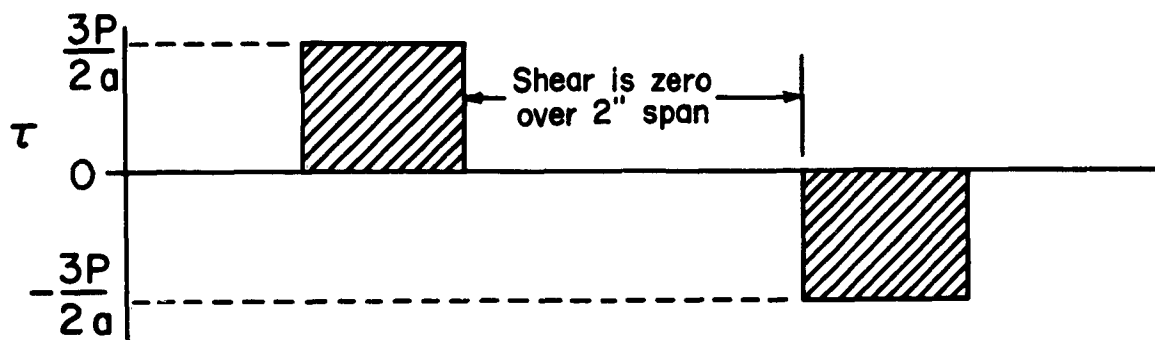


200-6-13-G

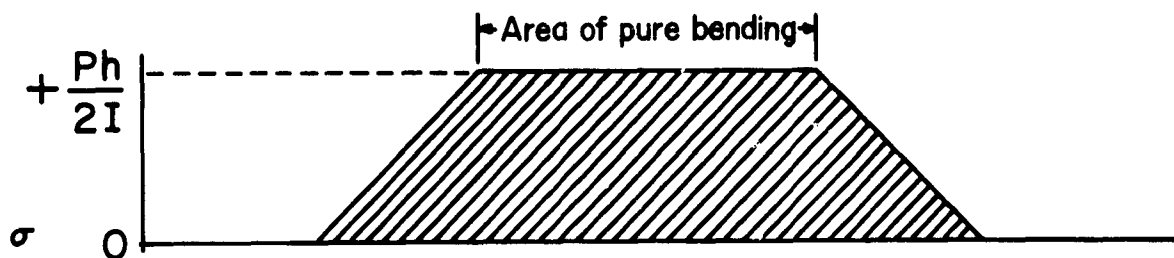
Fig. III-9 Typical Transverse Compressive Failures of Hollow Fiber Reinforced Composites.



LOADING DIAGRAM



SHEAR STRESS DIAGRAM



BENDING STRESS DIAGRAM
(COMPRESSION ON UPPER SURFACE)
(TENSION ON LOWER SURFACE)

Fig. III-10 Bend Test.

area is subjected to pure bending. These two values E_2 and E_3 were then averaged to give a single value E^* , the best estimate for the modulus for the specimen.

The shear and bending stresses were calculated from the equations

$$\sigma_{max} = \frac{3 P_{max}}{2 A}$$

and

$$\sigma_{b_{max}} = \frac{h_c P_{max}}{2 I_c}$$

where A is the cross sectional area of the rod, h_c is the thickness in the bending plane and I_c is the moment of inertia in the corresponding plane.

From previous tests, the modulus of elasticity of the resin was found to be about 0.52×10^6 psi. This value was used to calculate the modulus of the glass reinforcement from the equation

$$E_f^+ = \frac{E^* - v_b E_b}{v_f}$$

where the mark, +, denotes that the value is an estimate calculated from a bending test.

Fig. III-11 shows typical bend test failures. The uppermost specimens are solid and α increases toward the bottom. Table III-4 presents the results of the bending tests. The apparent modulus of the glass fibers varies considerably from one specimen to another, the average value being 10.77×10^6 psi. The values of modulus, obtained from the test, are plotted in Fig. III-12 for various values of α and fiber diameter.

A regression analysis made of the data in this figure yielded the relationship

$$E_f = 11.13 - 0.174\alpha - 146.4 d_f$$

Although this shows a slight reduction in fiber modulus with increasing α and d_f , the results are certainly not conclusive. The analysis showed the

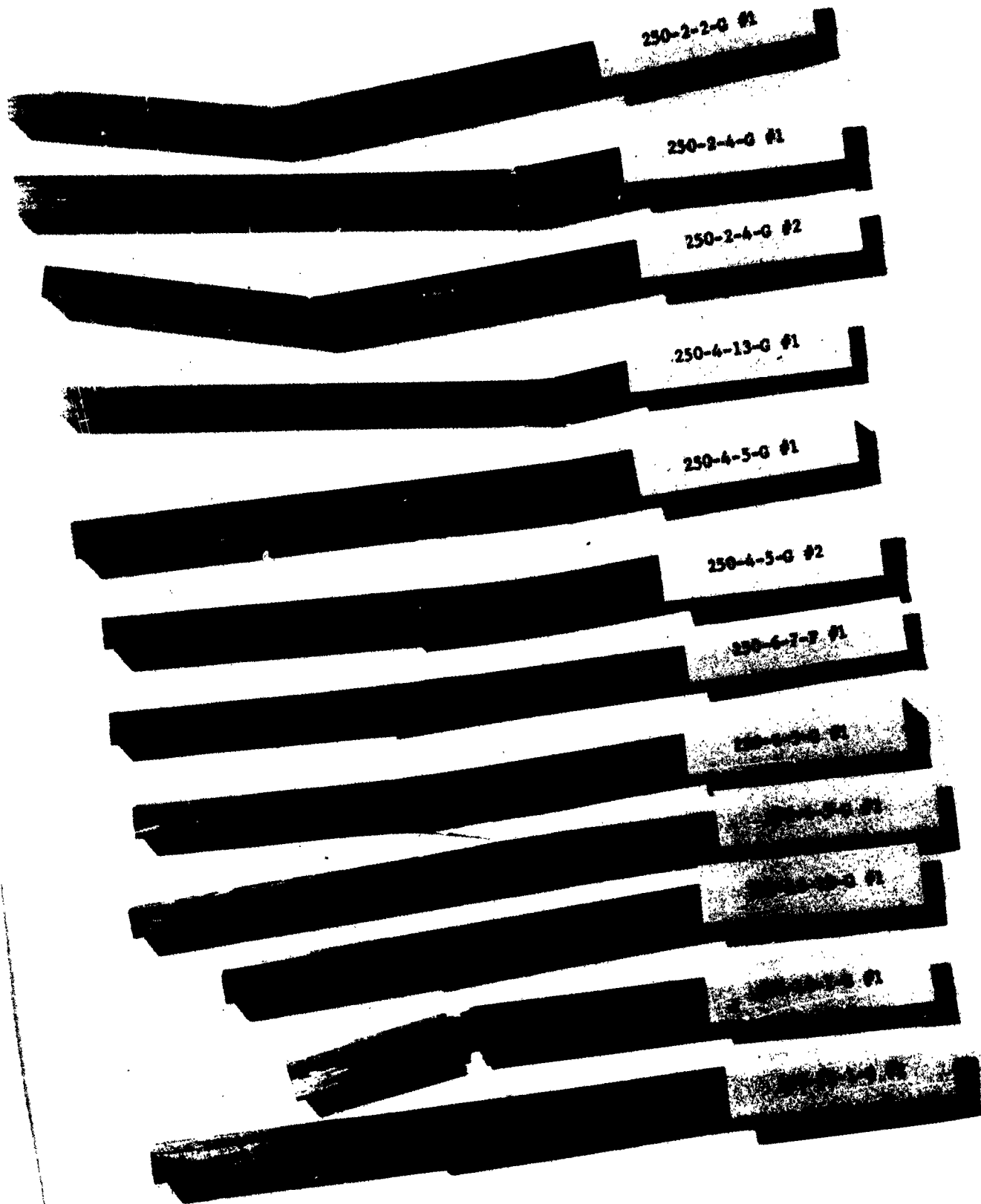


Fig. III-11 Typical Bend Test Failures.

TABLE III-4 RESULTS OF STATIC BEND TESTS

Designation	F_2 (psi)	F_3 (psi)	E^A (psi)	v_b	v_f	α	ρ_c (g/cc)	E_f (psi)	$\sigma_{b,max}$	C_f	T_{max}	Mode of Failure
250-10-10G#1	3.13×10^6	3.25×10^6	3.19×10^6	.366	.286	.741	1.15	10.50×10^6	40.4 ksi	141 ksi	2.69 ksi	Tension
-1G#2	4.57	4.24	4.05	.232	.387	.704	1.225	9.90	52.7	136.2	3.47	Tension
-1G#1	3.85	4.33	4.09	.232	.387	.704	1.225	10.00	48.7	125.6	3.93	Tension
250-6-5G#1	4.02	4.59	4.30	.364	.40	.612	1.41	10.40	63.4	159	3.75	Tension
-5G#2	4.22	4.01	4.11	.364	.40	.612	1.41	9.82	94.8	237	6.30	Tension
-7F#1	5.45	4.12	4.78	.276	.164	.60	1.45	10.50	196	422	10.10	Tension
-1G#1	4.35	4.65	4.50	.270	.376	.67	1.257	11.65	97	258	6.32	Tension
250-4-13G#1	4.75	6.05	5.40	.269	.560	.484	1.69	9.40	176	314	9.0	Tension
-5G#1	5.43	5.37	5.40	.246	.50	.58	1.53	10.53	54.2	108.5	4.24	Tension
-5G#2	4.84	5.58	5.72	.246	.50	.58	1.53	11.20	62.4	124.5	4.11	Tension
250-2-2G#1	8.42	8.13	8.27	.266	.724	0	2.10	11.10	72.3	98.5	4.75	Tension
-4G#1	15.70^{**}	12.0	13.80^{**}	.240	.760	0	2.14	—**	62.8	82.7	4.60	Compression
-4G#2	9.48	8.73	9.10	.240	.760	0	2.14	11.62	55.2	72.6	3.64	Tension
200-6-4G#1	5.12	5.17	5.14	.371	.403	.600	1.445	12.30	65.2	162	4.62	Shear-Tension
-3F#1	3.18	2.79	2.98	.332	.281	.7605	1.1	10.05	39.0	139	2.66	Tension-Shear
-3F#2	3.19	3.10	3.14	.332	.281	.7605	1.1	10.62	46.2	164	2.32	Tension
200-2-9G#1	10.16	10.10	10.13	.26	.74	0	2.15	13.5	41.4	56	3.8	Shear-Compression
-7G#1	4.29	10.42	7.36	.24	.76	0	2.09	9.56	52.4	69.0	3.55	Shear
-7G#2	—	7.72	7.72	.24	.76	0	2.07	10.00	88.2	116	6.0	Tension
150-G-14G#1	4.43	4.45	4.44	.31	.427	.618	1.42	10.03	66.4	155	4.46	Tension
-6G#1	4.19	3.94	4.06	.282	.399	.666	1.318	9.80	58.8	147	4.29	Tension
-6G#2	5.34	—	5.34	.282	.399	.666	1.318	13.20	63.4	159	4.28	Tension
150-2-12G#1	—	8.76	8.76	.286	.714	0	2.08	12.05	96.8	136	6.6	Tension-Compression
-15G#1	7.46	8.20	7.83	.267	.733	0	2.09	10.50	64.0	87.3	4.66	Tension
-15G#2	8.12	7.05	7.58	.267	.733	0	2.09	10.15	89.5	102	6.1	Tension
100-G-13F#1	4.10	3.89	4.00	.368	.382	.629	1.39	9.95	69.0	180	4.78	Tension
-13F#2	5.02	5.28	5.15	.368	.382	.629	1.39	12.95	70.5	184	4.48	Tension
-8G#1	4.33	4.51	4.42	.405	.40	.572	1.49	10.52	94.5	236	6.38	Compression-Tension
100-2-9G#1	6.84	7.61	7.225	.284	.716	0	2.06	9.88	123.3	172	8.36	Tension
-13G#1	7.72	7.81	7.765	.277	.723	0	2.08	10.53	101.2	140	7.5	Tension
-13G#2	7.30	8.40	7.85	.277	.723	0	2.08	10.68	110	152	7.25	Tension

** - Probable error, datum not considered valid.

+ - Calculated from tests.

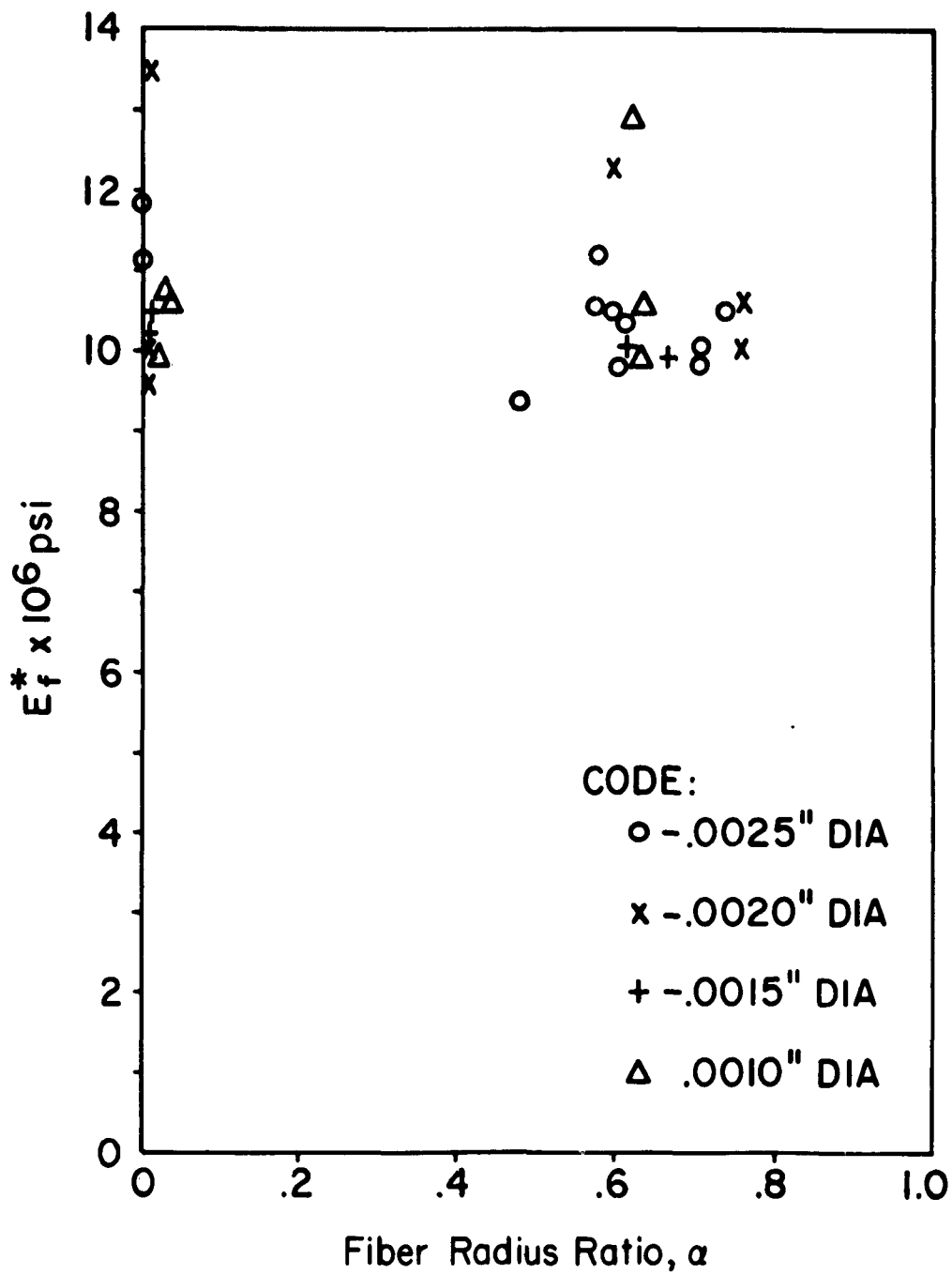


Fig. III-12 Apparent Glass Fiber Modulus, E_f^* , From Bend Test Data.

data to be nearly random and one should conclude that there is probably no correlation with fiber geometry.

d. Longitudinal tension

A great deal of difficulty was experienced in testing hollow fiber composites in tension. The low transverse compressive strength repeatedly caused failure in the testing machine grips. No successful tensile tests on composites have been made to date.

The usual result of a tensile test is either a longitudinal split along the rod or crushing the ends of the rod by the jaws of the testing machine. The shear strength of a composite is about 4000-5000 psi which can be converted into only about 2000 lb axial load. The full rod would require up to 10,000 lb to rupture. Necking down the rod to reduce the braking load to the limits of the grips requires the load to transfer across the fibers from the grips to the internally located test section, resulting in a longitudinal slit.

Attempts were made to perform tensile tests by modifying the specimen shape by varying the type of grips used. Slippage in the grips or shear and tensile failures away from the test section occurred, although some promise of future success was indicated by certain of the procedures.

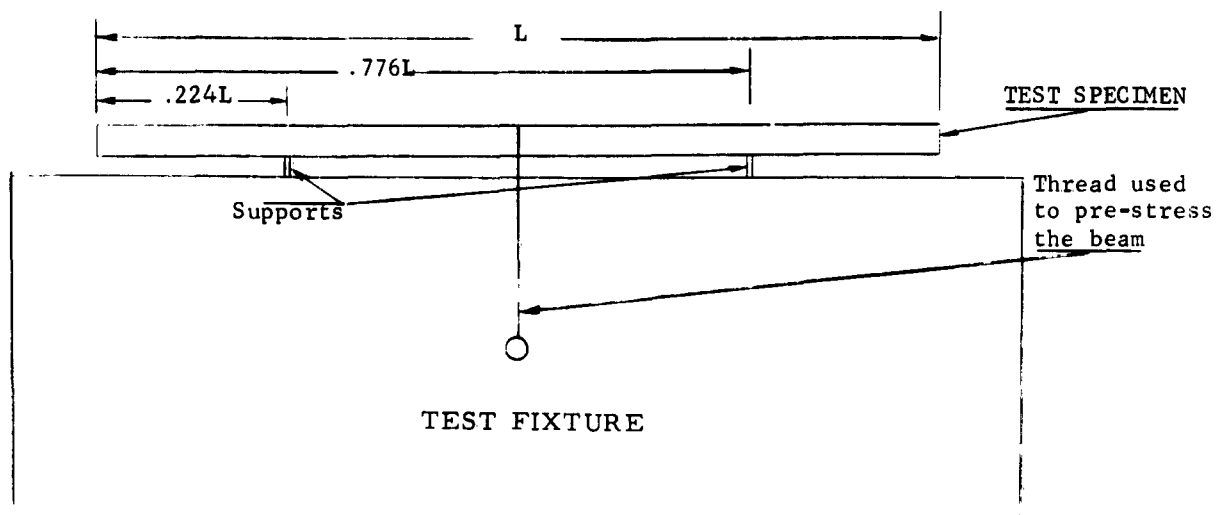
e. Dynamic properties

Several rods were excited to vibrate in a free-free mode by supporting them horizontally at their modal points and then suddenly releasing a force at the center point (Fig. III-13). This was done by severing a taut string tied to the center of each rod. A strain gage at the anti-node of each rod was coupled to an oscillograph which presented a time-amplitude plot of the rod vibrations (see Figs. III-14 and III-15).

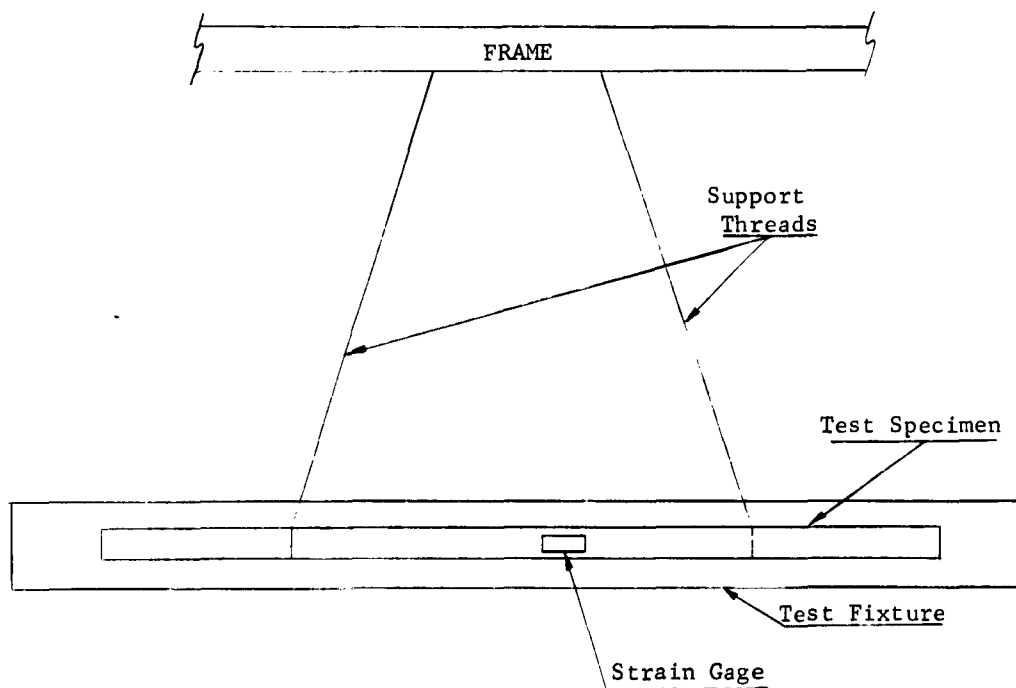
The initial vibrations after severing the string were of very large amplitude and distorted with higher harmonics. These initial vibrations soon died away, however, leaving a low small amplitude, sustained oscillation at constant frequency. This lowest natural frequency $f(n)$ and the ratio of the amplitude of one peak to that of the following peak x_1/x_2 were carefully measured. The modulus of elasticity was then calculated from the equation

$$E_c = \frac{\rho_c L^4}{32.2} \left(\frac{f(n)}{3.56h} \right)^2, \text{ psi}$$

where ρ_c is the composite density (lb/in³), L is overall beam length (inches) and h is the thickness of the beam (inches).



a) Top View



b) Front View

Fig. III-13 Dynamic Test Setup

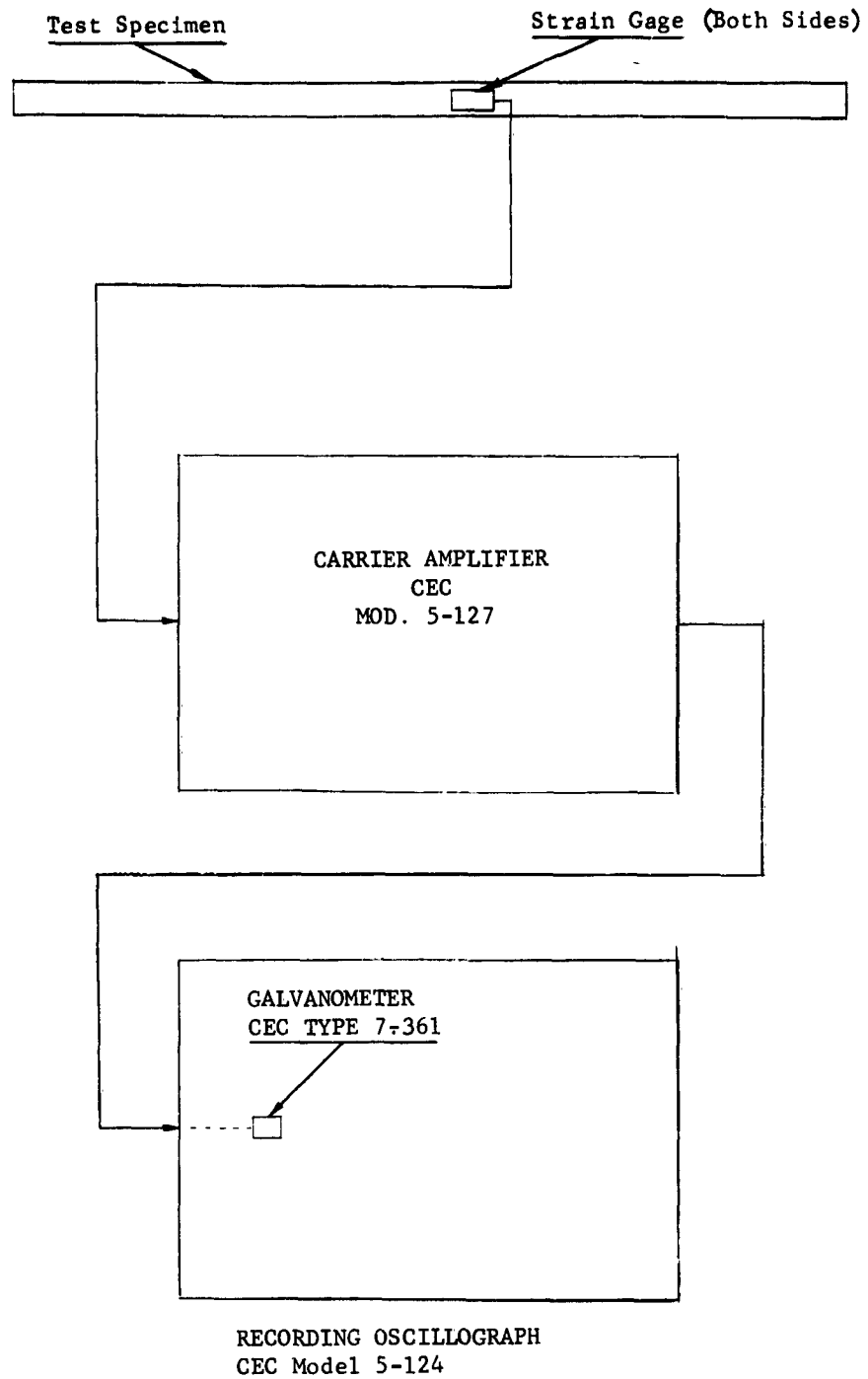
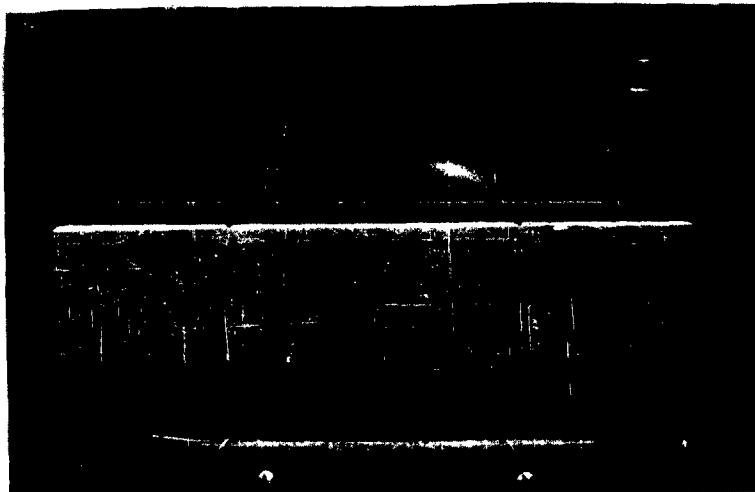


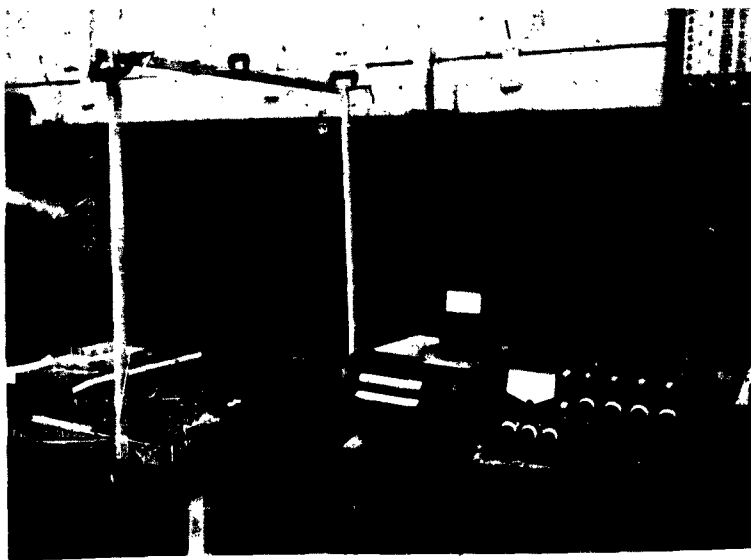
Fig. III-14 Instrumentation Setup For Dynamic Tests



a) Test Fixture



b) Test Setup



c) Instrumentation Setup

Fig. III-15 Dynamic Tests

Test results along with other pertinent information are presented in Table III-5.

C. Electrical properties measurement

The dielectric constants, dielectric strengths, dissipation factors and D. C. insulation resistance were measured on a complete group of hollow and solid fiber specimens. Measurements were made parallel and transverse to the fibers at 1 kilocycle and 1 megacycle. Specimens were tested after oven drying and then again after exposure to 50% relative humidity ambient air.

The following table summarizes the results.

Dielectric Constant at 1 KC	
Transverse to fibers	- 5 to 8
Parallel to fibers	- 6 to 8
Dielectric Constant at 1 MC	
Transverse to fibers	- 4 to 6
Parallel to fibers	- 5 to 6
Dissipation Factor at 1 KC	
Transverse to fibers	- 0.001 to 0.003
Parallel to fibers	- 0.001 to 0.002
Dissipation Factor at 1 MC	
Transverse to fibers	- 0.006 to 0.012
Parallel to fibers	- 0.008 to 0.024
D-C Insulation Resistivity	
Transverse to fibers	- 10^{15} ohm-cm
Parallel to fibers	- 10^{15} ohm-cm
60 Cycle Short Time Dielectric Strength	
Transverse to fibers	- 200 to 500 volts/mil
Parallel to fibers	- 100 volts/mil (max.)

1. Identification of samples

The test material consisted of ten groups of 3 composite rods. Each rod measured approximately 1/4" x 1/4" x 15". Groups represented variations in the glass fiber dimensions and were assigned identifying letters. Since all of the rods in a group were nearly identical, and since three rods were required

TABLE III-5

Results of Dynamic Bend Tests

Designation	Length inches	Width inches	Thickness inches	v_b --	v_f --	α --	f_c g/cc	$f(n)$ cps	E_c 6psi	E_f psi	$\frac{X_1}{X_2}$ --
150-2-6G	14.68	.322	.269	.216	.784	0	2.18	249.0	7.68	9.9	1.00580
150-6-2G	14.50	.257	.222	.308	.390	.66	1.34	201.7	4.33	10.7	1.00746
250-2-14G	13.19	.267	.240	.278	.722	0	2.11	282.1	7.94	10.8	1.00521

to make one test specimen, two specimens were formed randomly from the six similar rods of a group. Both were then marked with an identifying letter for the group. This single letter facilitated marking the small electrical test specimens and referring to them when discussing results. Table III-6 gives the sample designation and the corresponding identifications of specimen variables.

The electrical properties measured in this investigation were as follows:

60 Cycle Short Time Dielectric Strength
D-C Insulation Resistance
Dielectric Constant at 1 Kilocycle and 1 Megacycle
Dissipation Factor at 1 Kilocycle and 1 Megacycle

Each property was measured in two planes of the material: (a) parallel to the glass fibers, and (b) transverse to the fibers. All measurements were made at room temperature. Dielectric constant, dissipation factor and insulation resistance were measured after thorough drying and after exposure to room humidity; dielectric strength was measured only after exposure to room humidity.

2. Fabrication of electrical test specimens

a. Dielectric constant, dissipation factor and insulation resistance

For measurements parallel to the fibers, 64 blocks each about 1/4" long were cut from the rods with an 0.032" slitting saw on a bench milling machine and assembled in a removable clamping frame to form a 2" x 2" x 1/4" square with the fiber direction perpendicular to the 2" x 2" faces. Small drops of epoxy* resin were used to bond the adjacent block faces, care being exercised to see that no resin came in contact with the exposed hollow centers of the fibers. The 64-block assembly was then clamped tightly and the resin allowed to cure for 24 hours at room temperature. The 2" x 2" faces were sanded flat and parallel to remove irregularities caused by slight differences in the cut length of the nominally 1/4" x 1/4" x 1/4" rod sections. The truing of the faces was started with #240 and finished with #400 Carbimet silicon carbide grinding paper. The specimens were manually rubbed on the paper laid on a smooth flat surface.

For measurement transverse to the fibers, 8 (eight) blocks, each 2" long, were cut from the rods and assembled in the frame to form a 2" x 2" square with the fiber direction parallel to the 2" x 2" faces. The

* Epon 820, mixed 10 parts of resin to 1 of triethylene tetramine catalyst.

TABLE III-6

SAMPLE	IDENTIFICATION				α (5)			
	(1)	(2)	(3)	(4)				
A	250	-	2	-	1	-	G	0
	250	-	2	-	9	-	G	0
	250	-	2	-	13	-	G	0
B	250	-	4	-	9	-	G	0.5
	250	-	4	-	11	-	F	0.5
	250	-	4	-	15	-	G	0.5
C	250	-	6	-	2	-	F	0.67
	250	-	6	-	3	-	G	0.67
	250	-	6	-	8	-	G	0.67
D	200	-	2	-	4	-	G	0
	200	-	2	-	11	-	G	0
	200	-	2	-	15	-	F	0
E	250	-	10	-	2	-	F	0.8
	250	-	10	-	4	-	F	0.8
	250	-	10	-	9	-	F	0.8
G	150	-	6	-	7	-	G	0.67
	150	-	6	-	9	-	F	0.67
	150	-	6	-	10	-	G	0.67
H	150	-	2	-	3	-	G	0
	150	-	2	-	7	-	G	0
	150	-	2	-	8	-	G	0
I	100	-	6	-	7	-	F	0.67
	100	-	6	-	10	-	F	0.67
	100	-	6	-	11	-	F	0.67
J	100	-	2	-	5	-	G	0
	100	-	2	-	6	-	G	0
	100	-	2	-	7	-	G	0
K	200	-	6	-	7	-	G	0.67
	200	-	6	-	9	-	G	0.67
	200	-	6	-	15	-	G	0.67

NOTE: Sample F was machined but not used for electrical measurements.

- Col. #1 Outside diam. of glass fibers; 250 = 0.00250", 200 = 0.00200", etc.
 Col. #2 Ratio of fiber diameter to wall thickness. Ratio of 2 indicates solid fibers.
 Col. #3 Rod Number
 Col. #4 Estimated Rod Quality (G - Good, F - Fair)
 Col. #5 Ratio of Fiber I.D. to O.D.

blocks were cemented together with Epon 820 resin with no penetration of the rod ends by the resin. The 8-block assembly was clamped and the resin cured for 24 hours at room temperature. The 2" x 2" faces were then sanded flat and parallel using the same materials and procedure as for the parallel specimens. Since the total area of interfaces between the blocks amounts to only about 1% of the area of the 2" x 2" measurement surfaces, the resultant introduction of an extra 1% of epoxy resin seemed unlikely to affect the measurements significantly. The average thickness of the 2" x 2" blocks after sanding was determined from 5 (five) measurements per specimen within a 2" diameter circle using a machinist's micrometer with a 0.1 mil vernier. Fig. III-16 shows typical specimens of the two types.

After forming, the 2" x 2" specimens were air-dried in a forced-convection oven for 65 hours at 115°C, removed and cooled in a desiccator over Drierite. The specimens were kept in the desiccator until the completion of the "dry" measurements, except for brief periods during which the foil electrodes were being attached. Fig. III-17 shows typical specimens in the desiccator with leads attached for the "dry" measurements. The electrodes for these measurements consisted of 2" diameter discs of lead foil coated with Dow Corning Silicone Stop Cock Grease. These were rolled onto both of the 2" x 2" faces of the specimen so as to exclude air and conform to the surface. Fig. III-18 shows typical specimens with lead foil electrodes attached.

After the "dry" measurements, the specimens were exposed to ambient room humidity for 24 hours before re-measurement. The relative humidity varied between 40 and 50% at a temperature of 25°C ± 1°C during conditioning and measurement.

b. Dielectric strength

For measurements parallel to the fibers 5 (five) blocks each about 1" long were cut from the rods. Into the center of each 1/4" x 1/4" end of each block a flat-bottomed hole 0.125" in diameter was drilled to a depth such that about 0.10" of material remained between the bottoms of the holes. Every effort was made to insure that the axes of these holes were parallel and on the same center line. Fig. III-19 shows a specimen ready for test.

The first measurements of dielectric strength transverse to the fibers were made on short blocks, each about 0.4" long, cut from the 1/4" x 1/4" square rods. At the center of each 0.4" x 1/4" face of each block a flat-bottomed hole 0.125" in diameter was drilled to a depth such that about 0.10" of material remained between the bottoms of the holes. Again careful measurements insured that the holes had a common center line and their axes were parallel. Fig. III-20 shows this device ready for test. The electrodes used for these measurements consisted of two steel rods 0.125" in diameter mounted in a plastic fixture so they were axially in line. The adjacent faces were flat, with the circular edge slightly relieved. (Round-



Fig. III-16 Typical Assembled Specimens for Dielectric Constant, Dissipation Factor and Insulation Resistance Measurements.

Bottom: For Measurement Transverse to Fibers.
Top: For Measurement Parallel to Fibers.



Fig. III-17 Typical Specimens in Dessicator with Measurement Leads Attached.



Fig. III-18 Typical Dielectric Constant, Dissipation Factor and Insulation Resistance Specimens With Foil Electrodes Attached.

Bottom: For Measurement Transverse to Fibers.
Top: For Measurement Parallel to Fibers.

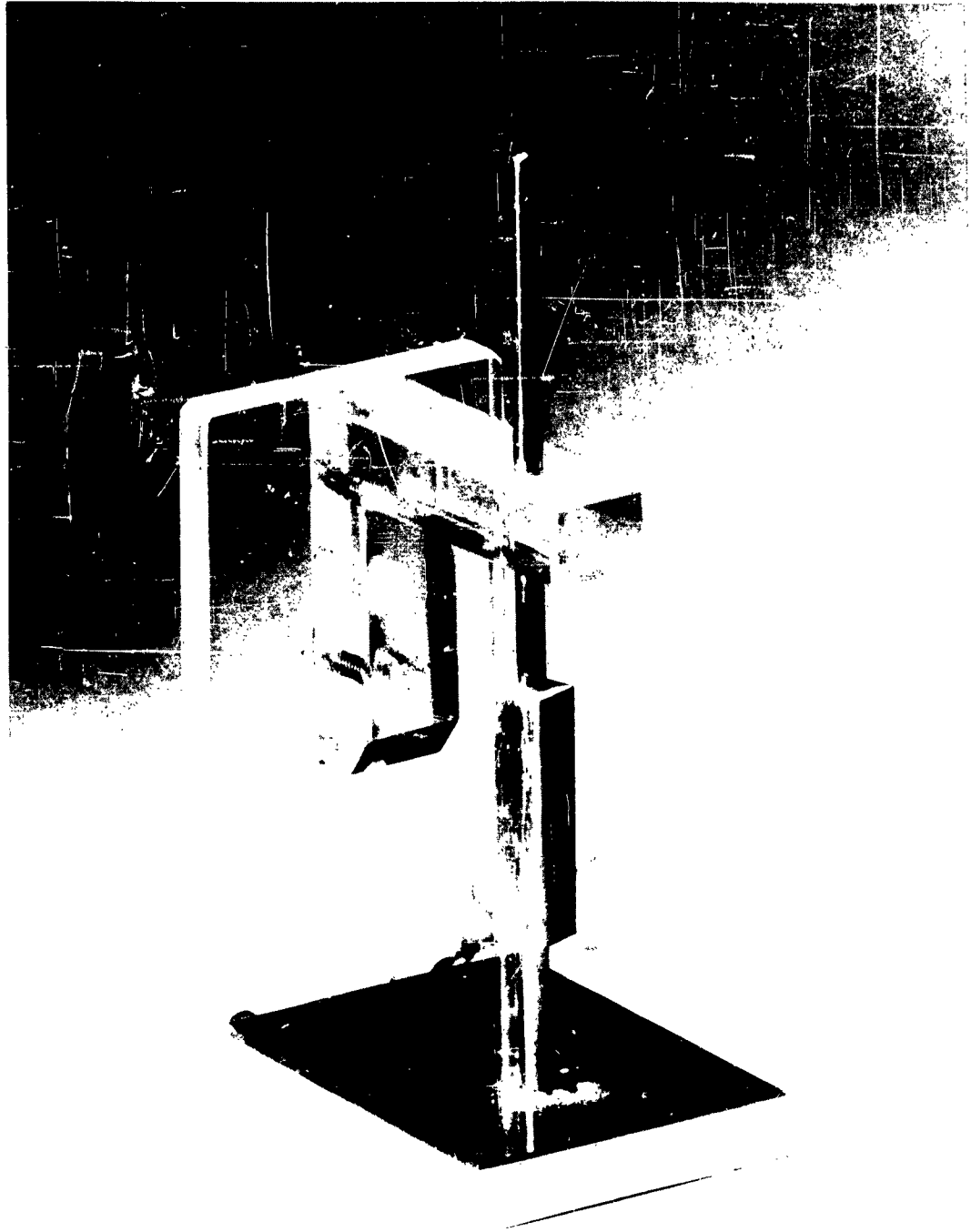


Fig. III-19 Dielectric Strength Electrodes with Specimens for Measurement Parallel to Fibers in Place.

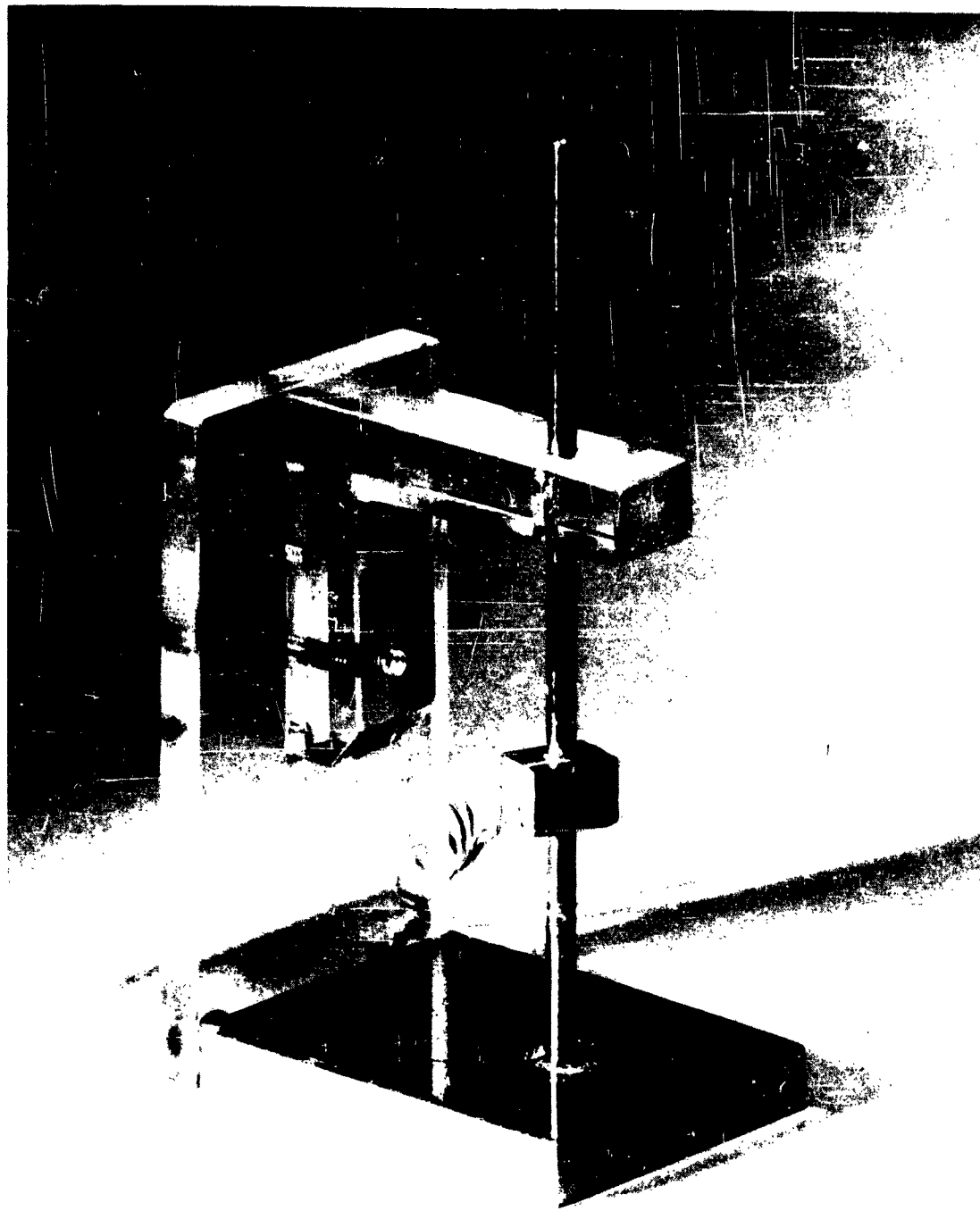
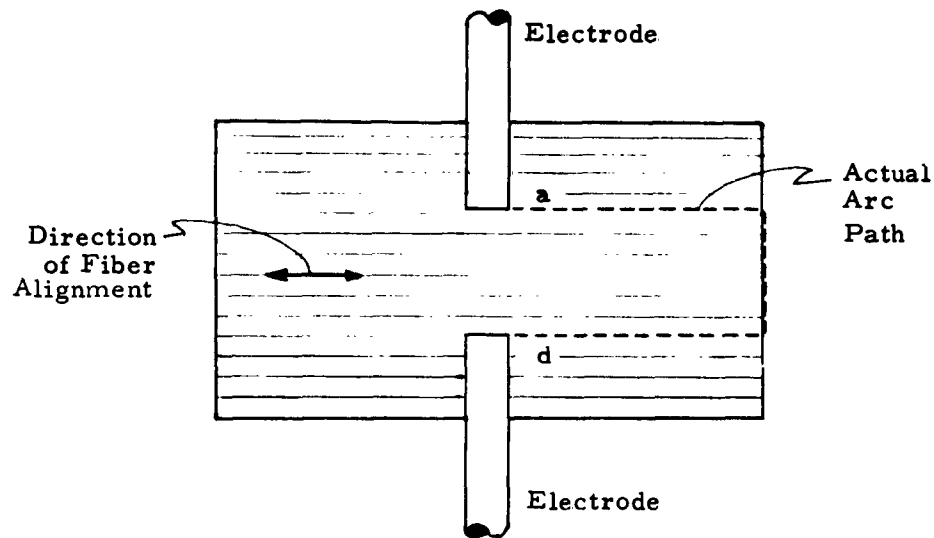


Fig. III-20 Dielectric Strength Electrodes with Specimen for Measurement Transverse to Fibers in Place.

ended electrodes were not used due to the difficulty in measuring the end separation). The thickness of material between the bottoms of the holes in each dielectric strength specimen was determined by inserting and bottoming the electrode pins, applying a machinist's micrometer over the free ends of the pins, then subtracting the total pre-measured length of the pins. The dielectric strength samples were not dried. They were conditioned for 24 hours at ambient room humidity before measurement. Unfortunately, these first rods were too short and flashover occurred around path a-b-c-d as indicated in the sketch below instead of across the desired path a-d. It was evident that a longer specimen was required.



DIELECTRIC STRENGTH TEST SPECIMEN

The transverse dielectric strength specimen which finally proved successful was a long rod into which five sets of 0.125" diam., flat-bottomed electrode holes were drilled. The end holes were at least 1" in from the nearest rod end, and the inter-hole spacing was also 1". These 1" spacings were sufficient to prevent flashover lengthwise of the rod. The spacing between the bottoms of the holes of each pair was maintained at about 0.10", so that these tests were made on approximately this thickness of material.

To prevent flashover in the plane perpendicular to the longest rod axis, a special jig, shown schematically with specimen in place in Fig. III-21, was constructed to increase the flashover path length in this plane. In this jig the 7" specimen was clamped with the electrode holes vertically disposed between two 1" wide Lucite strips, with vinyl tape gaskets between the Lucite

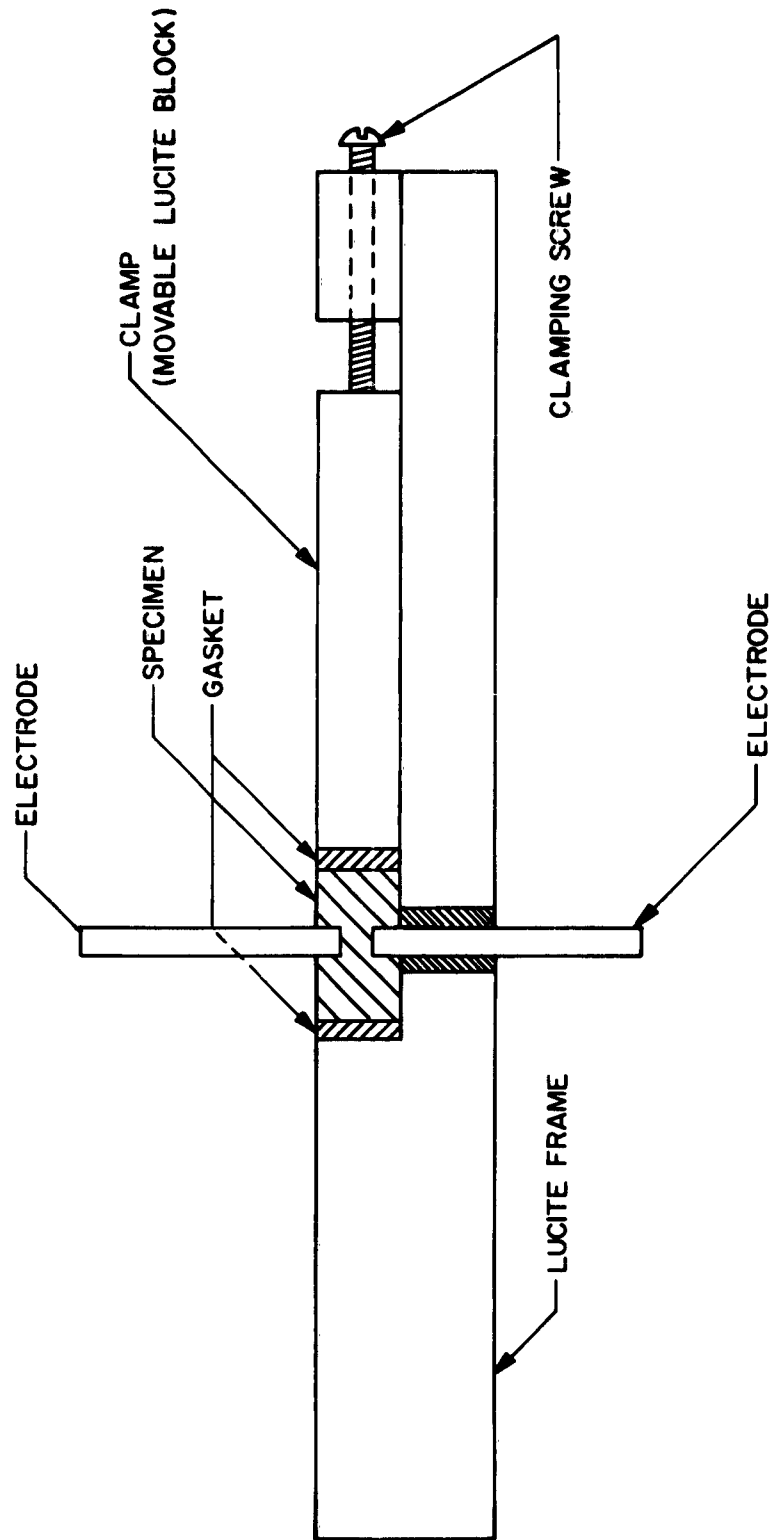


Fig. III-21 Schematic Cross Section of Epoxy-Glass Specimen in Transverse Dielectric Strength Test Fixture.

and the 7" x 14" sides of the specimen. Since these strips were, like the specimens, also about 1/4" thick, they provided an extension of the creepage path on each side amounting to 2 1/4". Tight clamping which produced compression of the vinyl gaskets, prevented creepage through the interface between specimen and the extension strips. The clamp was constructed of Lucite and was provided with drilled holes for the passage of the lower electrode into the lower electrode hole.

3. Instrumentation

a. Dielectric constant and dissipation factor at 1 kilocycle

These measurements were made with a General Radio Type 716 CR Bridge fed by a General Radio 1210C Oscillator. A General Radio Type 1232A Null Detector was used to indicate bridge balance.

b. Dielectric constant and dissipation factor at 1 megacycle

These measurements were made with a Wayne-Kerr Type 601 Radio Frequency Bridge powered by a General Radio Type 1330A oscillator. A communications receiver was used as an audible-type null detector.

c. D-C insulation resistance

For these measurements, a Keithley Model 240 Regulated High Voltage Supply gave 400 volts ($\pm 1\%$); a Keithley Model 410 Micro-microammeter was used to measure current and the resistance was calculated from Ohm's Law.

d. Dielectric strength

For these measurements, A General Electric Cat 153x355 60-cycle 2 KVA Test Set was used to obtain dielectric breakdowns. This set is equipped to give a motor-driven 500 volts per second rate of voltage rise. The dielectric strength was calculated from the relation

$$\text{Dielectric Strength} = \frac{\text{Dielectric Breakdown Potential (Volts)}}{\text{Thickness (Mils)}}$$

4. Test procedure

So far as the rod-like raw material would permit, the measurement procedures used follow these standard test methods for electrical properties:

Dielectric Constant and Dissipation Factor - ASTM D 150-54T
Insulation Resistance - ASTM D 257-58
Dielectric Strength - ASTM D 149-59

Each sample was subjected to the following sequential procedure:

1. Drying and cooling to room temperature.
2. Attachment of foil electrodes.
3. Measurement of "dry" insulation resistance parallel and transverse to fibers.
4. Measurement of "dry" dielectric constant and dissipation factor at 1 megacycle, parallel and transverse to fibers.
5. Measurement of "dry" insulation resistance parallel and transverse to fibers.
6. Removal from desiccator and conditioning for 24 hours at ambient room temperature and humidity.
7. Measurement of dielectric constant and dissipation factor at 1 kilocycle and ambient humidity parallel and transverse to fibers.
8. Measurement of dielectric constant and dissipation factor at 1 megacycle and ambient humidity parallel and transverse to fibers.
9. Measurement of dielectric strength at ambient humidity parallel and transverse to fibers on each of 5 (five) specimens.

5. Results

The results from measurement of all ten samples are tabulated in Table III-7 through Table III-10. The results have also been plotted as a function of α (the ratio of inside to outside fiber diameter) for the following fiber diameters: 0.00250", 0.00200", 0.00150" and 0.00100".

a. Dielectric constant (ϵ') (see Figs. III-22 through 25)

The decrease in dielectric constant as α increases is evident from the curves and can be attributed to the greater proportion of air in the samples made from higher α fibers. The difference between the 1 kc values for ϵ' of the specimens "dry" and at 50% RH is small and suggests moderate moisture pickup, probably on the outer surfaces, since the solid fiber specimens change much like the hollow fiber ones. The 1 mc values of ϵ' are generally lower than the 1 kc values although the curves maintain the same general shapes and slopes. These 1 mc values show only negligible differences between the "dry" and 50% RH values.

TABLE III-7

DIELECTRIC CONSTANT AND DISSIPATION FACTOR AT KILOCYCLE

Sample	Conditioning	Dielectric Constant		Dissipation Factor	
		Parallel	Transverse	Parallel	Transverse
A	Dry	8.2	7.9	.002	.002
B	Dry	6.7	6.6	.001	.002
C	Dry	5.7	5.3	.001	.001
D	Dry	8.5	8.0	.002	.002
E	Dry	5.5	4.7	.003	.003
G	Dry	6.7	5.8	.001	.002
H	Dry	8.8	7.5	.001	.001
I	Dry	6.9	5.4	.002	.003
J	Dry	7.9	7.5	.002	.001
K	Dry	5.9	5.4	.004	.003
A	At 40-50% RH*	7.4	8.0	.002	.001
B	At 40-50% RH	6.8	6.5	.002	.002
C	At 40-50% RH	5.9	5.1	.001	.002
D	At 40-50% RH	8.3	7.9	.002	.002
E	At 40-50% RH	5.8	4.9	.002	.003
G	At 40-50% RH	6.6	5.8	.001	.004
H	At 40-50% RH	7.8	7.4	.002	.001
I	At 40-50% RH	6.9	5.4	.002	.003
J	At 40-50% RH	8.0	7.6	.001	.001
K	At 40-50% RH	5.9	5.5	.001	.001

* Relative Humidity

TABLE III-8

DIELECTRIC CONSTANT AND DISSIPATION FACTOR AT 1 MEGACYCLE

Sample	Conditioning	Dielectric Constant		Dissipation Factor	
		Parallel	Transverse	Parallel	Transverse
A	Dry	5.9	6.5	.0062	.0061
B	Dry	5.1	5.3	.0066	.0078
C	Dry	4.3	3.8	.0068	.0051
D	Dry	5.5	6.1	.0070	.0082
E	Dry	4.0	3.4	.0075	.0066
G	Dry	5.5	4.7	.0098	.0098
H	Dry	6.6	6.2	.0065	.0069
I	Dry	5.7	4.5	.0088	.0078
J	Dry	6.7	6.3	.0060	.0072
K	Dry	4.8	4.2	.0067	.0071
A	At 40-50% RH*	5.9	6.1	.0062	.0084
B	At 40-50% RH	5.1	5.3	.0066	.0073
C	At 40-50% RH	4.5	3.9	.0066	.0053
D	At 40-50% RH	6.6	6.2	.0089	.0087
E	At 40-50% RH	4.0	3.5	.0068	.0054
G	At 40-50% RH	5.3	4.8	.024	.011
H	At 40-50% RH	6.5	6.2	.0067	.0070
I	At 40-50% RH	5.7	4.3	.0087	.012
J	At 40-50% RH	6.6	6.3	.0067	.007
K	At 40-50% RH	4.8	4.3	.0067	.0068

* Relative Humidity

TABLE III-9

D-C INSULATION RESISTANCE

Sample	Conditioning	(in ohm-cm*)	
		Parallel	Transverse
A	Dry	8.6×10^{14}	1.9×10^{15}
B	Dry	7.5×10^{14}	1.9×10^{15}
C	Dry	7.0×10^{14}	8.5×10^{14}
C	Dry	8.9×10^{14}	1.5×10^{15}
E	Dry	5.4×10^{14}	7.9×10^{14}
G	Dry	1.7×10^{15}	4.1×10^{14}
H	Dry	7.9×10^{14}	1.5×10^{15}
I	Dry	1.4×10^{15}	1.7×10^{15}
J	Dry	2.3×10^{14}	2.4×10^{14}
K	Dry	2.6×10^{15}	2.6×10^{15}
A	At 40-50% RH**	2.6×10^{12}	7.8×10^{13}
B	At 40-50% RH	7.8×10^{13}	2.0×10^{15}
C	At 40-50% RH	7.0×10^{14}	5.9×10^{14}
D	At 40-50% RH	4.4×10^{11}	8.9×10^{11}
E	At 40-50% RH	1.3×10^{15}	1.5×10^{15}
G	At 40-50% RH	2.5×10^{15}	3.9×10^{14}
H	At 40-50% RH	6.5×10^{15}	1.5×10^{15}
I	At 40-50% RH	1.9×10^{15}	1.9×10^{15}
J	At 40-50% RH	5.2×10^{15}	2.4×10^{14}
K	At 40-50% RH	6.2×10^{14}	4.0×10^{14}

* This is a combined volume and surface resistivity. Because of the small specimen size, guard electrodes which permit the separation of these two types of resistivity could not be used.

** Relative Humidity

TABLE III-10

60 CYCLE SHORT TIME
DIELECTRIC STRENGTH

Sample	<u>(volts/mil)</u>	
	Parallel	Transverse
A	104	490*
B	42	290
C	45	420*
D	29	500*
E	36	200
G	45	300
H	37	430*
I	45	180
J	63	480*
K	50	330

* Tested under oil; all other values obtained in air.

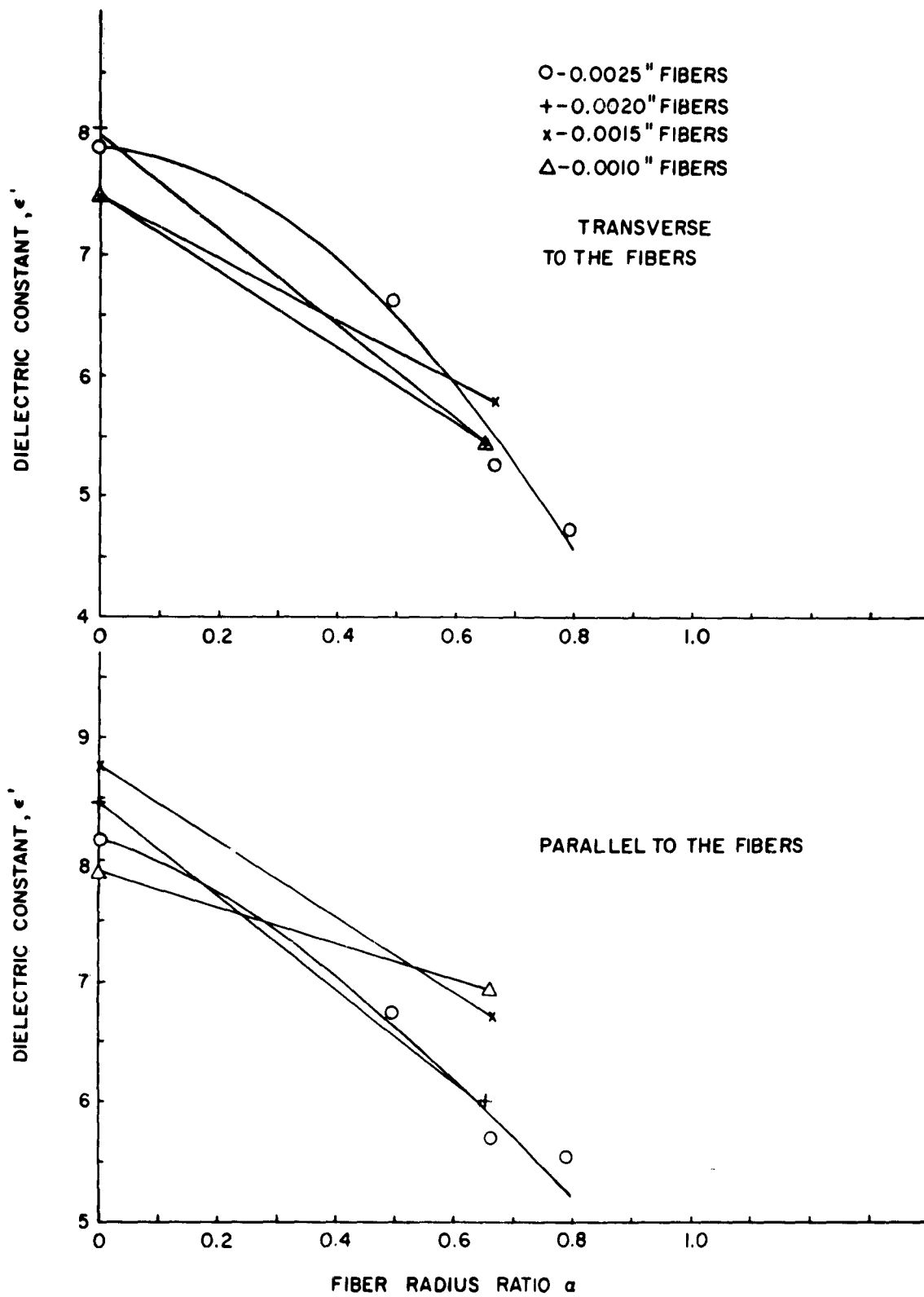


Fig. III-22 Dielectric Constant at 25°C.

Conditioning - Dry, Frequency - 1 kc

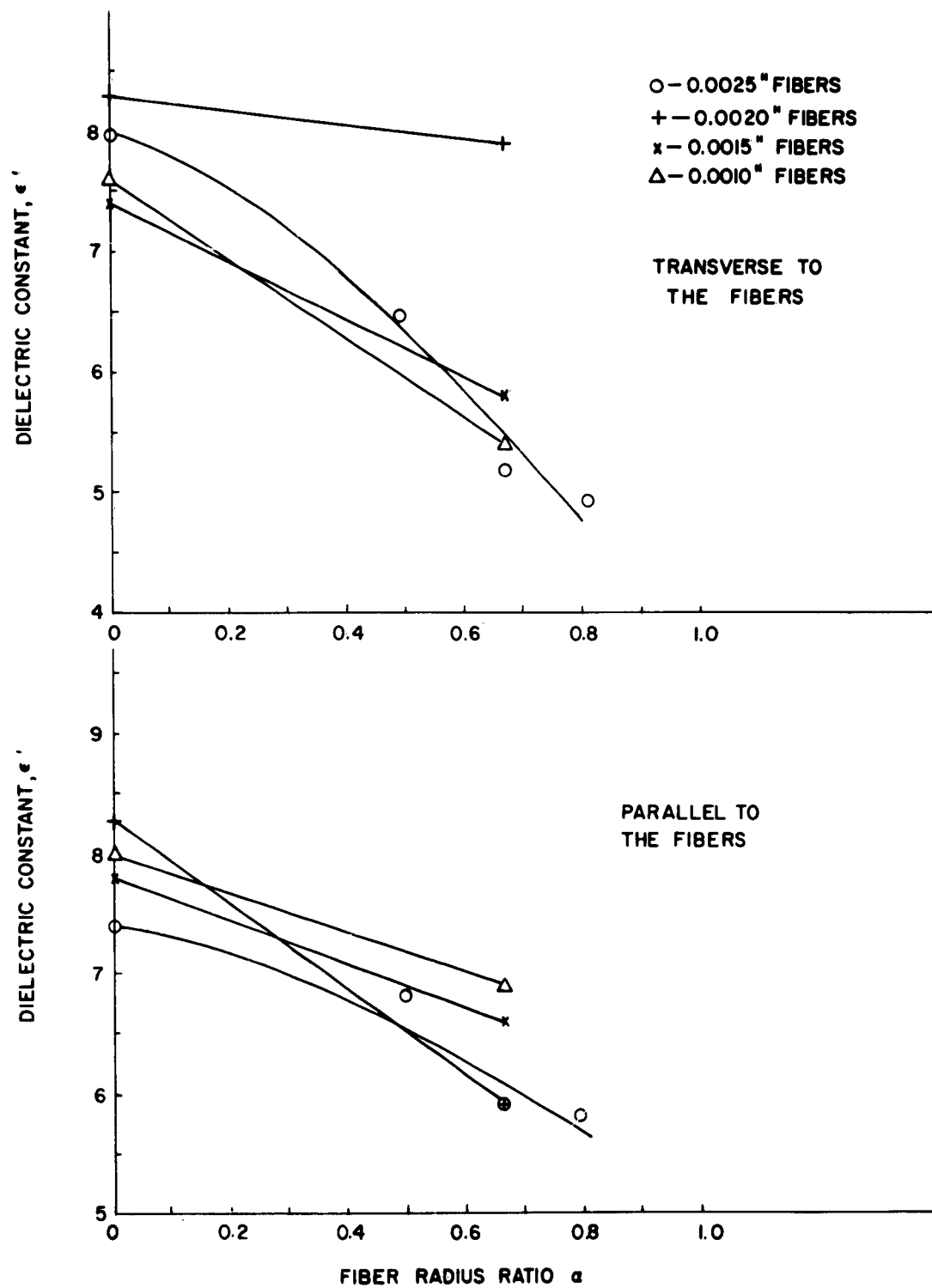


Fig. III-23 Dielectric Constant at 25°C.

Conditioning - at 50% Relative Humidity, Frequency - 1 kc

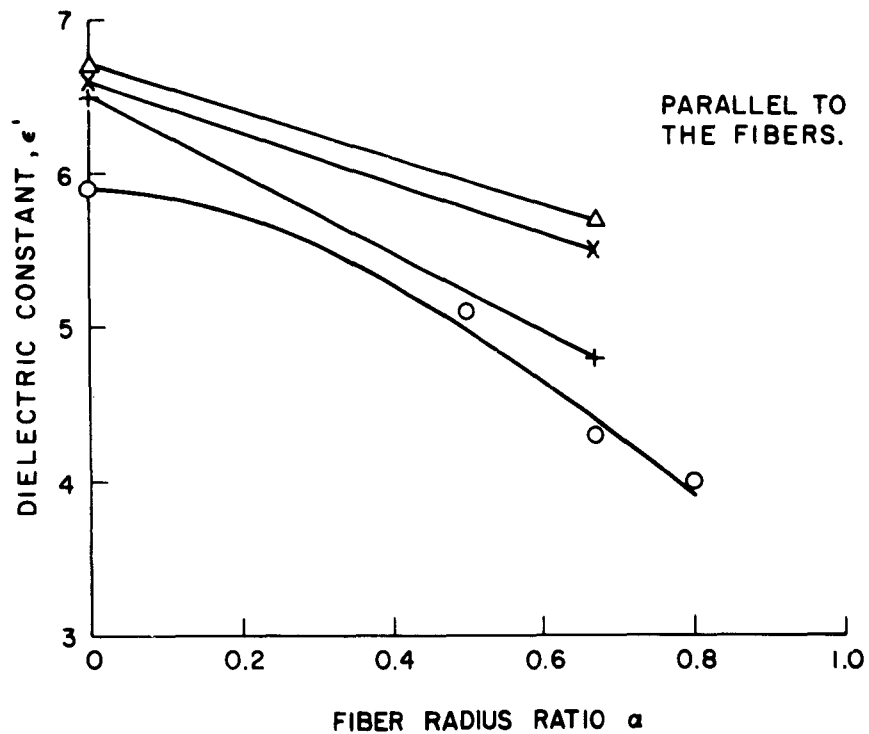
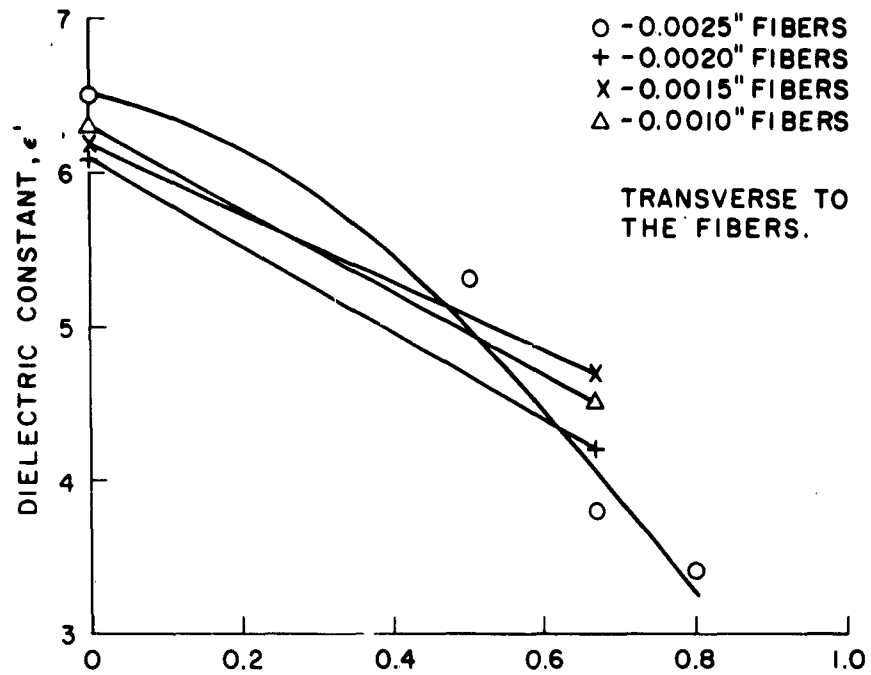


Fig. III-24 Dielectric Constant at 25°C.

Conditioning - Dry, Frequency - 1 mc

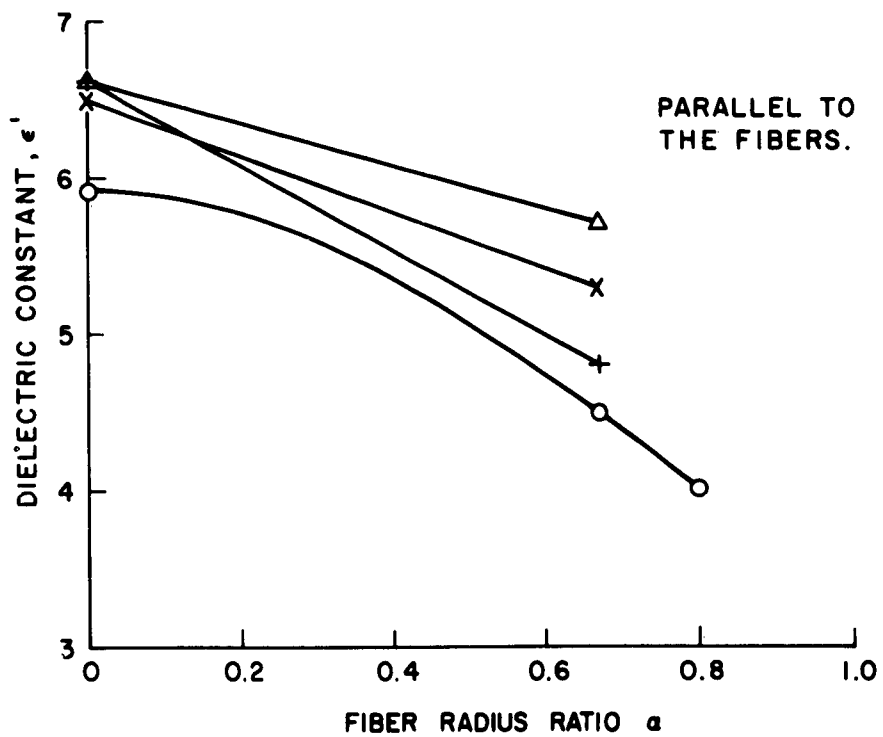
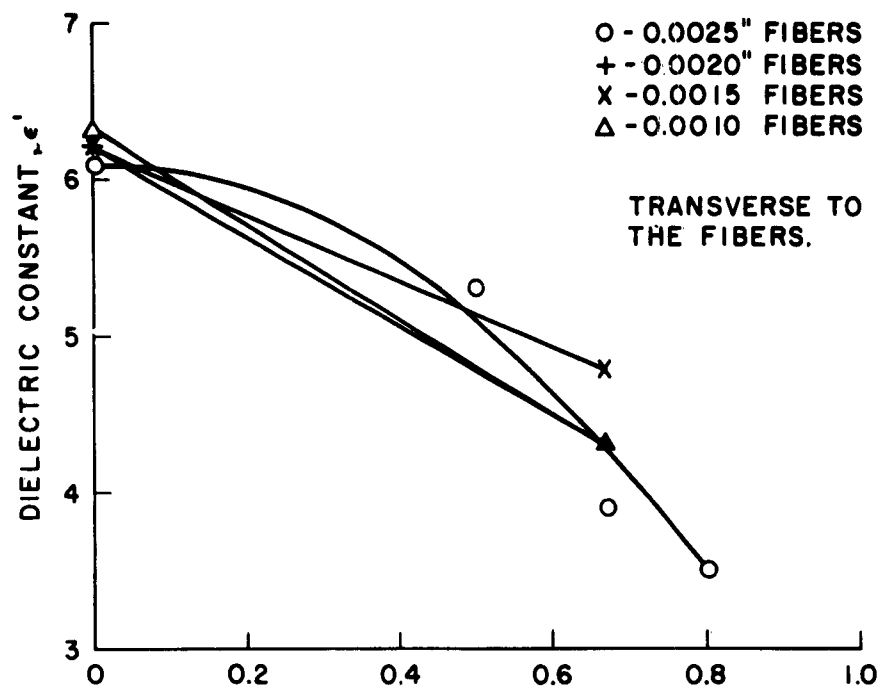


Fig. III-25 Dielectric Constant at 25°C.

Conditioning - at 50% Relative Humidity, Frequency - 1 mc

b. Dissipation factor (ϵ'') (see Figs. III-26 through 29)

These curves have been plotted to a scale which does not accentuate non-significant variations. For some unknown reason there is a slight tendency for the values to increase as α increases; however, the trend is not conclusive. Variations could easily be caused by minor differences in resin content, cure cycle, and the like. The same is true for the effects of humidity; no significant effects are evident. There is, however, a very pronounced correlation of ϵ'' with frequency. Values at 1 mc are considerably higher than those at 1 kc.

c. D-C insulation resistivity (ρ) (see Figs. III-30 through 33)

In interpreting these curves it should be remembered that, in insulation resistance measurements, only changes of a decade or more can be considered significant. With this in mind, the "dry" values show no conclusive trend when α is varied. At 50% RH the variations of ρ with α no longer follow a consistent pattern: the 0.0025" and 0.0020" samples show increases in ρ parallel to the fibers as α increases, while the other two sizes show insignificant changes. For the transverse samples the 0.0025", 0.0020", and 0.0010" samples increase in ρ as α increases while the 0.0015" sample decreases.

It is evident that the anomalies occur not only in the hollow fiber specimens, but in the solid fiber one. Noting that the value of ρ for glass is very high (about 10^{16} ohm/cm) leads one to believe that the unusual behavior is caused either by the resin or by the surface contamination of the specimen. Subsequent investigations should employ a different type of specimen to separate these effects.

d. Dielectric strength (D.S.) (see Figs. III-34 and 35)

The parallel D.S. values indicate that breakdown in this direction takes place along an internal creepage path containing air pockets. This is the characteristic of inhomogeneities such as cavities or completely impregnated regions. While low creepage breakdowns might be expected to take place along the hollow fibers, the fact that the solid fiber samples also broke down at or below 100 volts/mil indicates that axially oriented voids exist in the composites.

The transverse dielectric strength curves show a more consistent behavior. D.S. tends to decrease with increasing α as might be expected from the increase in air content at the higher α values. The consistently high transverse D.S. values for solid fiber specimens suggest that the axially oriented voids discussed above must be of very minute transverse cross-section. This supports the conclusion that these voids are oriented parallel with the fibers.

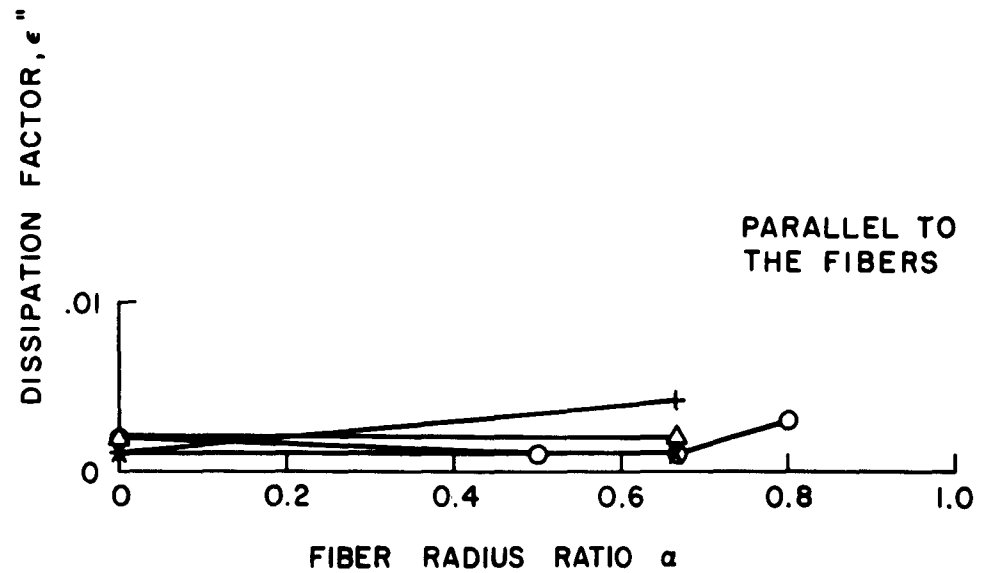
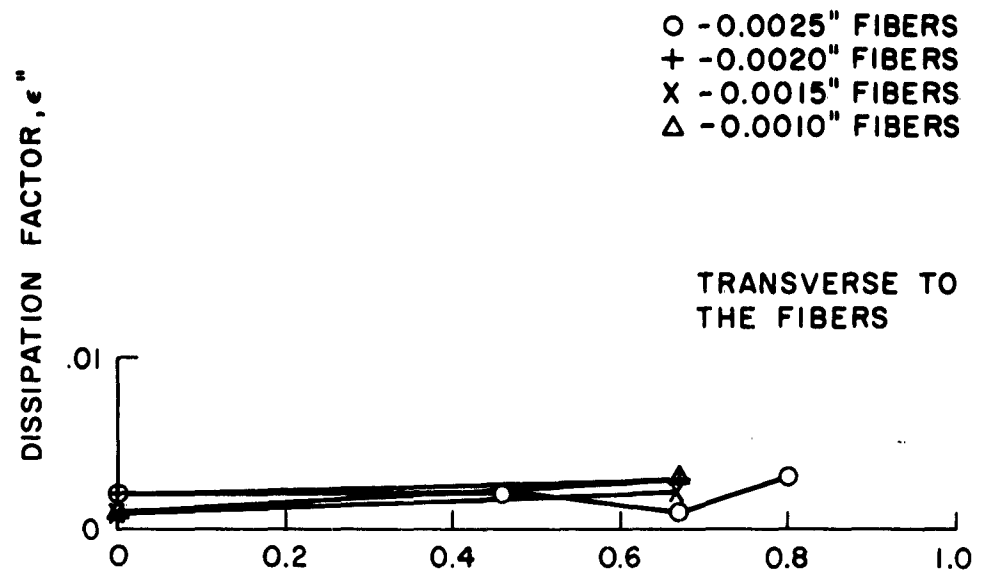


Fig. III-26 Dissipation Factor at 25°C.

Conditioning - Dry, Frequency - 1 kc

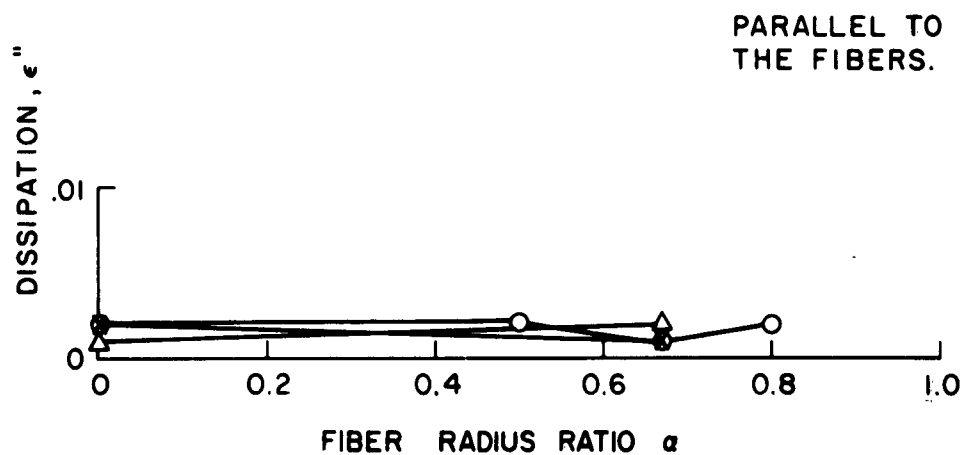
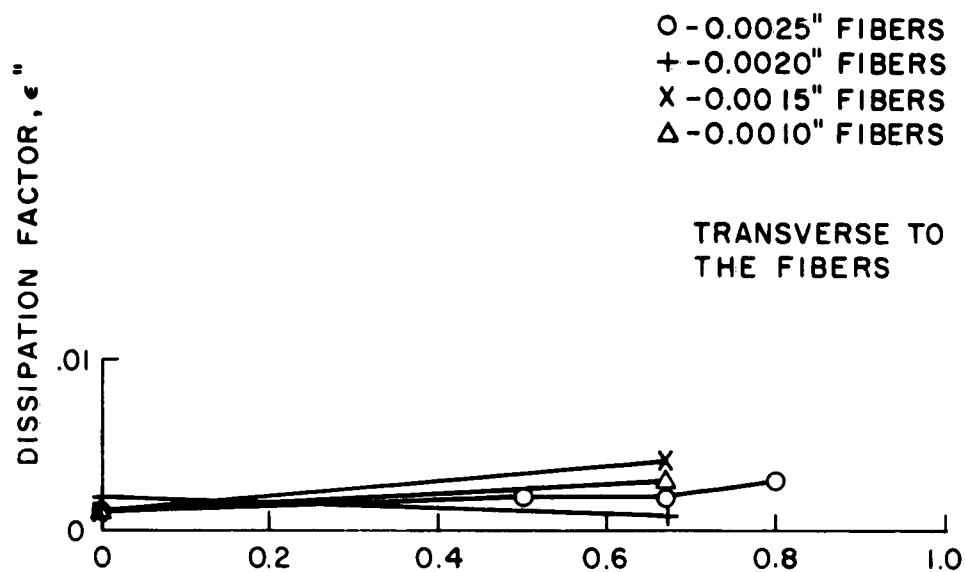


Fig. III-27 Dissipation Factor at 25°C.

Conditioning - at 50% Relative Humidity, Frequency - 1 kc

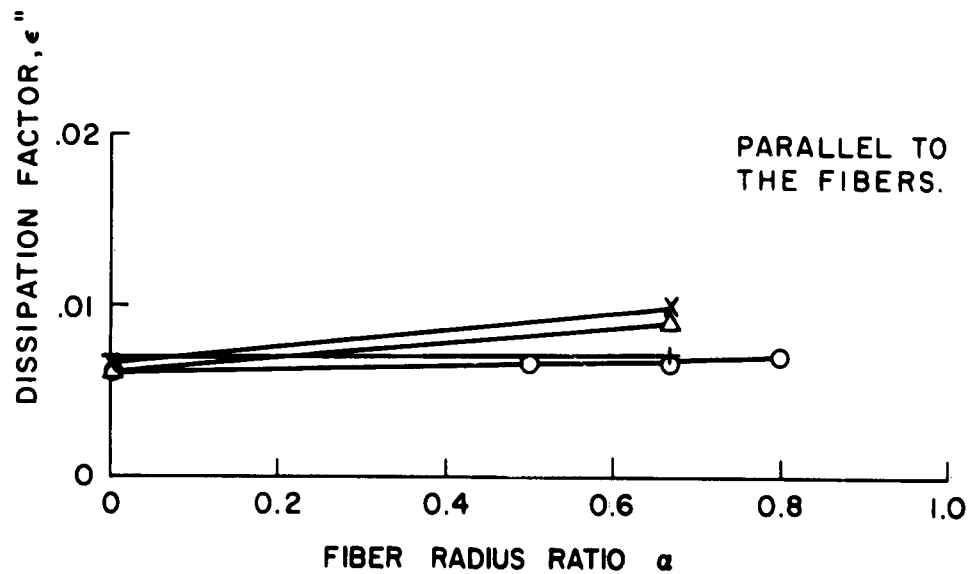
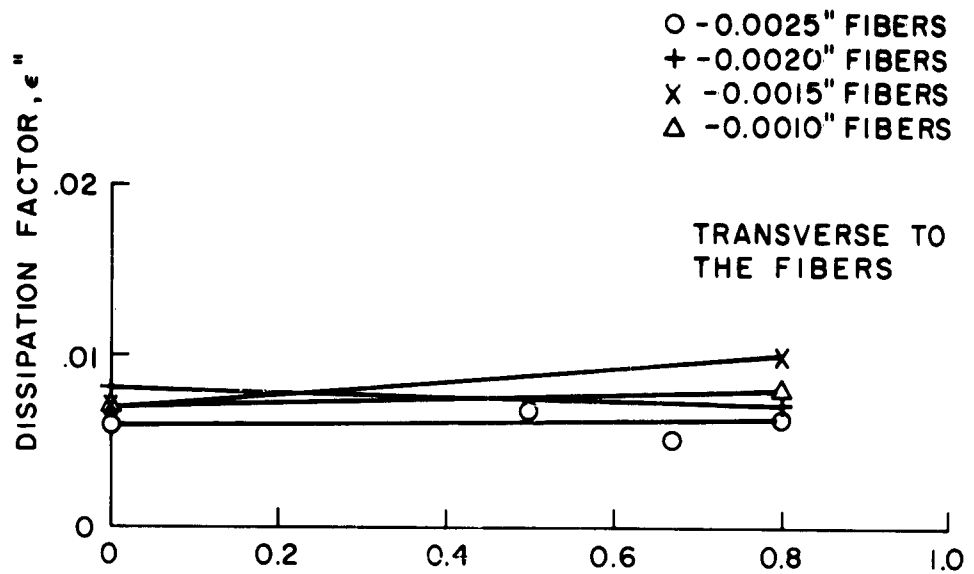


Fig. III-28 Dissipation Factor at 25°C.

Conditioning - Dry, Frequency - 1 mc

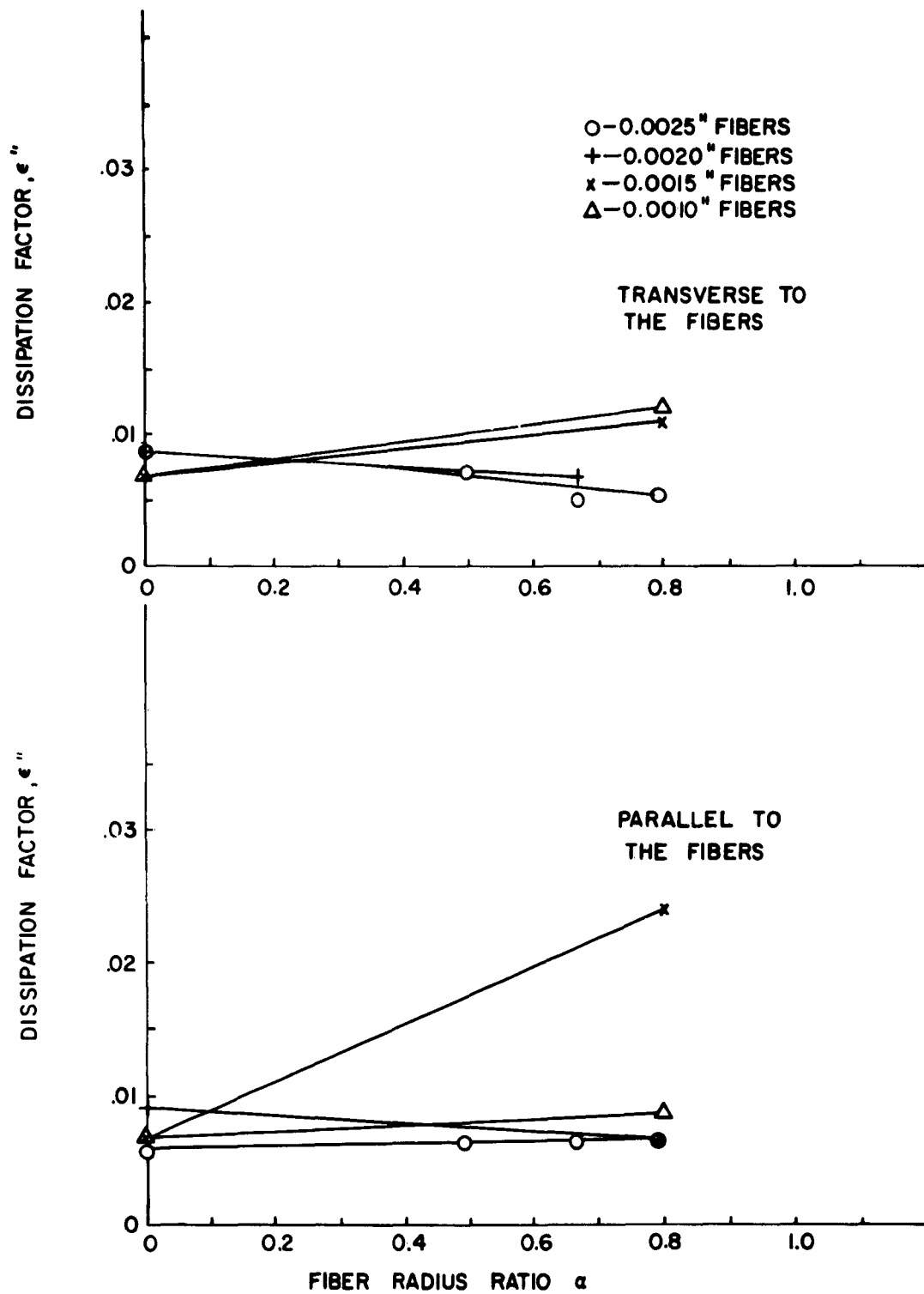


Fig. III-29 Dissipation Factor at 25°C.

Conditioning - at 50% Relative Humidity, Frequency - 1 mc

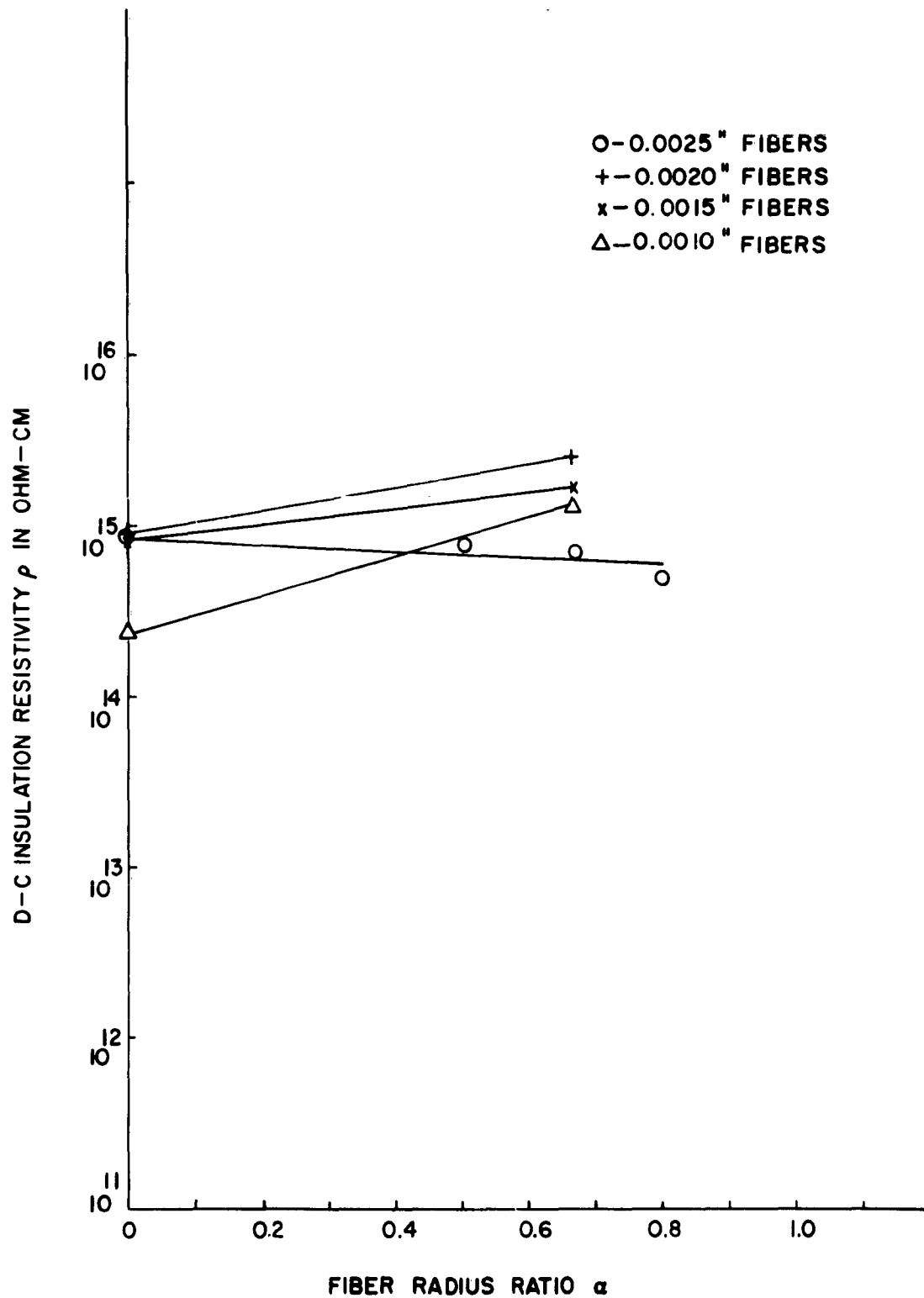


Fig. III-30 D-C Insulation Resistance at 25°C.

Conditioning - Dry, Direction - Parallel

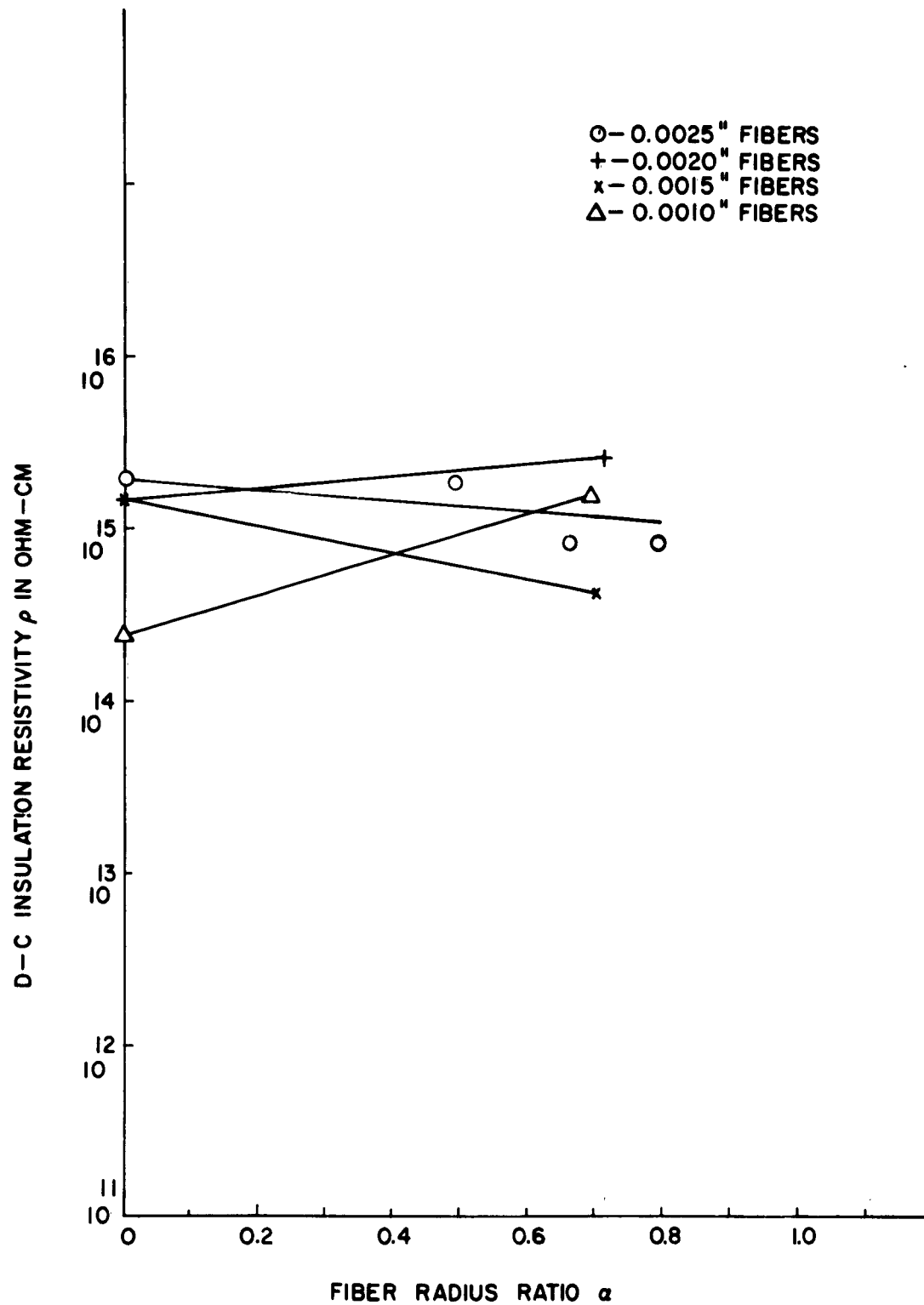


Fig. III-31 D-C Insulation Resistance at 25°C.

Conditioning - Dry, Direction - Transverse

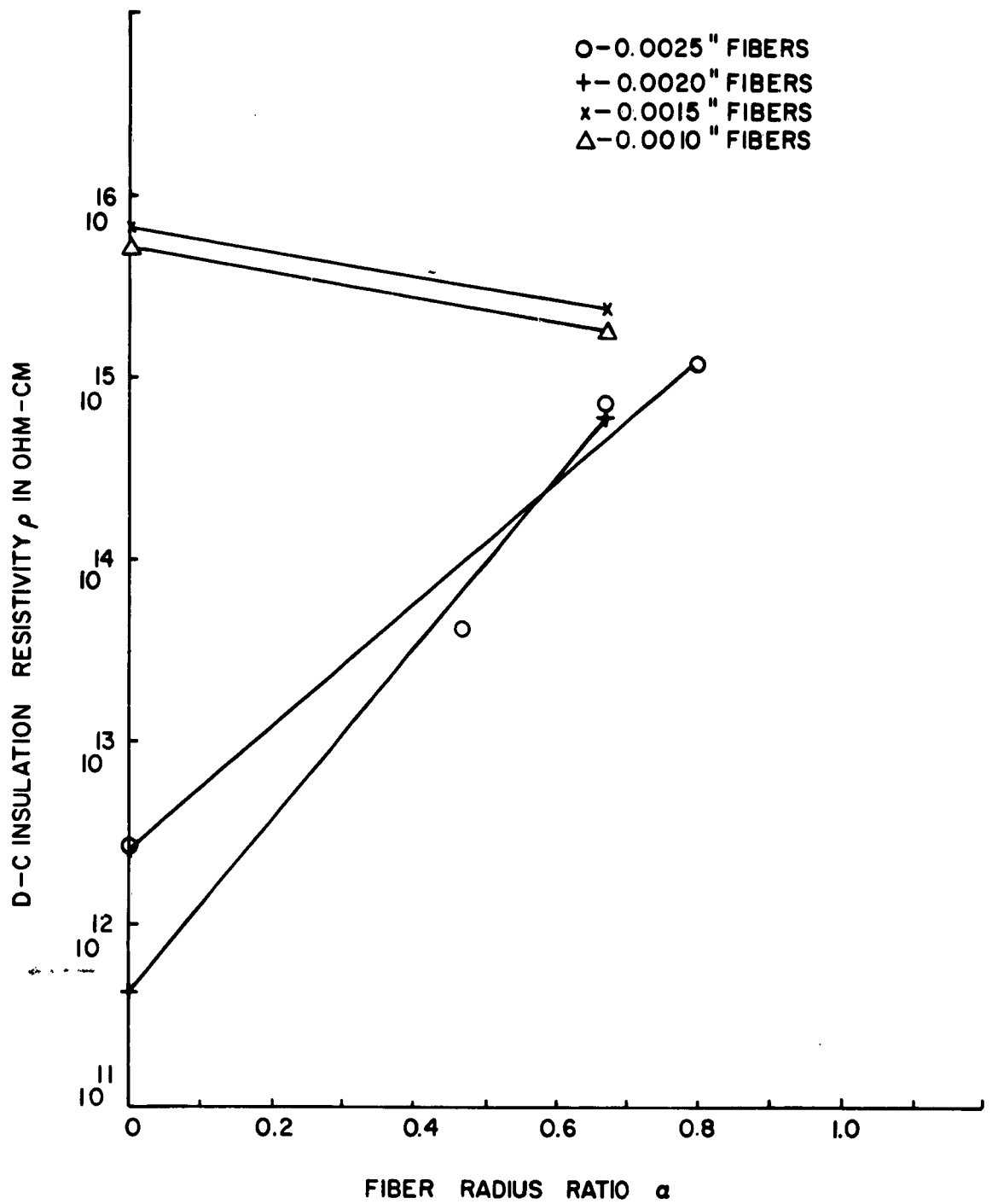


Fig. III-32 D-C Insulation Resistance at 25°C.

Conditioning - at 50% Relative Humidity, Direction - Parallel

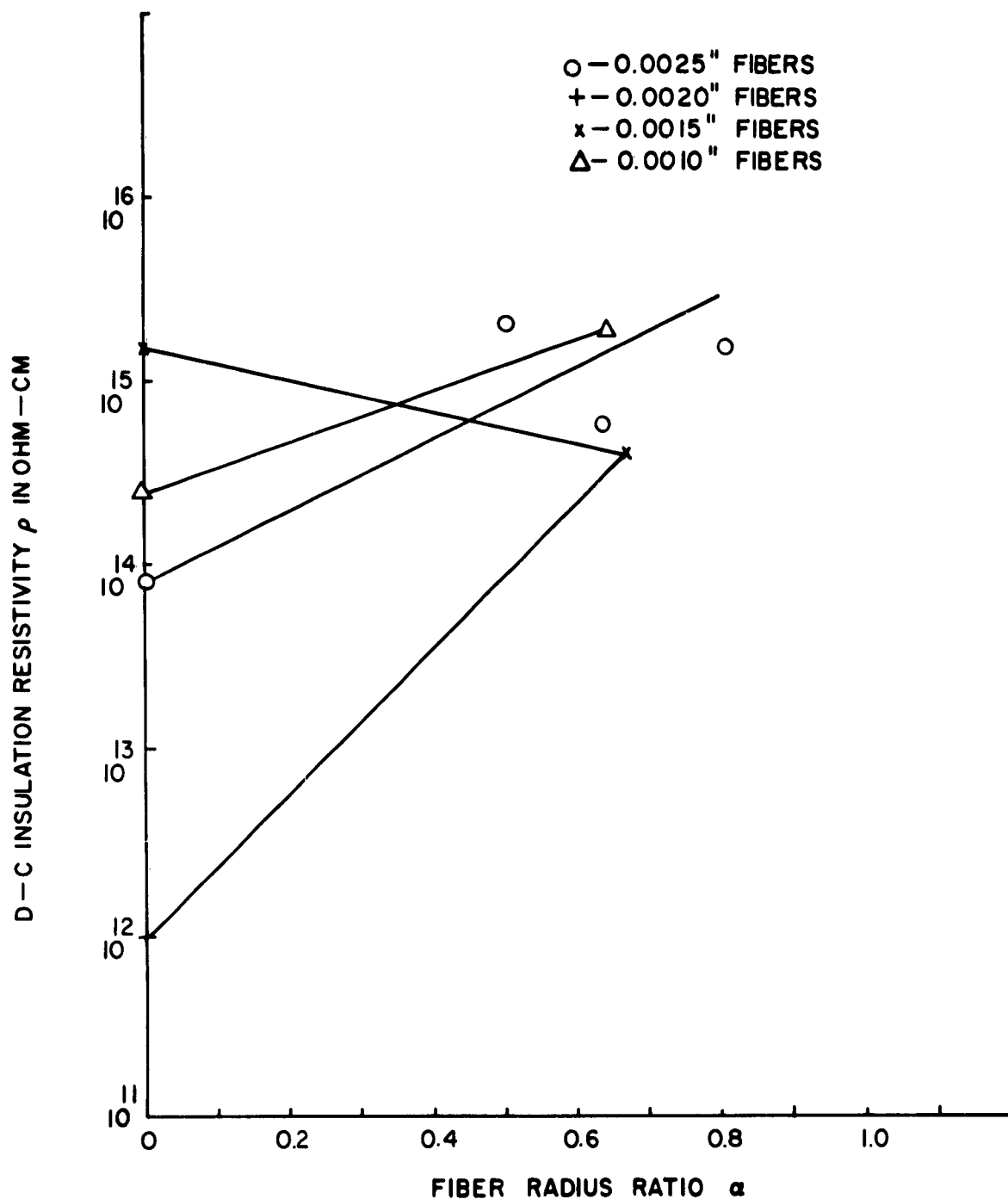


Fig. III-33 D-C Insulation Resistance at 25°C.

Conditioning - at 50% Relative Humidity, Direction - Transverse

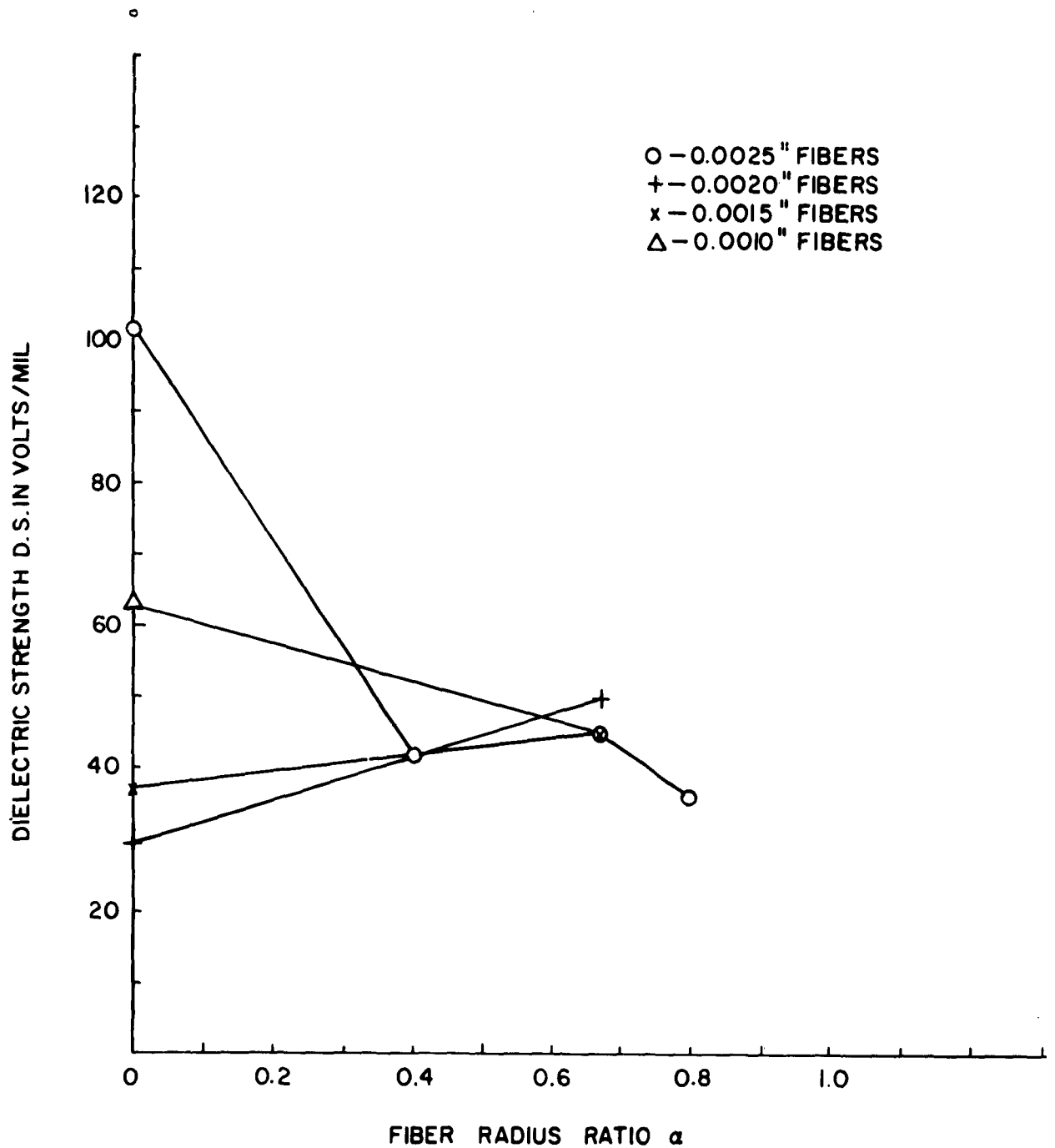


Fig. III-34 60 Cycle Short Time Dielectric Strength at 25°C.

Conditioning - at 50% Relative Humidity, Direction - Parallel

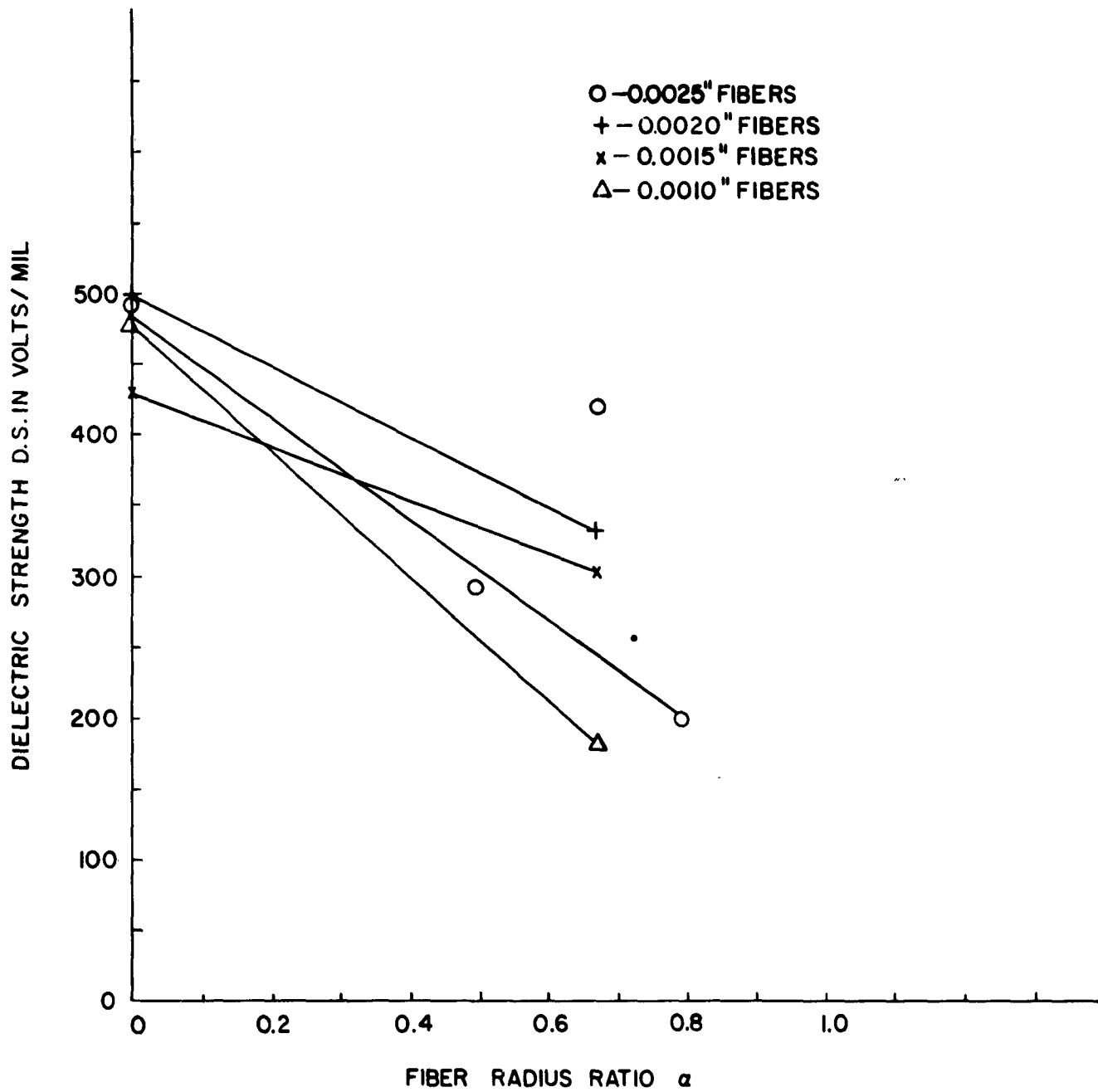


Fig. III-35 60 Cycle Short Time Dielectric Strength at 25°C.

Conditioning - at 50% Relative Humidity, Direction - Transverse

IV. Analysis

Prediction of the structural performance of a composite material requires the evaluation of the strength and stiffness of the material under various types of loads. However, a composite material subjected to even simple external loads has a complex internal state of stress which is not susceptible to exact analysis. In order to evaluate the performance of such materials, approximate solutions for the internal stresses must be utilized. When estimates of the internal stress field are available, the external behavior can be readily derived.

For certain loading conditions, the material must be treated as an inhomogeneous composite, to investigate the internal stress field. Thus, for example, the definition of ultimate tensile strength requires an understanding of the stress distribution in the two constituents, including all localized stress concentrations, so that the mode of internal failure and the quantitative failure level can be predicted. The difficulty of this problem implies a degree of inaccuracy of the results which may well limit their value to qualitative comparisons of the various potential constituents and geometries.

For other loading conditions the material may be treated as a quasi-homogeneous material having certain average or effective properties. Thus, for example, the deflection under a uniaxial load can be related to that load by the use of an effective modulus of elasticity. This effective material approach is of value for the determination of such things as the acoustic impedance under large (relative to the characteristic dimension of the inhomogeneities) wavelength excitations, behavior under hydrostatic pressure, fiber stability evaluation, as well as for the various elastic constants of the composite material. These properties are, in effect, integrations of the internal stress field characteristics and thus, it appears that the errors are likely to be smaller and the results more suitable for quantitative analysis.

The analytical work described herein is largely concerned with the latter type of structural behavior. The analyses presented treat the major overall structural characteristics of hollow glass fiber composites, namely, the elastic constants of the material. In section A, below, the evaluation of these elastic constants is described. Determination of certain aspects of the internal stress distribution are inherent in these studies and are also discussed in that section. The significance of certain of the results is apparent only when used in a structural analysis. The results of such static analyses are described in section B. Further the dynamic structural behavior is considered in section C.

A. Material Analysis

The material treated consists of an epoxy matrix reinforced with straight and parallel hollow glass cylindrical fibers oriented in one or two directions. For the case of uniaxial stiffening, the effective elastic constants are those of a transversely isotropic medium having five principal constants. The work herein has provided estimates of, or bounds to, four of these constants. In the present notation, the studies have defined the axial modulus, E_1 , the transverse modulus, E_2 , and the Poisson's ratios associated with axial loading, ν_{21} , and with transverse loading, ν_{23} . The shear rigidity in the longitudinal plane, G_{12} , has been the subject of some study and certain approximations have been obtained. However, a complete model does not exist and G_{12} remains undefined and is a required output of future research. The remaining elastic constants (including E_3 , ν_{23} , ν_{12} , ν_{31} and G_{23}) are defined as functions of the aforementioned known constants and are thus available.

The model used to define the elastic constants considers the material to be composed of a series of composite tubes containing a hollow glass fiber surrounded by a coaxial tube of binder material with volume fractions of the constituents equal to the average volume fractions found in the composite material. The tubes are considered to vary in size from some arbitrary maximum value, which is small with respect to a composite material specimen being considered, down to zero diameter so that the entire material may be comprised of an assembly of such cylinders. When proper consideration is given to the lateral boundary conditions the evaluation of the behavior of a single such tube is adequate to define the behavior of the composite. This is discussed further in the description of the individual elastic constants.

The material is anisotropic and the fiber and matrix properties have different relative effects upon the various elastic constants. Any perturbation of the properties of a given constituent (for example a change in the fiber hollowness) will have a total effect which can only be evaluated by considering a structural application. For example, the results of the computation of the elastic constants of a biaxially reinforced plate show wide variations of Young's modulus as a function of loading direction and fiber orientation and the optimum orientation cannot be defined until the structural environment is specified. In part 2 below, plate buckling is treated as a typical environment and optimum orientation is then readily determined.

Further the effects of density as well as elastic properties must be considered and thus several structural environments are evaluated from a structural efficiency point of view.

1. Longitudinal elastic constants

The longitudinal elastic constants (those defined by material displacements under a load parallel to the direction of fiber orientation) are determined by applying an axial displacement to the material. Each of the previously described composite cylinders which are considered to comprise this material will have a radial displacement at the outer surface which is proportional to the outer radius. The resulting displacement field is thus a compatible one and the behavior of the composite is defined by the behavior of a single composite cylinder containing one hollow glass fiber.

Young's modulus

The inside radius of the fiber, r_o , and the radius of the fiber-binder interface, r_f , and the outer radius of the binder, r_b , define the geometry. An average axial displacement, $\bar{\epsilon}_z$, requires an average stress over the end face, $\bar{\sigma}_z$, which defines the axial modulus, E_1 , namely:

$$E_1 = \frac{\bar{\sigma}_z}{\bar{\epsilon}_z} \quad (1)$$

The radial displacement, u , for this problem is (see, for example, ref. 16):

$$u_f = \frac{1-\nu_f}{E_f} \left(\frac{p r_f^2 r}{r_f^2 - r_o^2} \right) + \frac{1+\nu_f}{r E_f} \left(\frac{p r_o^2 r_f^2}{r_f^2 - r_o^2} \right) - \nu_f r \frac{\sigma_{zf}}{E_f} \quad (2)$$

$$\text{for } r_o \leq r \leq r_f$$

$$u_b = \frac{1-\nu_b}{E_b} \left(\frac{p r_f^2 r}{r_b^2 - r_f^2} \right) - \frac{1+\nu_b}{r E_b} \left(\frac{p r_f^2 r_b^2}{r_b^2 - r_f^2} \right) - \nu_b r \frac{\sigma_{zb}}{E_b} \quad (3)$$

$$\text{for } r_f \leq r \leq r_b$$

where p equals the radial stress at the interface between the fiber and binder.

σ_z equals axial stress (which is constant over each material).

The axial strain is constant and the axial displacement is thus linear. The axial strain is:

$$\epsilon_{zf} = \frac{\sigma_{zf}}{E_f} - \frac{2\nu_f}{E_f} \left(\frac{p r_f^2}{r_f^2 - r_0^2} \right) \quad (4)$$

for $r_0 \leq r \leq r_f$

$$\epsilon_{zb} = \frac{\sigma_{zb}}{E_b} + \frac{2\nu_b}{E_b} \left(\frac{p r_f^2}{r_b^2 - r_f^2} \right) \quad (5)$$

for $r_f \leq r \leq r_b$

From the definition of $\bar{\sigma}_z$:

$$\bar{\sigma}_z = \nu_f \sigma_{zf} + \nu_b \sigma_{zb} \quad (6)$$

The boundary condition requires that

$$\epsilon_{zf} = \epsilon_{zb} = \bar{\epsilon} \quad (7)$$

Compatibility requires that

$$u_f(r_f) = u_b(r_f) \quad (8)$$

Substitution of eqs. (4), (5) and (6) into (7) and of eqs. (2), (3) and (6) into (8) yields:

$$2p \left[\frac{\nu_b}{E_b} \left(\frac{r_f^2}{r_b^2 - r_f^2} \right) + \frac{\nu_f}{E_f} \left(\frac{r_f^2}{r_f^2 - r_0^2} \right) \right] + \sigma_{zb} \left[\frac{1}{E_b} + \frac{1}{E_f} \left(\frac{\nu_b}{\nu_f} \right) \right] = \frac{\bar{\sigma}_z}{\nu_f E_f} \quad (9)$$

$$p \left[\frac{1}{E_f} \left(\frac{r_f^2 + r_0^2}{r_f^2 - r_0^2} - \nu_f \right) + \frac{1}{E_b} \left(\frac{r_b^2 + r_f^2}{r_b^2 - r_f^2} + \nu_b \right) \right] + \sigma_{zb} \left[\frac{\nu_b}{E_b} + \frac{\nu_f}{E_f} \left(\frac{\nu_b}{\nu_f} \right) \right] = \frac{\nu_f \bar{\sigma}_z}{\nu_f E_f} \quad (10)$$

The solution of these two simultaneous equations yields the two unknowns, p and σ_{zb} , as functions of $\bar{\sigma}_z$. When these are evaluated, equations (5) and (7) can be used to obtain $\bar{\sigma}_z$ as a function of $\bar{\epsilon}$. Eq. (1) will then define E_1 . The result is the following expression for effective modulus:

$$\frac{E_1}{E_{av}} = \frac{E_b (A_1 - A_3 B) + E_f (A_2 - A_4 B')}{E_b (A_1 - A_3) + E_f (A_2 - A_4)} \quad (11)$$

where

$$A_1 = \frac{\nu_f + 2\nu_v}{\nu_f} - \nu_f$$

$$A_2 = \frac{1 + \nu_v + \nu_f}{\nu_b} + \nu_b$$

$$A_3 = 2\nu_f^2 \left(\frac{\nu_f + \nu_v}{\nu_f} \right)$$

$$A_4 = 2\nu_b^2 \left(\frac{\nu_f + \nu_v}{\nu_b} \right)$$

$$B = \frac{\nu_b \nu_f E_f + \nu_f \nu_b E_b}{\nu_f (\nu_f E_f + \nu_b E_b)} = \frac{\nu_b}{\nu_f} B'$$

$$E_{av} = \nu_f E_f + \nu_b E_b$$

The result has been normalized with respect to the weighted average modulus, E_{av} . This latter quantity is the modulus obtained by neglecting Poisson's effects and assuming plane sections remain plane. Thus, it can be obtained from eq. (11) by setting $\nu_f = \nu_b = 0$, which yields:

$$E_1 = E_{av}$$

The same result is obtained for $\nu_f = \nu_b \neq 0$.

Poisson ratio effects:

The effect of non-zero Poisson ratios on the effective longitudinal modulus, E_1 , is evaluated by considering the following extreme numerical examples.

Consider: $\nu_v = 0$ $\nu_f = \nu_b = 0.5$

$$\text{Case I: } \nu_f = 0 \quad \nu_b = 0.4 \quad \frac{E_f}{E_b} = 20$$

$$\frac{E_1}{E_{av}} = 1.005$$

$$\text{Case II: } \nu_f = 0.4 \quad \nu_b = 0 \quad \frac{E_f}{E_b} = 20$$

$$\frac{E_1}{E_{av}} = 1.005$$

$$\text{Case III: } \nu_f = 0 \quad \nu_b = 0.4 \quad \frac{E_f}{E_b} = 1$$

$$\frac{E_1}{E_{av}} = 1.04$$

$$\text{Case IV: } \nu_f = 0.4 \quad \nu_b = 0 \quad \frac{E_f}{E_b} = 1$$

$$\frac{E_1}{E_{av}} = 1.09$$

The conclusion is that differing Poisson's ratio have a negligible effect on the axial modulus unless $\nu_f E_f$ and $\nu_b E_b$ are approximately equal, in which case the effect is small but perhaps not negligible.

Shear stress effects:

The above study treated boundary conditions of uniform axial displacement. Because of the symmetry of the structure, this resulted in a constant-strain displacement field. The effect of a constant axial stress boundary condition should be considered. Both of these effects introduce a load transfer between fiber and matrix. Since load is transferred between matrix and fiber by shear stresses, a study has been performed to evaluate the effect of shear stresses on the modulus. The model is as shown in Fig. IV-1 and consists of a fiber surrounded by a matrix which in turn is imbedded within another material. The fiber and matrix constitute an inclusion in the average material.

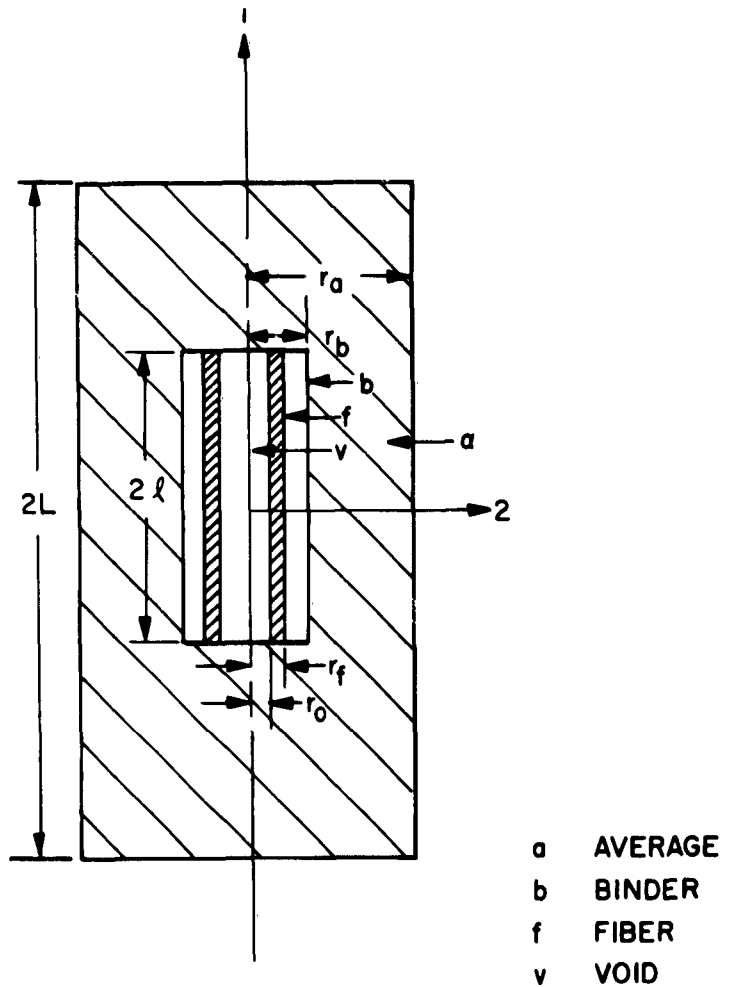


Fig. IV-1 Model for Determination of Effect of Shear Deformation on the Elastic Modulus of Uniaxially Stiffened Material.

The method of approach is to consider the model with a uniform stress applied to the end faces, and to determine the average longitudinal strain. The problem cannot be solved exactly and a shear lag type analysis is utilized herein. The method is not aimed at the determination of an exact stress distribution, but rather at an approximation of the contribution of the internal shear stresses to the longitudinal extension. The need for refinement of some of the initial assumptions will be largely determined by the results obtained with this model.

Load is applied parallel to the fiber direction. The fiber is assumed to carry only extensional stresses and the matrix to transmit only shear stresses. The material surrounding this typical fiber-matrix element is assumed to have uniform characteristics which are those to be evaluated. This "average" material will have the effective properties of the composite. No stress is transmitted axially from the end fiber to the average material. Shear stresses in the average material are considered to decay in a negligible distance from the inclusion interface.

For equilibrium of a fiber element in the axial direction:

$$\tau + \left(\frac{r_f^2 - r_o^2}{2r_f} \right) \frac{d\sigma_f}{dz} = 0 \quad (12)$$

where τ = shear stress in matrix material
 σ_f = axial stress in fiber

For equilibrium of the composite in the axial direction:

$$\left(\frac{r_f^2 - r_o^2}{r_a^2} \right) \sigma_f + \left(\frac{r_a^2 - r_f^2}{r_a^2} \right) \sigma_a = \bar{\sigma} \quad (13)$$

where σ_a = axial stress in average material
 $\bar{\sigma}$ = applied axial stress

The axial displacements in the fiber, u_f , and in the average material, u_a , define the binder shear strain, γ , as follows:

$$u_a - u_f = (r_b - r_f) \gamma \quad (14)$$

Differentiating eq. (14) with respect to z , and using Hookes law, yields:

$$\frac{\sigma_a}{E_a} - \frac{\sigma_f}{E_f} = \left(\frac{r_b - r_f}{G_b} \right) \frac{d\gamma}{dz}$$

Differentiating again, yields:

$$\frac{1}{E_a} \frac{d\sigma_a}{dz} - \frac{1}{E_f} \frac{d\sigma_f}{dz} = \left(\frac{r_b - r_f}{G_b} \right) \frac{d^2 \tau}{dz^2} \quad (15)$$

where

E_a	=	effective Young's modulus of the composite
E_f	=	Young's modulus of the fiber
G_b	=	shear modulus of the binder

Differentiating eq. (13) and substituting the result and eq. (12) into eq. (15) yields:

$$\frac{d^2 \tau}{dz^2} - \beta^2 \tau = 0 \quad (16)$$

where

$$\beta^2 = \frac{2G_b r_f}{E_f (r_b - r_f) (r_f^2 - r_b^2)} \left[1 + \frac{E_f}{E_a} \left(\frac{r_f^2 - r_b^2}{r_a^2 - r_b^2} \right) \right]$$

The solution to eq. (16) is of the form

$$\tau = A \sinh \beta z + B \cosh \beta z$$

The boundary conditions are:

$$\tau(0) = 0$$

$$\sigma_f(l) = 0$$

$$\therefore B = 0$$

$$A = \frac{G_b \bar{\sigma} r_a^2}{\beta E_a (r_b - r_f) (r_a^2 - r_b^2) \cosh \beta l}$$

and

$$\tau = \frac{G_b \bar{\sigma} r_a^2 \sinh \beta z}{\beta E_a (r_b - r_f) (r_a^2 - r_b^2) \cosh \beta l} \quad (17)$$

From eqs. (12) and (17):

$$\sigma_f = - \frac{\bar{\sigma} r_a^2 E_f}{[E_a(r_a^2 - r_b^2) + E_f(r_f^2 - r_o^2)]} \left(\frac{\cosh \beta z}{\cosh \beta l} - 1 \right) \quad (18)$$

From eqs. (13) and (18):

$$\sigma_a = \frac{\bar{\sigma} r_a^2}{r_a^2 - r_b^2} \left\{ 1 + \frac{\left(\frac{\cosh \beta z}{\cosh \beta l} - 1 \right)}{\left[\frac{E_a}{E_f} \left(\frac{r_a^2 - r_b^2}{r_f^2 - r_o^2} \right) + 1 \right]} \right\} \quad (19)$$

With the stress distribution established, the displacements can be determined and the average strain will be defined. From Hookes Law, and the strain-displacement relation for uniaxial stress:

$$\frac{du_a}{dz} = \frac{\sigma_a}{E_a} \quad (20)$$

The average strain, $\bar{\epsilon}$, need only be considered over the length of the fiber since deviations from average stress are considered small over the end region; thus,

$$\bar{\epsilon} = \frac{1}{l} u_a(l) \quad (21)$$

The effective modulus, E_a , is given by:

$$E_a = \frac{Q}{\bar{\epsilon}} \quad (22)$$

From eqs. (19) through (22) the following equation for the effective modulus is obtained:

$$v_i \left[1 + \left(\frac{1 - v_i}{v_i} \right) \frac{E_a}{v_f E_f} \right] + \frac{\tanh \beta l}{\beta l} = 1 \quad (23)$$

where

$$(\beta l)^2 = \frac{2G_b}{E_f} \left(\frac{1}{1 - \alpha^2} \right) \left(\frac{l}{r_f} \right)^2 \left(\frac{v_f^{1/2}}{1 - v_f^{1/2}} \right) \left[1 + \frac{E_f}{E_a} \left(\frac{v_f v_i}{1 - v_i} \right) \right] \quad (24)$$

- v_i = volume fraction of inclusion relative to model
 v_t = volume fraction of tube relative to inclusion
 v_f = volume fraction of fiber relative to inclusion

For a meaningful model the inclusion is a small volume fraction. Thus, the modulus is found by setting $v_i = 0$ in eqs. (23) and (24):

$$\frac{1}{v_f} \left(\frac{E_a}{E_f} \right) + \frac{\tanh \beta l}{\beta l} = 1 \quad (25)$$

where

$$(\beta l)^2 = \frac{2G_b}{E_f} \left(\frac{1}{1-\alpha^2} \right) \left(\frac{l}{r_f} \right)^2 \left(\frac{v_t^{1/2}}{1-v_t^{1/2}} \right) \quad (26)$$

The modulus, E_a , is plotted in Fig. IV-2 for two values of $1/r_f$ and of α . The weighted average of the constituent moduli is used as the normalizing factor, so that the reduction of modulus due to shear deformations is indicated by a modulus ratio less than unity. (In this case, neglect of extensional stresses in the binder reduces the weighted average, E_{av} , to: $E_{av} = v_f E_f$) For the solid fibers the modulus ratio is seen to be very close to unity for even a very small aspect ratio of $1/r_f = 100$. This corresponds to a length of only 0.05" for conventional glass filaments used in filament wound construction. The curves for $1/r_f = 10$ are shown to indicate the aspect ratios necessary to provide a significant contribution from the shear modulus considered. These curves are shown for both solid and hollow fibers.

It is clear from figure IV-2 that the contribution of shear deformations to effective axial modulus is small, for glass-reinforced plastics. It was shown above that the effect of different Poisson's ratios upon the axial modulus for glass-plastic composites is small. It therefore appears that the weighted average of the constituent moduli is an adequate measure of the effective axial modulus of uniaxially stiffened glass-plastic composites. This is the value used in subsequent studies of biaxial stiffening and structural efficiency. For other reinforced-matrix materials it is recommended that eq. (11) be used to evaluate the axial modulus unless the stiffening fibers are of extremely short length in which case they should probably be treated as randomly oriented particles.

Poisson's ratio

Using the model of concentric cylinders of glass and plastic, the effective Poisson's ratio, ν_{21} , is readily defined:

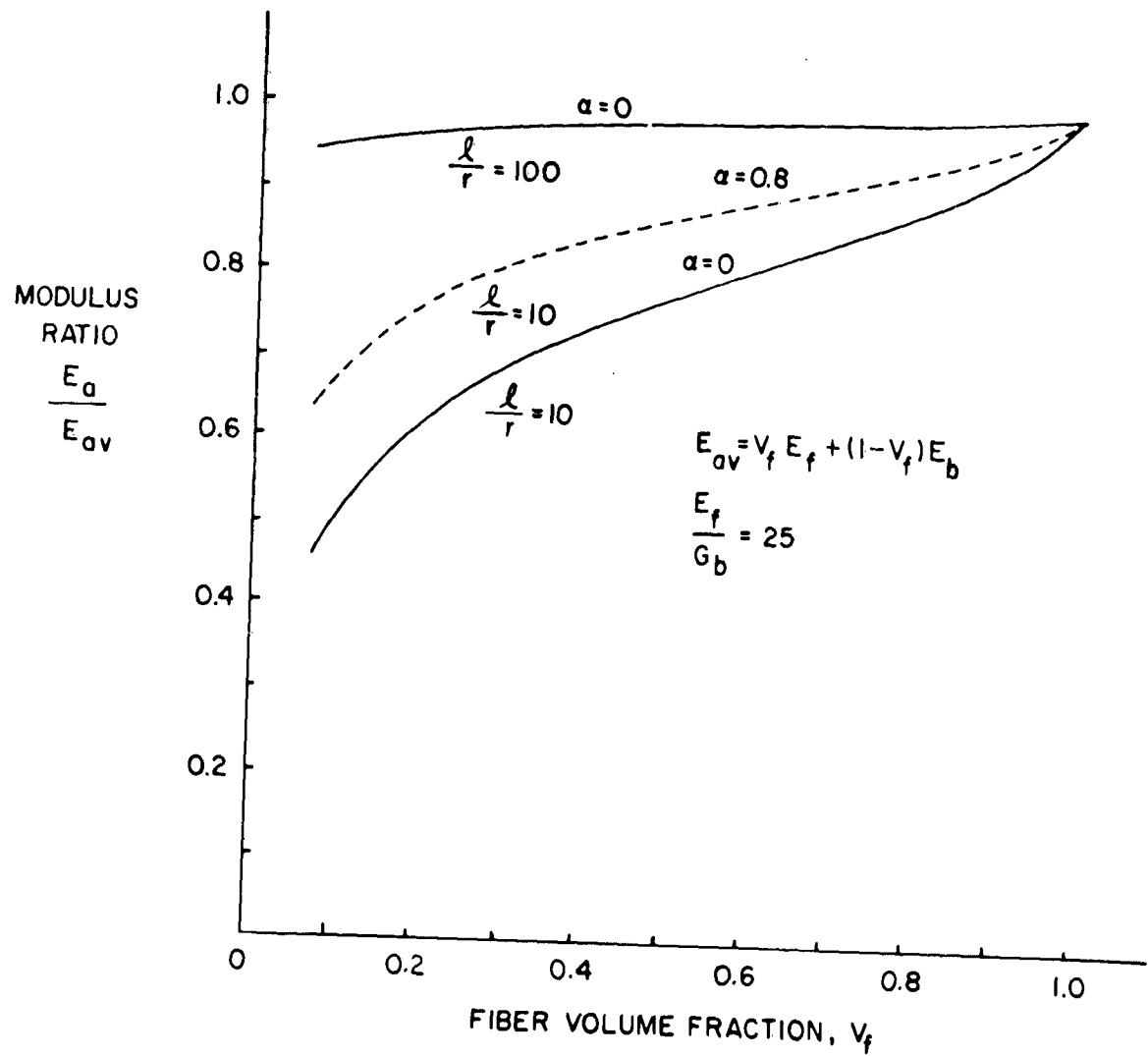


Fig. IV-2 Variation of Modulus with Fiber Volume Fraction and Fiber Length, Showing Effect of Shear Deformations.

$$\nu_{21} = - \frac{u_b(r_b)}{r_b \bar{\epsilon}_z} \quad (27)$$

Using the values of p and σ_z obtained from eqs. (9) and (10), $u_b(r_b)$ and $\bar{\epsilon}_z$ can be evaluated from eqs. (3) and (5) respectively (noting eq. 7). Substitution of these results into eq. (27) yields:

$$\nu_{21} = \frac{\nu_f E_f C_1 + \nu_b E_b C_2 \nu_b}{\nu_f E_f C_3 + \nu_b E_b C_2} \quad (28)$$

where

$$C_1 = 2\nu_f(1-\nu_b^2)(\nu_f+\nu_0) + \nu_b(1+\nu_b)\nu_b$$

$$C_2 = (1-\nu_f-2\nu_f^2)\nu_f + 2(1-\nu_f^2)\nu_0$$

$$C_3 = 2(1-\nu_b^2)(\nu_f+\nu_0) + (1+\nu_b)\nu_b$$

For a glass-plastic composite which has 30 % plastic with $\nu_b = 0.35$ and $\nu_f = 0.20$ it is found that ν_{21} varies only from 0.238 to 0.244 as α varies from 0 to 0.9. This is shown in Fig. IV-3.

Interface pressure

Different Poisson's ratios for the fiber and the matrix result in radial interface stresses when the composite is subjected to axial load or to temperature changes. The longitudinal property analysis required the evaluation of this stress under axial load. The resulting interface stress, p , for an axial stress, $\bar{\sigma}_z$, is:

$$p = \frac{\bar{\sigma}_z(\nu_f - \nu_b)}{D_1 + \frac{\nu_b E_b}{\nu_f E_f} D_2 + \frac{\nu_f E_f}{\nu_b E_b} D_3} \quad (29)$$

where

$$D_1 = (1+\nu_b) + (1-\nu_b)(2-\nu_f-\nu_b-4\nu_b\nu_f) + \nu_0(1+\nu_f)$$

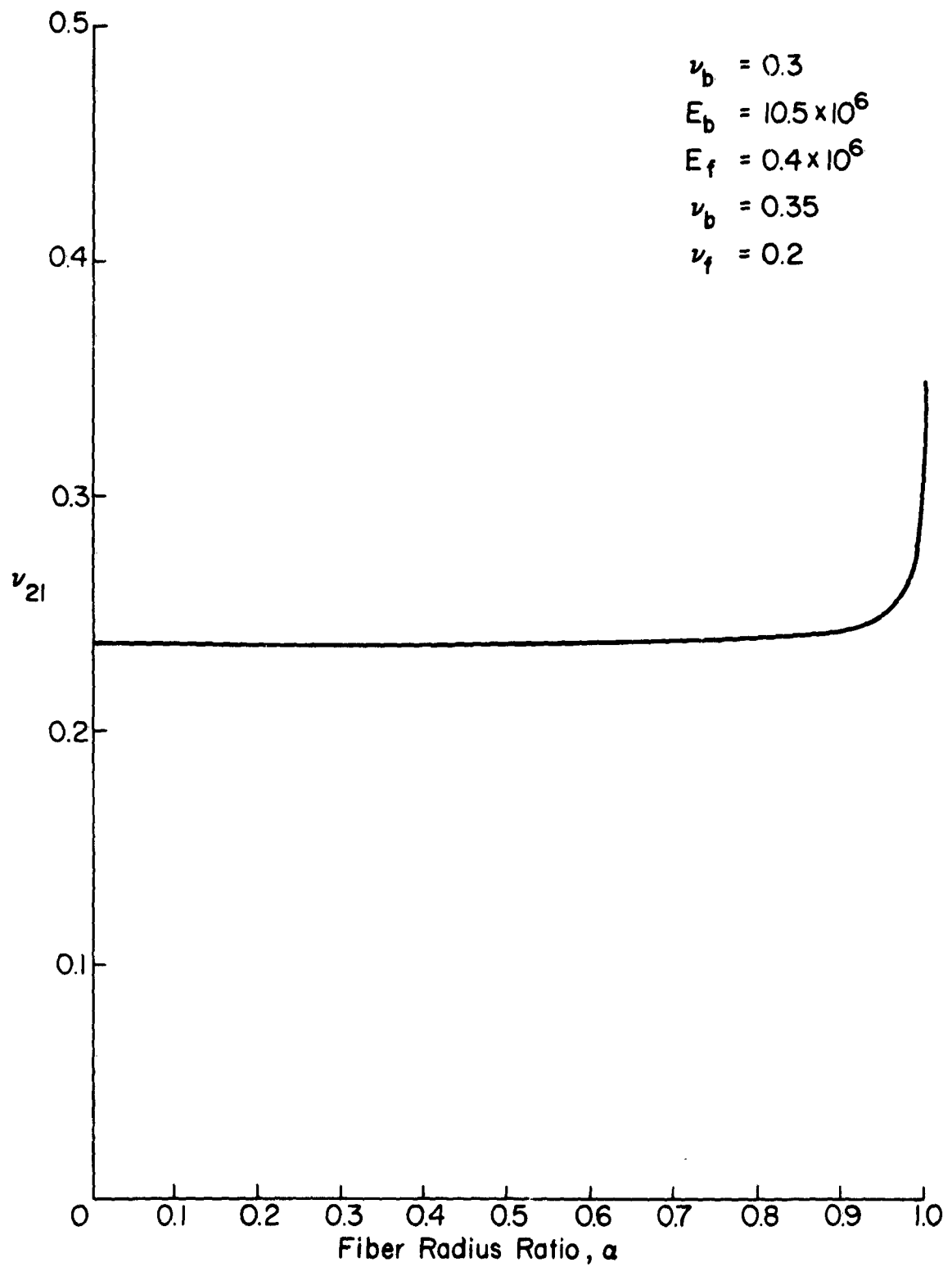


Fig. IV-3 Poisson's Ratio for Glass Plastic Composites Loaded Parallel to the Stiffening Fibers.

$$D_2 = (1 + \nu_f) [(1 - \nu_b)(1 - 2\nu_f) + \nu_b]$$

$$D_3 = (1 + \nu_b) [(1 - \nu_b)(1 - 2\nu_b) + 1]$$

2. Transverse elastic constants

The model used for the evaluation of the transverse elastic constants is geometrically the same as that used for the longitudinal constants. The hollow fiber cylinders are randomly distributed over the transverse plane and it is assumed that the composite is isotropic in this plane. Since the fiber diameters are very small compared to their lengths, it will be assumed that the cylinder will be in plane strain when tractions normal to the fiber direction and independent of location along the fiber are applied. The moduli are evaluated by strain energy techniques. The method is described in Appendix A and the results are as follows:

$$G_{23}^* \geq \frac{G_b}{1 + \frac{2(1-\nu_b)\nu_f A_4^\sigma}{1-2\nu_b}} \quad (30)$$

$$G_{23}^* \leq G_b \left[1 - \frac{2(1-\nu_b)}{1-2\nu_b} \nu_f A_4^\epsilon \right] \quad (31)$$

$$\bar{K}^* = \bar{K}_b \frac{\phi(1-\alpha^2)(1+2\nu_b\nu_f) + 2(1 + \frac{\alpha^2}{2\nu_f})\nu_b\nu_b}{\phi(1-\alpha^2)\nu_b + (1 + \frac{\alpha^2}{2\nu_f})(2\nu_b + \nu_f)} \quad (32)$$

The bounds for the plane strain bulk modulus coincide. The constants A_4^σ and A_4^ϵ are evaluated as described in the appendix. The bulk and shear moduli so defined are denoted as \bar{K}^* and G_{23}^* , respectively. For an isotropic homogeneous material:

$$\bar{K} = \frac{E}{2(1+\nu)(1-2\nu)}$$

and

$$G_{23} = \frac{E}{2(1+\nu)}$$

where E = Young's modulus
 ν = Poisson's ratio

Fig. IV - 4 shows the variation of \bar{K}^* with the ratio, α , of inner to outer diameters of the hollow fibers for two different volume fractions binder, v_b . The bulk modulus is normalized with respect to the equivalent quantity for binder, \bar{K}_b , or fiber, \bar{K}_f . Note that the curves cross at $\alpha = 0.94$. This is the diameter ratio for which the effective bulk modulus of a hollow fiber is the same as that for the binder. Figure IV-5 shows a similar relationship for the normalized shear modulus with three volume fractions considered. Computed points are presented by the plotted symbols, and curves are drawn connecting the points for $v_b = 0.2$ to indicate the nature of the property variation.

The values shown in Figs. IV-4 and IV-5, along with the axial composite properties, can be used to obtain Young's modulus and Poisson's ratio in the transverse plane. The latter properties can then be used in the expressions for the elastic constants of biaxially stiffened materials.

3. Elastic constants for biaxially stiffened material

The applications for hollow fiber reinforced plastics are expected to include filament wound structures. It is therefore important to study the characteristics of the hollow fiber composites with biaxial stiffening. For this purpose, the material may be considered as a laminate of orthotropic plates alternately oriented in each of two directions. Each plate has a single fiber orientation direction and the elastic constants of each plate are the uniaxially stiffened properties described in the previous section. The relationship between those properties and the laminate properties are available. (See, for example, ref. 2) Hence the studies of the uniaxially stiffened material can be used to analyze the behavior and determine the desirable geometry of actual filament wound structures, designed by stiffness considerations.

The coordinate system used in the following work is shown in Fig. IV-6. The laminate consists of layers of fibers in each of two directions, A_1 and B_1 , inclined at equal and opposite angles, ϕ , to the y axis. A large number of layers in each of the A and B directions are considered so that bending and extensional characteristics will be of the same form. In each plate the l direction is parallel to fibers and the modulus in that direction may be taken a E_{av} , for each layer.

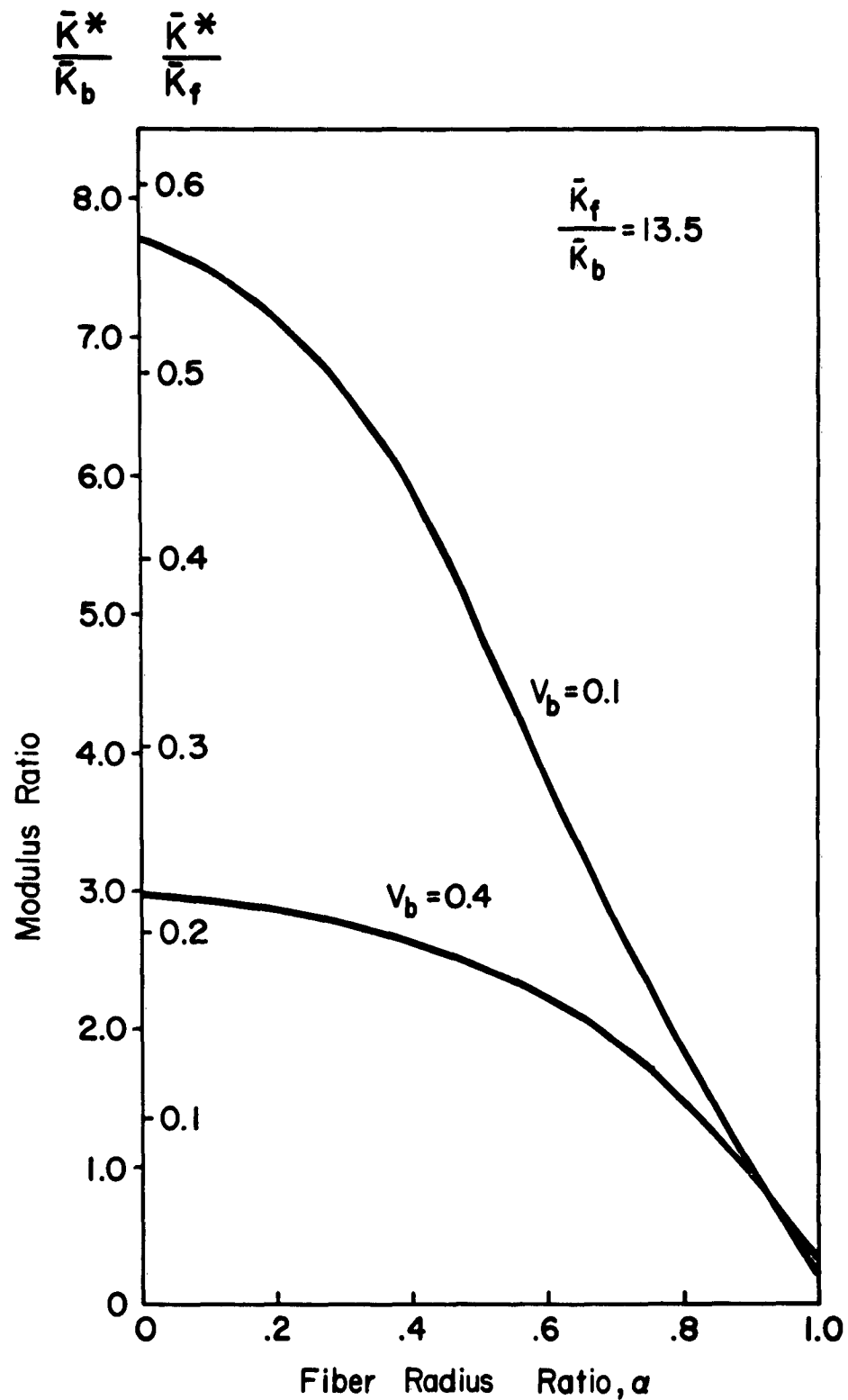


Fig. IV-4 Effective Transverse Plane Strain Bulk Modulus, \bar{K}^* , of Hollow Fiber Composites.

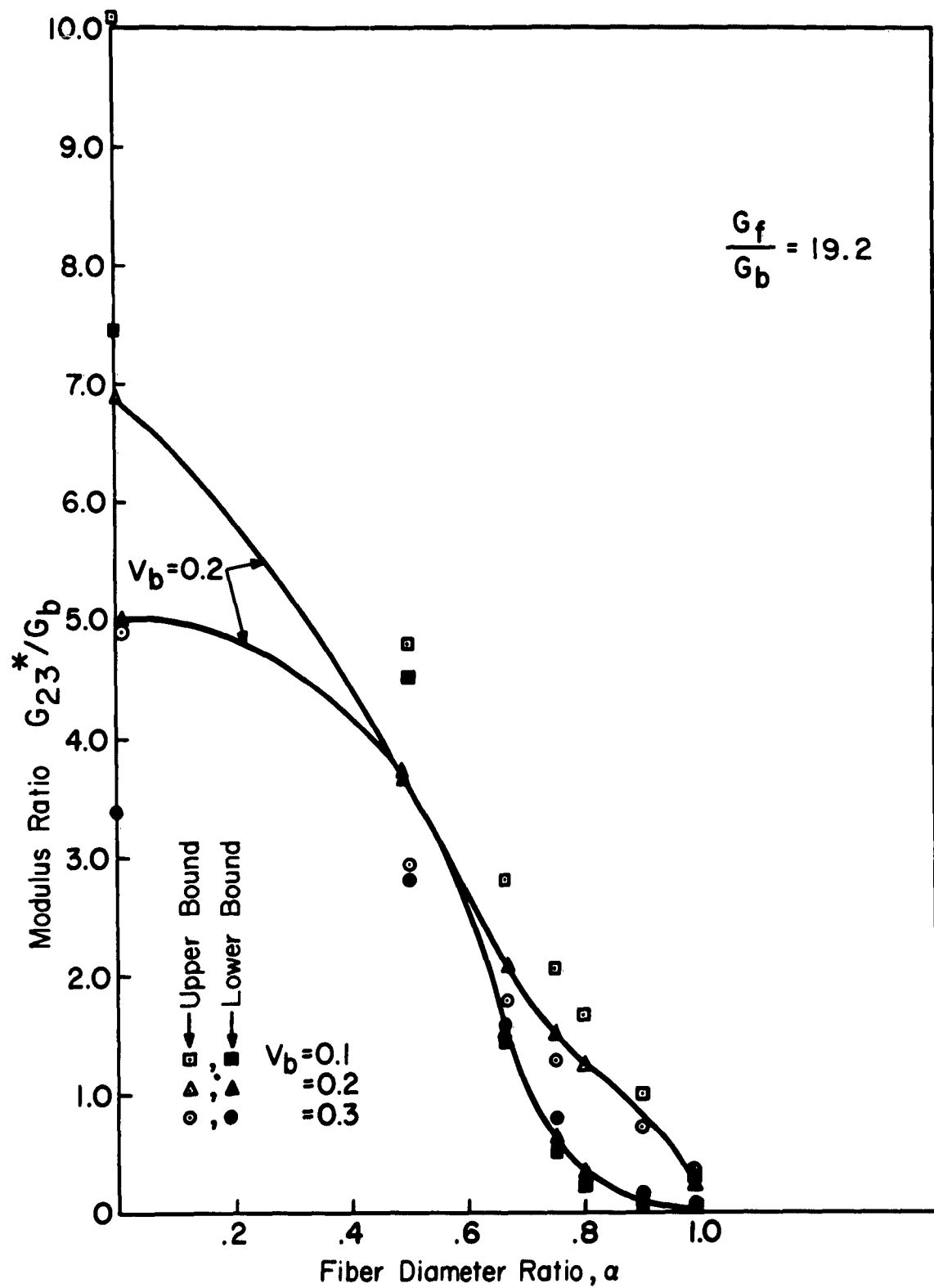


Fig. IV-5 Effective Transverse Shear Modulus, G_{23}^* , of Hollow Fiber Composites.

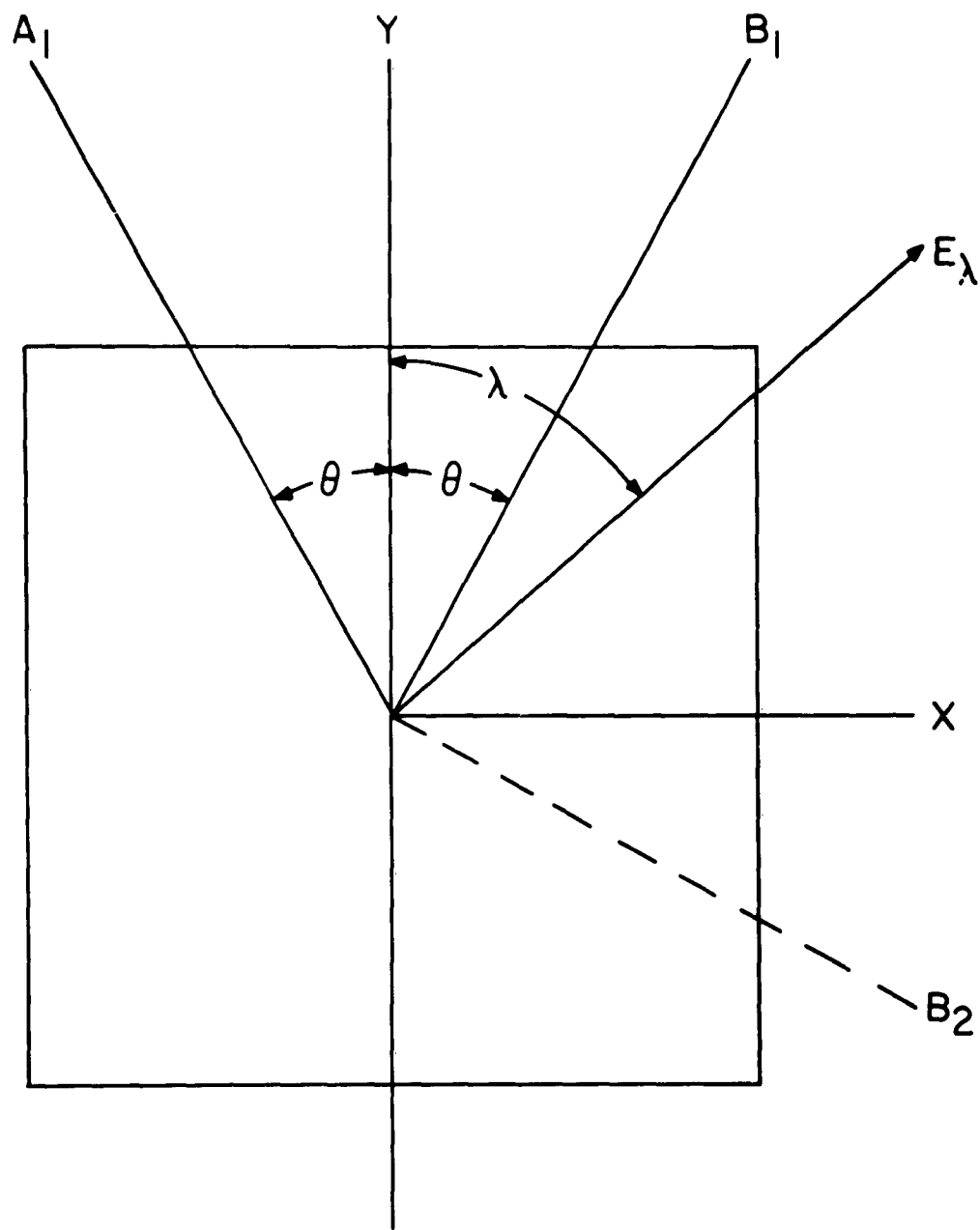


Fig. IV-6 Coordinate System for Laminate of Orthotropic Plates.

The modulus in the 2 direction will be obtained as described previously. The shear modulus, G_{12} , is also required. A model for this remains to be developed. The influence of these moduli on a composite is shown in Fig. IV-7 for values representative of glass-plastic composites. The strong influence of Θ and G_{12} are apparent.

For a fixed Θ it is important to note that the properties vary considerably with direction. Figures IV-8 show this variation. The ratio of Young's modulus at any angle, λ , to the y axis divided by the uniaxially stiffened modulus for the same fiber geometry is plotted against the loading direction, λ . The existence of the wide property variations in Figs. IV-7 and IV-8 indicates that a criterion for the evaluation of multi-directional properties is necessary. Such a criterion should be a mode of failure which involves biaxial stress fields. The criterion selected is the buckling strength of an orthotropic plate compressed in one direction. This will be discussed further in section B-2 below.

B. Structural Analysis

The properties determined in section IV-A can be used to evaluate the performance of hollow glass fibers for various structural applications. The potential of this hollow fiber material can be studied by treating uniaxial stiffening. More refined evaluations can then be performed for biaxial stiffening using the pertinent structural criteria. Structural efficiency studies of uniaxially stiffened material are presented below and then as an example, a stability evaluation of biaxially stiffened plates is presented.

1. Structural efficiency analysis

The fact that hollow fibers result in a variation of the material density, as well as of the mechanical properties, requires that material comparisons be made on a weight basis and thus, that a structural efficiency analysis be utilized. In the work that follows, hollow fiber composites are compared on this basis to solid fiber composites of the same binder geometry.

Young's modulus

As described in section IV-A, the modulus in the axial direction is adequately represented by:

$$E_1 = V_f E_f + V_b E_b \quad (33)$$

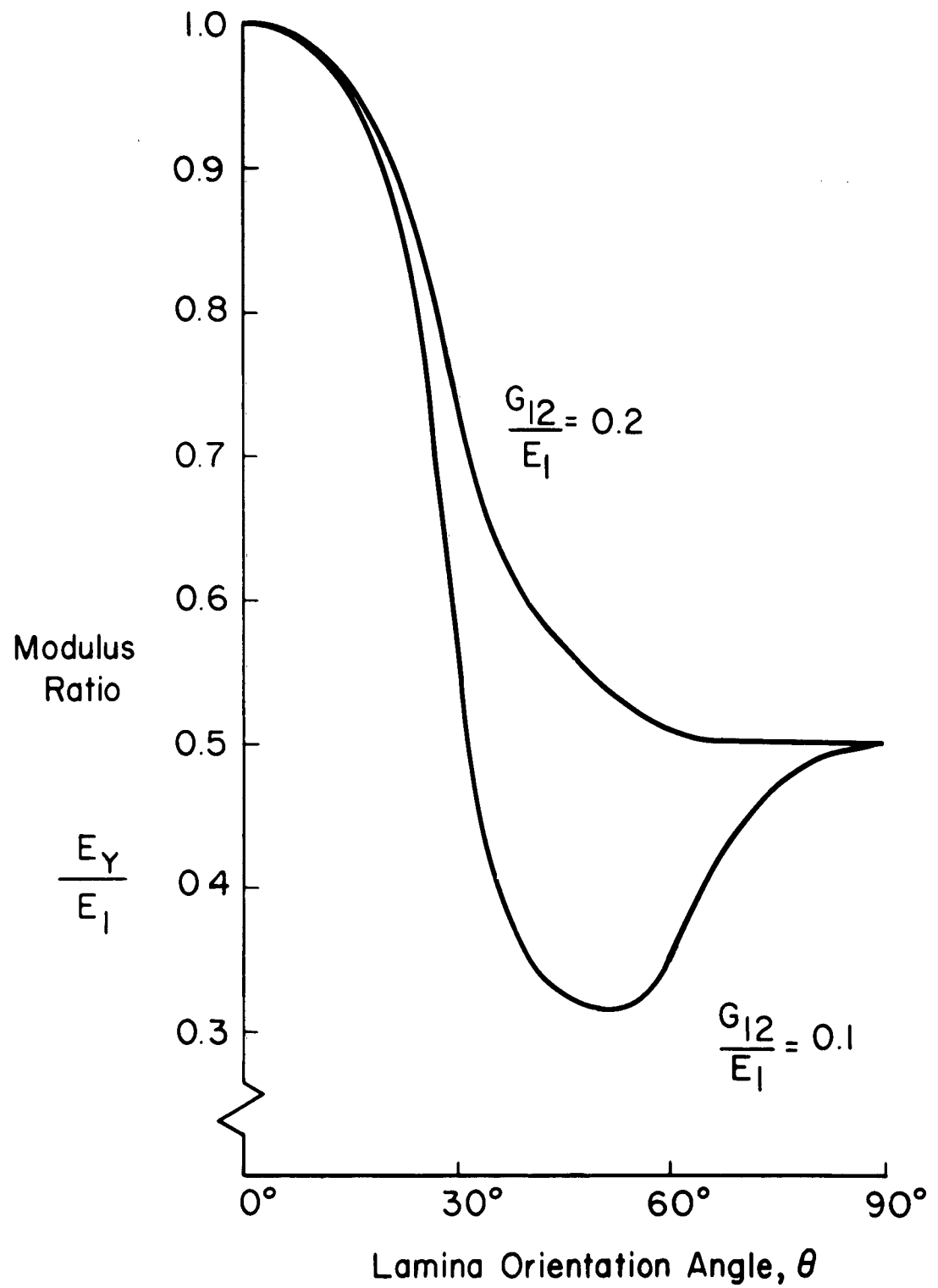


Fig. IV-7 Principal Laminate Modulus as a Function of Lamina Orientation.

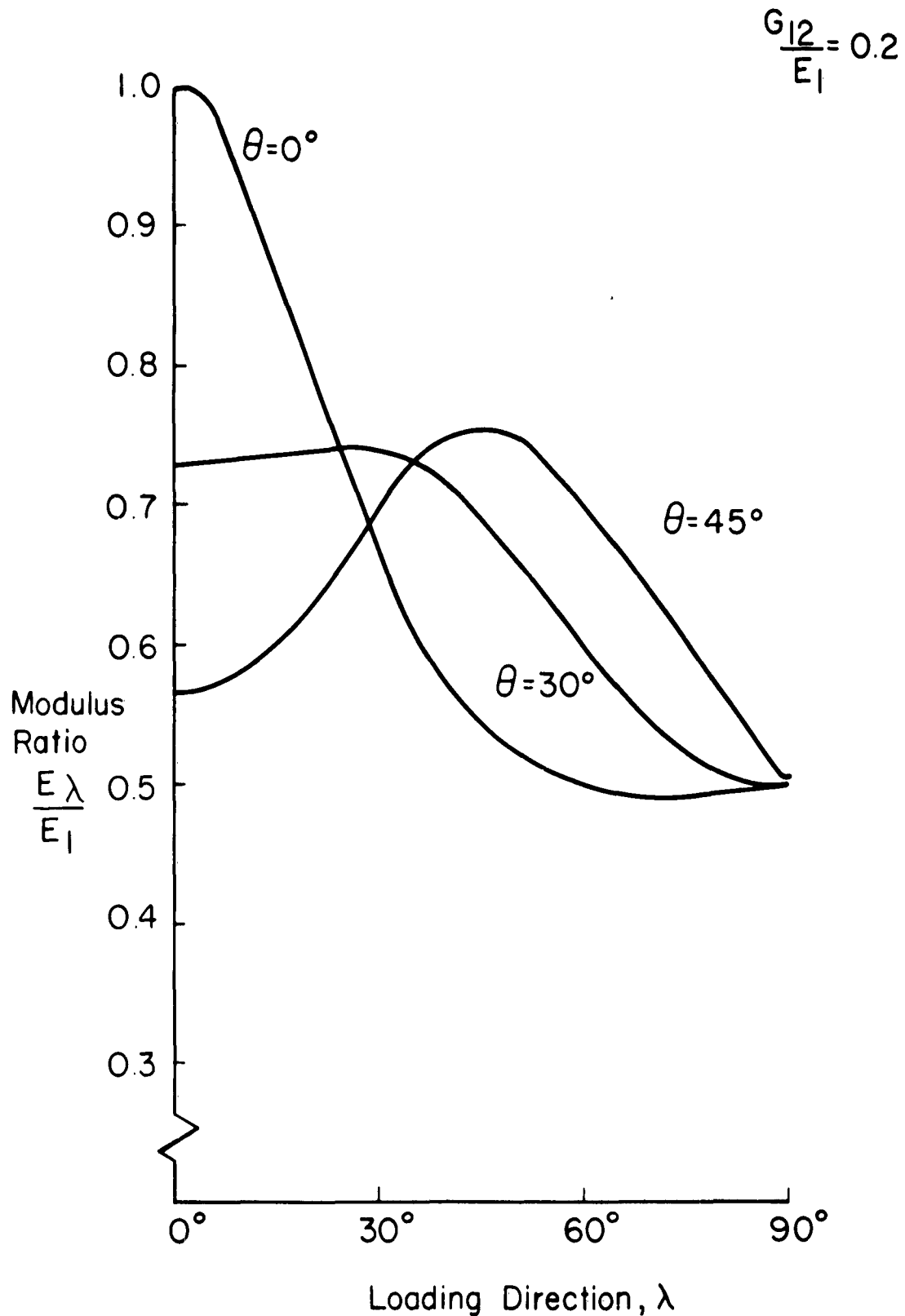


Fig. IV-8 Variation of Laminate Modulus with Direction (For $E_2 = 0.5 E_1$)

a. $G_{12}/E_1 = 0.2$

$$\frac{G_{12}}{E_1} = 0.1$$

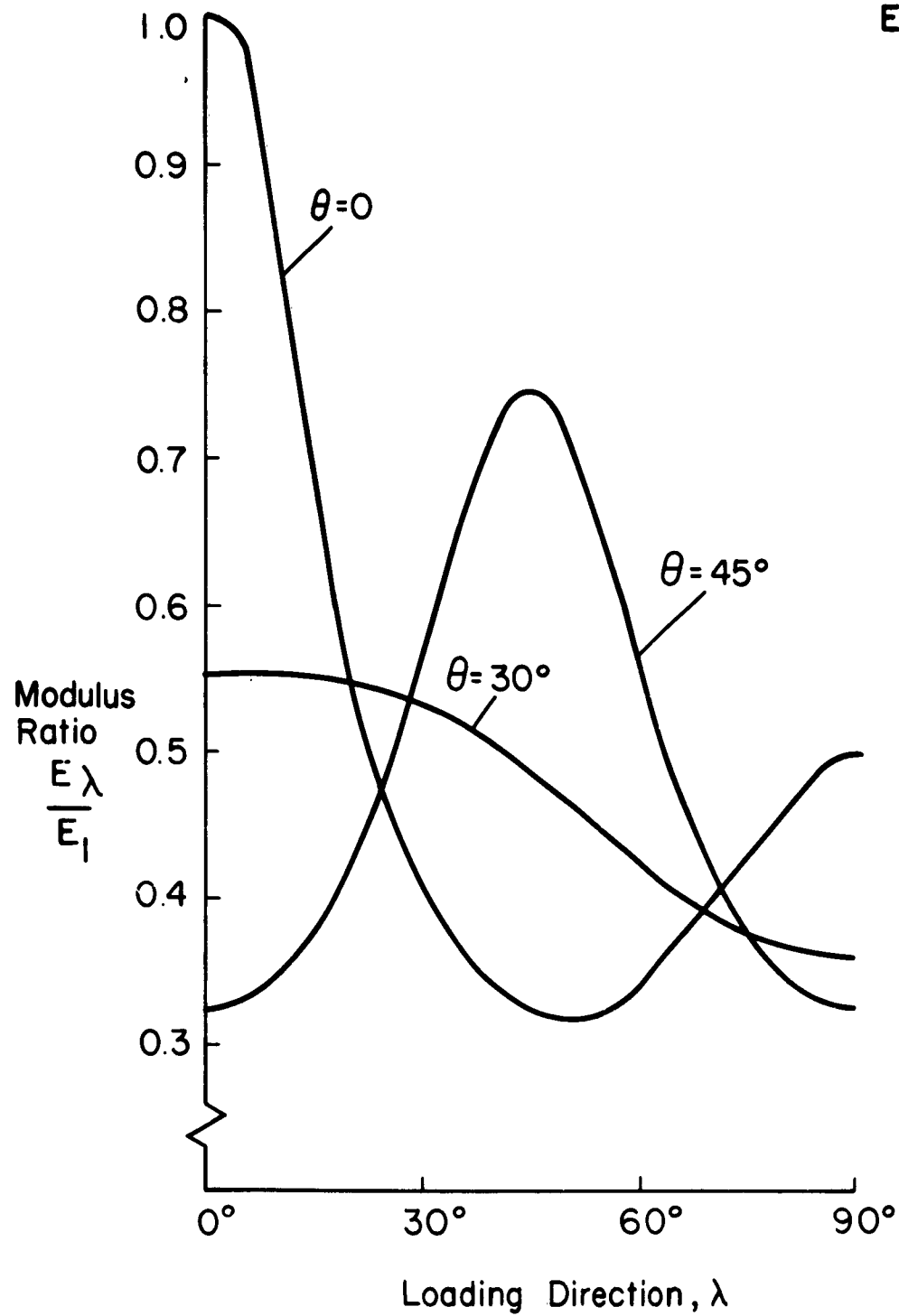


Fig. IV-8 b. $G_{12}/E_1 = 0.1$

which may be rewritten as:

$$E_i = (1 - v_b)(1 - \alpha^2) E_f + v_b E_b \quad (34)$$

This is normalized with respect to the solid fiber material of the same binder geometry yielding:

$$M \equiv \frac{E_{ih}}{E_{is}} = \frac{(1 - v_b)(1 - \alpha^2) + v_b \frac{E_b}{E_f}}{(1 - v_b) + v_b \frac{E_b}{E_f}} \quad (35)$$

Density

The average weight-density of the material, ρ_c , is given by (neglecting the weight of included air):

$$\rho_c = v_f \rho_f + v_b \rho_b \quad (36)$$

which may be rewritten as:

$$\rho_c = (1 - v_b)(1 - \alpha^2) \rho_f + v_b \rho_b \quad (37)$$

This is normalized with respect to the solid fiber material of the same binder geometry, yielding:

$$N \equiv \frac{\rho_{ch}}{\rho_{cs}} = \frac{(1 - v_b)(1 - \alpha^2) + v_b \frac{\rho_b}{\rho_f}}{(1 - v_b) + v_b \frac{\rho_b}{\rho_f}} \quad (38)$$

Equations (37) and (38) are plotted in Fig. IV-9.

Modulus-density ratio

The modulus to density ratios for hollow fiber composites normalized with respect to equivalent solid fiber composites are given by:

$$\frac{\left(\frac{E_i}{\rho_c}\right)_h}{\left(\frac{E_i}{\rho_c}\right)_s} = \frac{M}{N} = \eta_i \quad (39)$$

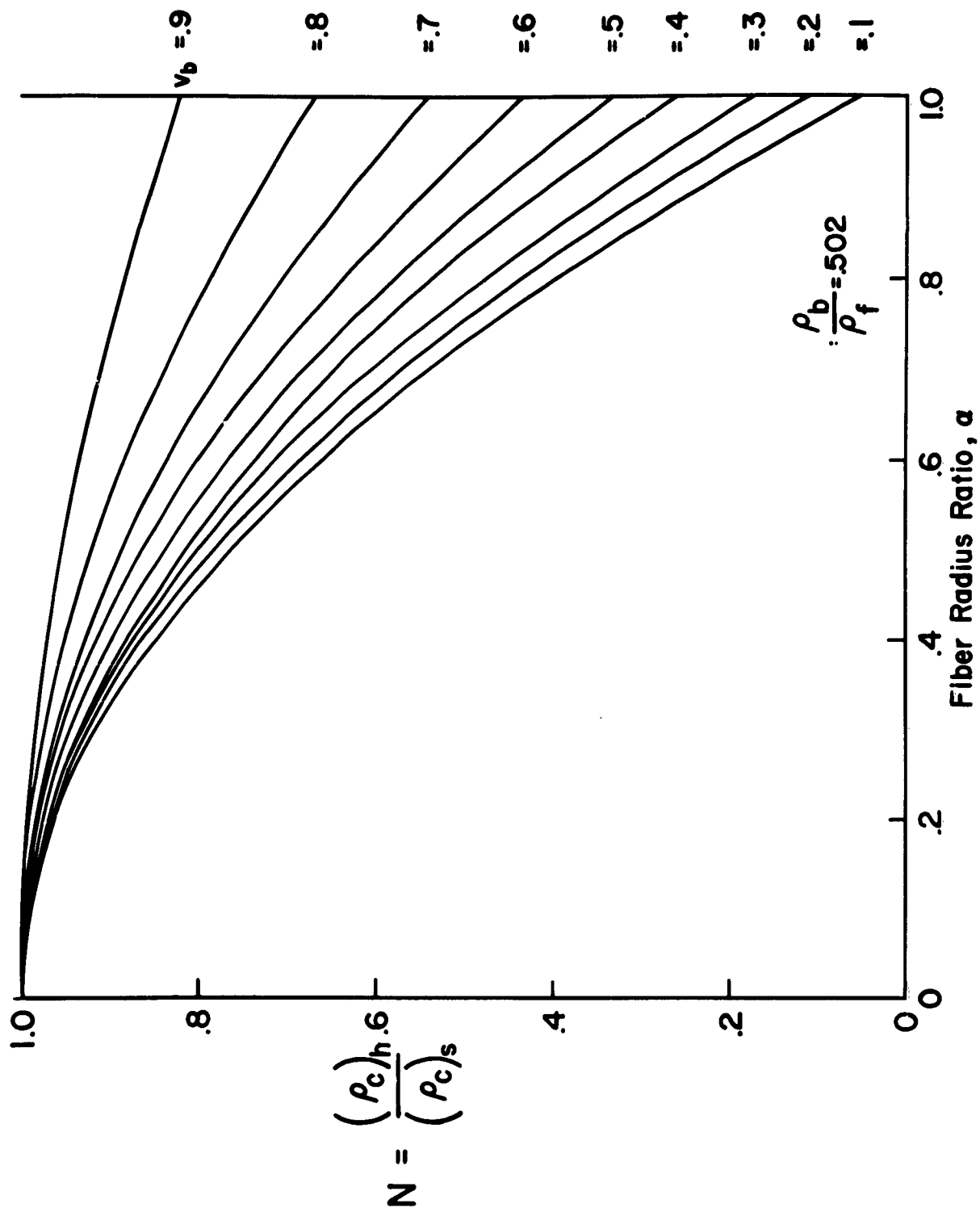


Fig. IV-9 a. Ratio of Densities of Hollow Fiber Composites to Solid Fiber Composites.

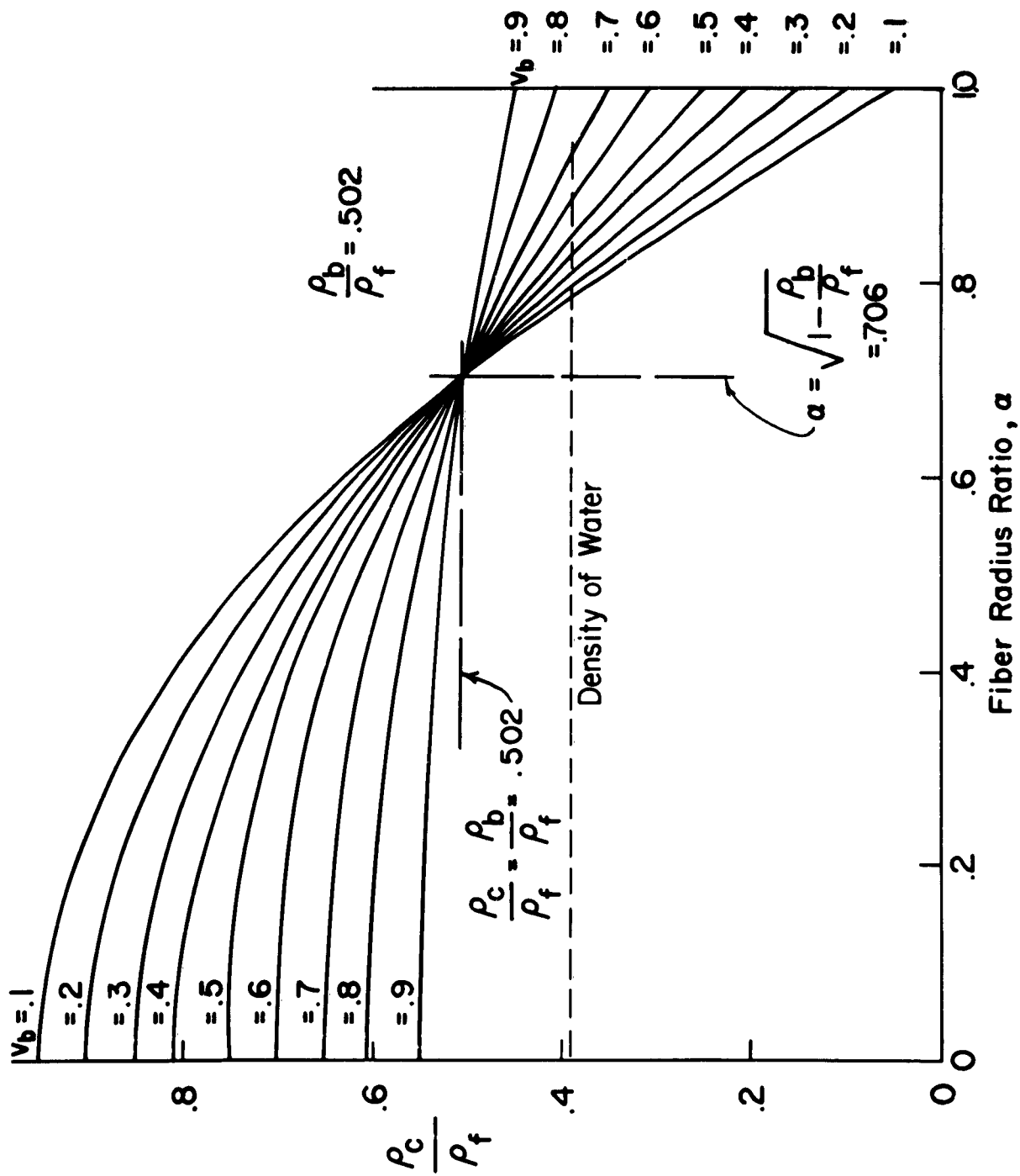


Fig. IV-9 b. Density of Hollow Fiber Composites.

and are plotted in Fig. IV-10a.

Tensile strength

The average stress in the composite under an axial load is:

$$\sigma_c = v_f \sigma_f + v_b \sigma_b \quad (40)$$

In the elastic range the stresses will be essentially the plane strain stress distribution. Thus, eq. (40) may be rewritten as:

$$\sigma_c = \sigma_f \left[(1-v_b)(1-\alpha^2) + v_b \frac{E_b}{E_f} \right] \quad (41a)$$

or

$$\sigma_c = \sigma_b \left[(1-v_b)(1-\alpha^2) \frac{E_f}{E_b} + v_b \right] \quad (41b)$$

Although inelastic effects and uncertain interior stress distributions will contribute to failure, a first strength estimate may be made using eqs. (41). Treating the fiber failure as the cause of composite failure, one obtains the hollow to solid strength ratio as:

$$\frac{\sigma_{ch}}{\sigma_{cs}} = \frac{(1-v_b)(1-\alpha^2) + v_b \frac{E_b}{E_f}}{(1-v_b) + v_b \frac{E_b}{E_f}} \quad (42)$$

From eq. (35), it is seen that:

$$\frac{\sigma_{ch}}{\sigma_{cs}} = M$$

Thus, the ratio of strength-density ratios will be the same as the ratio of modulus-density ratios. That is:

$$\frac{\left(\frac{\sigma_c}{\rho_c}\right)_h}{\left(\frac{\sigma_c}{\rho_c}\right)_s} = \frac{M}{N} = \eta, \quad (43)$$

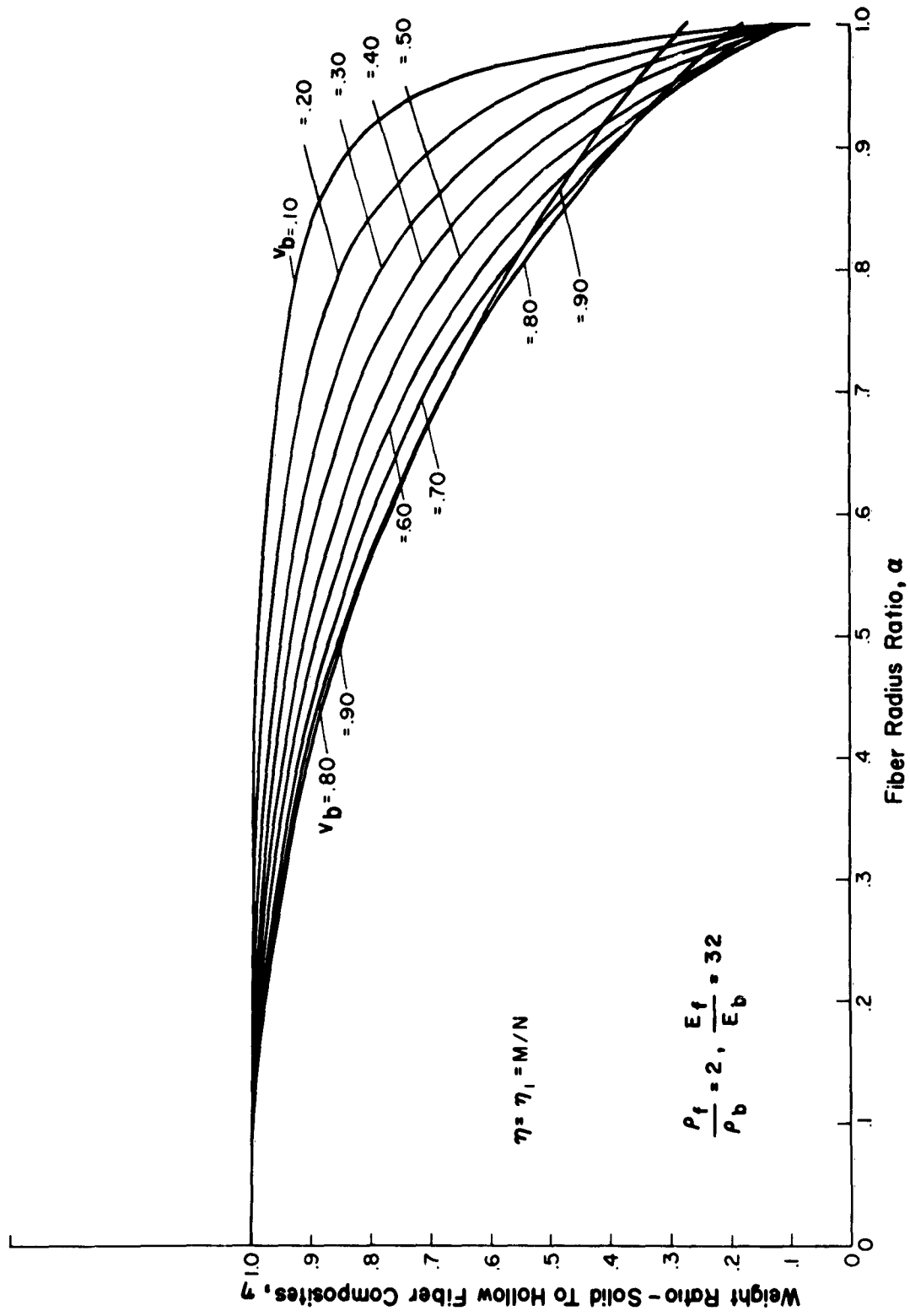


Fig. IV-10 Structural Efficiency and Hollow Fiber Composites

a. Structural Criterion is Axial Stiffness or Ultimate Tensile Strength

and the results in Fig. IV-10a are applicable.

Bending strength - slender beams

The maximum bending stress in a cantilever beam with a tip load, P , is given by:

$$\sigma = \frac{PLh}{2I} \quad (44)$$

where:

$$L = \text{beam length}$$

$$I = \frac{bh^3}{12}$$

for a rectangular cross section of dimensions b and h .

To perform the structural efficiency study, the cross section shape is held constant. That is, a constant ratio is maintained between the width b and thickness h .

$$e = \frac{b}{h}$$

Thus, eq. (44) becomes:

$$\sigma_c = \frac{6PL}{eh^3} \quad (45)$$

The weight of this beam is:

$$W = bhL\rho_c = eh^2L\rho_c \quad (46)$$

From eq. (45):

$$h = \left(\frac{6PL}{e\sigma_c} \right)^{1/3} \quad (47)$$

Substituting eq. (47) into (46), the weight is related to the strength of the composite.

$$W = eL\rho_c \left(\frac{6PL}{e\sigma_c} \right)^{2/3}$$

or simply

$$W = c_1 \frac{\rho_c}{\sigma_c^{2/3}} \quad (48)$$

The efficiency of the material in supporting the load P at a length L is inversely proportional to the weight.

Comparing the efficiencies of hollow and solid fiber reinforced beams, based upon the bending strength criteria, and using the strength definition of eq. (41a)

$$\frac{\left(\frac{\sigma_c^{2/3}}{\rho_c} \right)_h}{\left(\frac{\sigma_c^{2/3}}{\rho_c} \right)_s} = \frac{M^{2/3}}{N} = \eta_2 \quad (49)$$

Curves of this equation are presented Fig. IV-10b.

Beam deflection

An analysis of bending deflection for the cantilever beam treated above exemplifies the advantages of hollow fibers with regard to minimizing deflection under load. The deflection of the loaded end of the beam is

$$\Delta = \frac{PL^3}{3E_c I} \quad (50)$$

Again, we can let $b/h = e$,

$$\Delta = \frac{PL^3}{eh^4 E_c} \quad \text{or} \quad h^4 = \frac{4PL^3}{\Delta e E_c} \quad (51)$$

The weight of the beam is

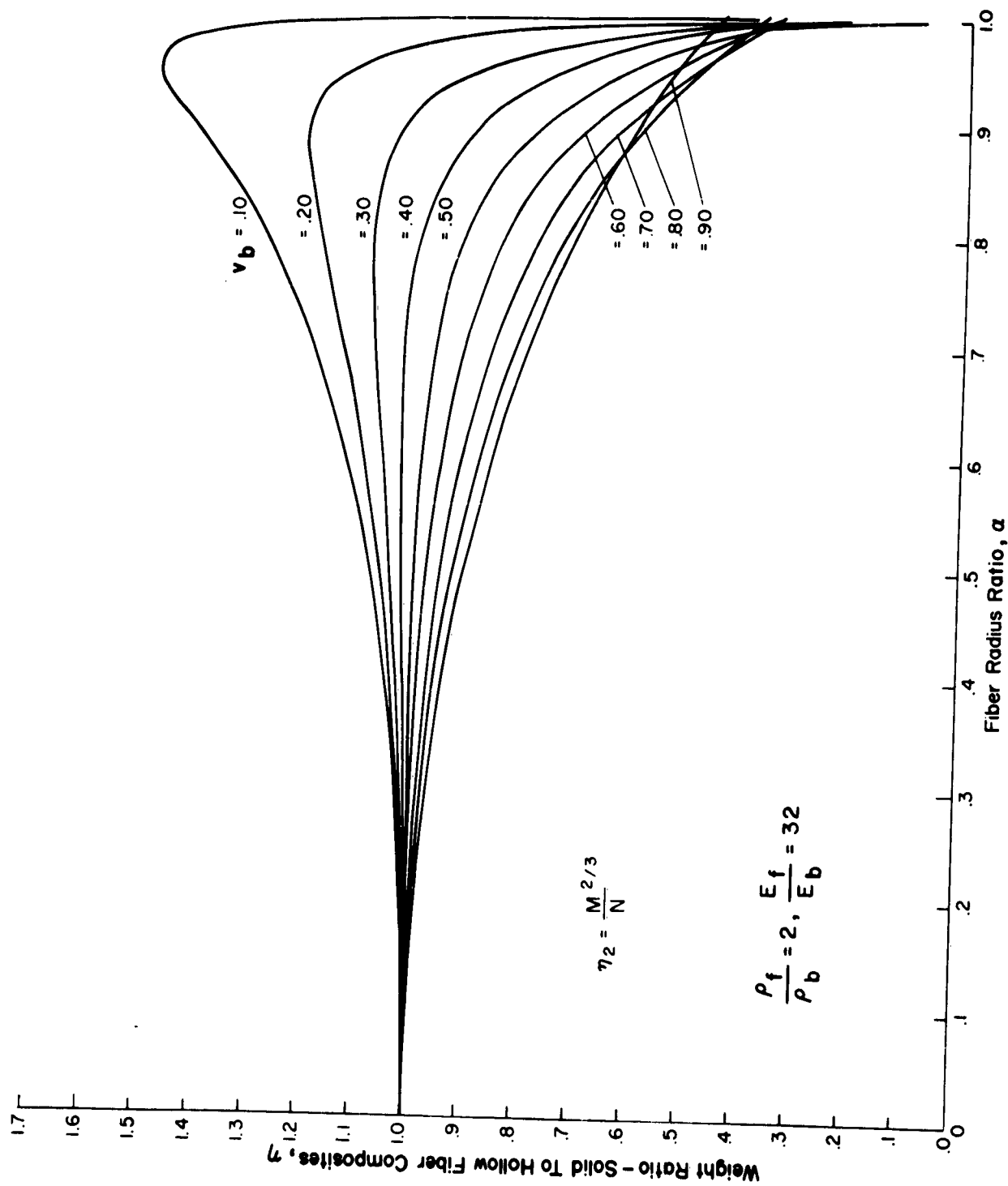


Fig. IV-10 b. Structural Criterion is Bending Strength of Slender Beams.

$$\begin{aligned}
 W &= bhL\rho_c \\
 &= eL\rho_c \left[\frac{4PL^3}{\Delta e E_c} \right]^{1/2} \\
 &= C_3 \frac{\rho_c}{E_c^{1/2}}
 \end{aligned} \tag{52}$$

The comparative efficiency of any two beams can be defined as the weight ratio for equal deflections. Thus, the comparison of efficiencies of hollow fiber to solid glass fiber reinforced plastics with regards to stiffness is,

$$\frac{\left(\frac{E_c^{1/2}}{\rho_c} \right)_h}{\left(\frac{E_c^{1/2}}{\rho_c} \right)_s} = \frac{M^{1/2}}{N} = \eta_3 \tag{53}$$

This equation is plotted in Fig. IV-10c.

Column buckling

Euler's formula for the critical buckling load of a long, slender column with hinged ends and having an axially applied load is

$$P_{cr} = \frac{\pi^2 E_c I}{L^2} \tag{54}$$

where I is the least moment of inertia.

An efficient column has equal bending resistance in all directions and, therefore, is usually of circular cross-section. The structural efficiency analysis is therefore performed on a circular cross-section column so that:

$$I = A r_o^2$$

where r_o = radius of gyration of the composite cross section

A = cross-section area

Thus

$$\sigma_{cr} = \pi^2 E_c \left(\frac{r_o}{L} \right)^2$$

or

$$\sigma_{cr} = (\pi^2 E_c)^{1/2} \left(\frac{r_o^2}{A} \right)^{1/2} \left(\frac{P_{cr}}{L^2} \right)^{1/2} \quad (55)$$

where $\frac{P_{cr}}{L^2}$ is the structural index

$\frac{r_o^2}{A}$ is a non-dimensional cross-sectional characteristic.

The column weight is

$$W = AL\rho_c = \frac{P_{cr}}{\sigma_{cr}} L\rho_c \quad (56)$$

Thus

$$W = \frac{L^3 \rho_c}{(\pi^2 E_c \frac{r_o^2}{A})^{1/2}} \left(\frac{P_{cr}}{L^2} \right)^{1/2}$$

or

$$W = C_5 \frac{\rho_c}{E_c^{1/2}} \quad (57)$$

And the relative efficiency of the rod in column buckling is seen to be the same as for the beam deflection criterion. Thus

$$\frac{\left(\frac{E_c^{1/2}}{\rho_c} \right)_h}{\left(\frac{E_c^{1/2}}{\rho_c} \right)_s} = \frac{M^{1/2}}{N} = \eta_3 \quad (58)$$

The curves of Fig. IV-10c are applicable to the buckling criterion also.

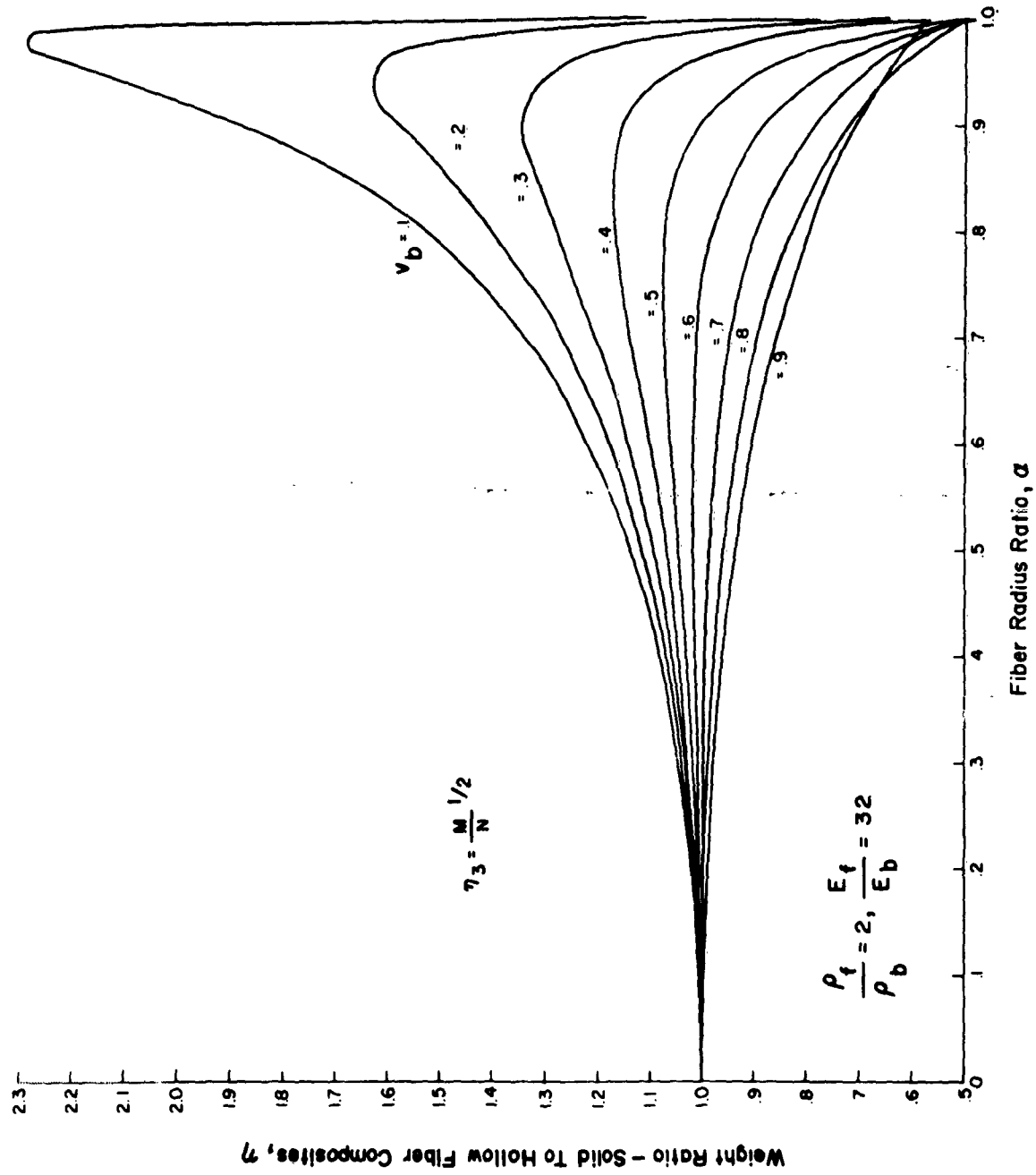


Fig. IV-10 c. Structural Criterion is Column Buckling or Bending Stiffness.

The efficiency data may also be plotted to show the weight of a hollow fiber element with respect to an equivalent solid fiber element. This is demonstrated in Fig. IV-10d for the column buckling case.

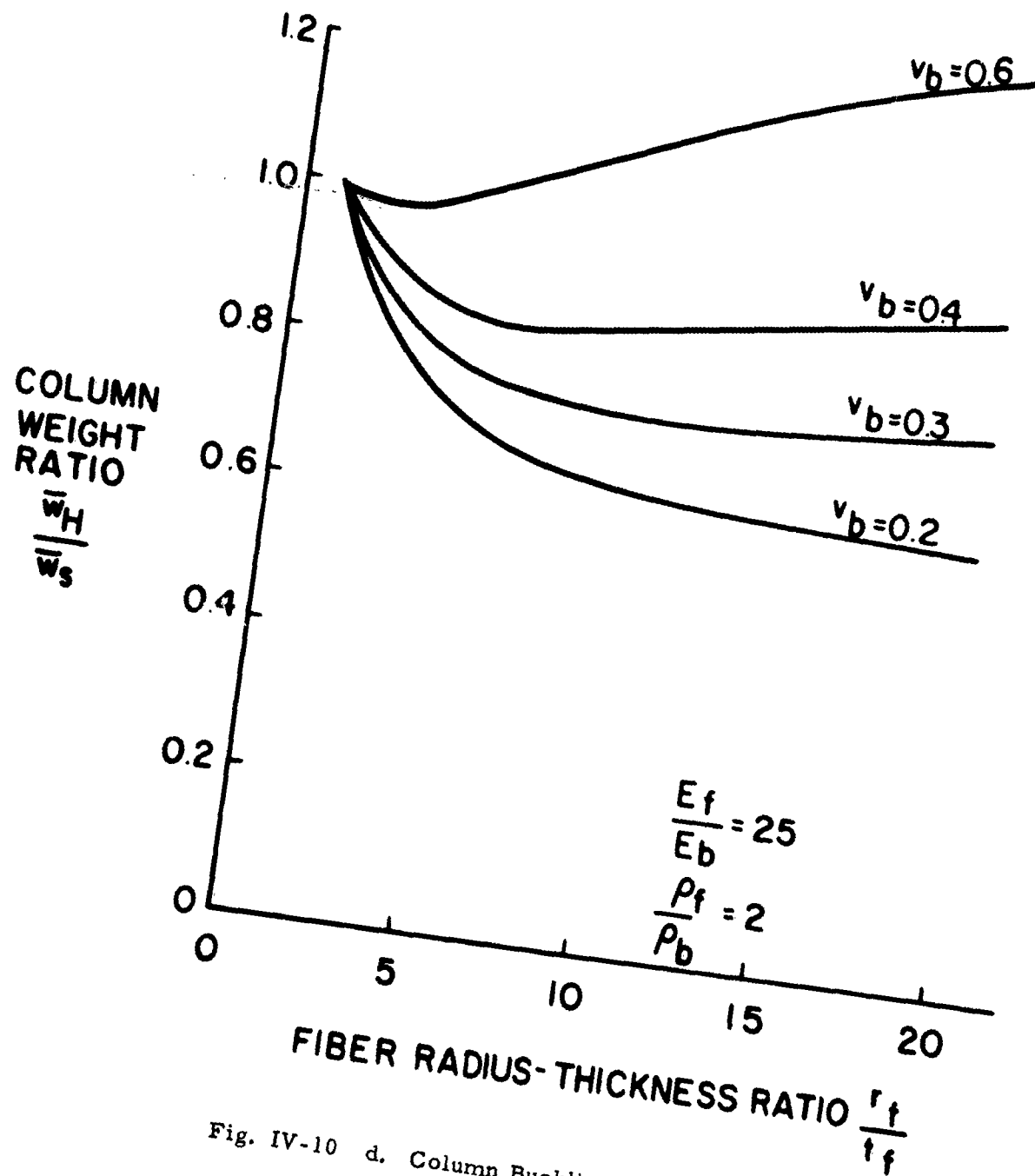


Fig. IV-10 d. Column Buckling Efficiency Normalized with Respect to Solid Fibers

Compressive strength

There is evidence to support the short compression specimen failure theory for filamentary structures presented in ref. 3 which states that failure is initiated by buckling instabilities of individual fibers. Buckling of these small columns (microbuckling) can be treated as buckling on an elastic foundation. This problem was studied in ref. 3, but is presented here in somewhat different form to indicate the effect of certain foundation characteristics.

Ref. 7, pages 108-112, gives the following equation for a long, slender column (in this case an individual fiber) supported continuously by an elastic foundation

$$P_{cr_f} = \frac{2\pi^2 E_f I_f}{(L/m)^2} = \sigma_{cr_f} A_f \quad (59)$$

where L/m is the half wave length of the buckling mode. This value L/m is related to the column properties as well as the spring constant of the supporting medium by

$$\frac{L}{m} = \pi \left(\frac{E_f I_f}{\psi} \right)^{1/4} \quad (60)$$

The foundation modulus ψ (lb/in²) represents the magnitude of the force exerted by the foundation per unit length, per unit lateral displacement.

From eqs. (59) and (60) and substituting for A_f and I_f

$$\sigma_{cr_f} = \left(\frac{E_f \psi}{\pi} \right)^{1/2} \left(\frac{1+\alpha^2}{1-\alpha^2} \right)^{1/2} \quad (61)$$

If, as a first estimate, it is assumed that the foundation modulus is the same for hollow and solid fibers, the critical stress ratio will be

$$\frac{(\sigma_{cr_f})_h}{(\sigma_{cr_f})_s} = \left(\frac{1+\alpha^2}{1-\alpha^2} \right)^{1/2} \quad (62)$$

From eqs. (41) and (62):

$$\frac{(\sigma_{cr_c})_h}{(\sigma_{cr_c})_s} = \left(\frac{1+\alpha^2}{1-\alpha^2} \right)^{1/2} M$$

And thus the structural efficiency for maximum compression stress is:

$$\frac{\left(\frac{\sigma_{cr_c}}{\rho_c} \right)_h}{\left(\frac{\sigma_{cr_c}}{\rho_c} \right)_s} = \left(\frac{1+\alpha^2}{1-\alpha^2} \right)^{1/2} \left(\frac{M}{N} \right) = \eta_4 \quad (63)$$

This equation is plotted in Fig. IV-10e.

From eq. (61), it can be seen that, as $\alpha \rightarrow 1$, $\sigma_f \rightarrow \infty$. At high values of α , other failure modes will occur. The following discussion considers such other possible modes and initial estimates of relative magnitudes are made. For high values of α , it is seen that σ_b will rapidly approach its maximum allowable value. Since

$$\sigma_b = \sigma_f \frac{E_b}{E_f}$$

for the glass-plastic composite:

$$\sigma_b = \frac{\sigma_f}{34}$$

and a 10 ksi plastic strength would be adequate for a 340 ksi glass failure stress. Thus the limiting fiber radius ratio for this mode will be above, $\alpha = 0.8$. This is shown on Fig. IV-11. Also shown on this figure is the shape of the glass failure stress curve of eq. (61).

Still another phenomenon occurs as $\alpha \rightarrow 1$, namely, the collapse of the thin walls by local buckling. The buckling mode would be a sinusoidal wave about the initial neutral axis of the thin wall. As a first estimate, the failure stress for an unsupported cylinder is used (ref. 7, page 440)

$$\sigma_{f_{cr}} = \frac{2 E_f (r_f - r_o)}{(r_o + r_f) \sqrt{3(1-\nu_f^2)}} \quad (64)$$

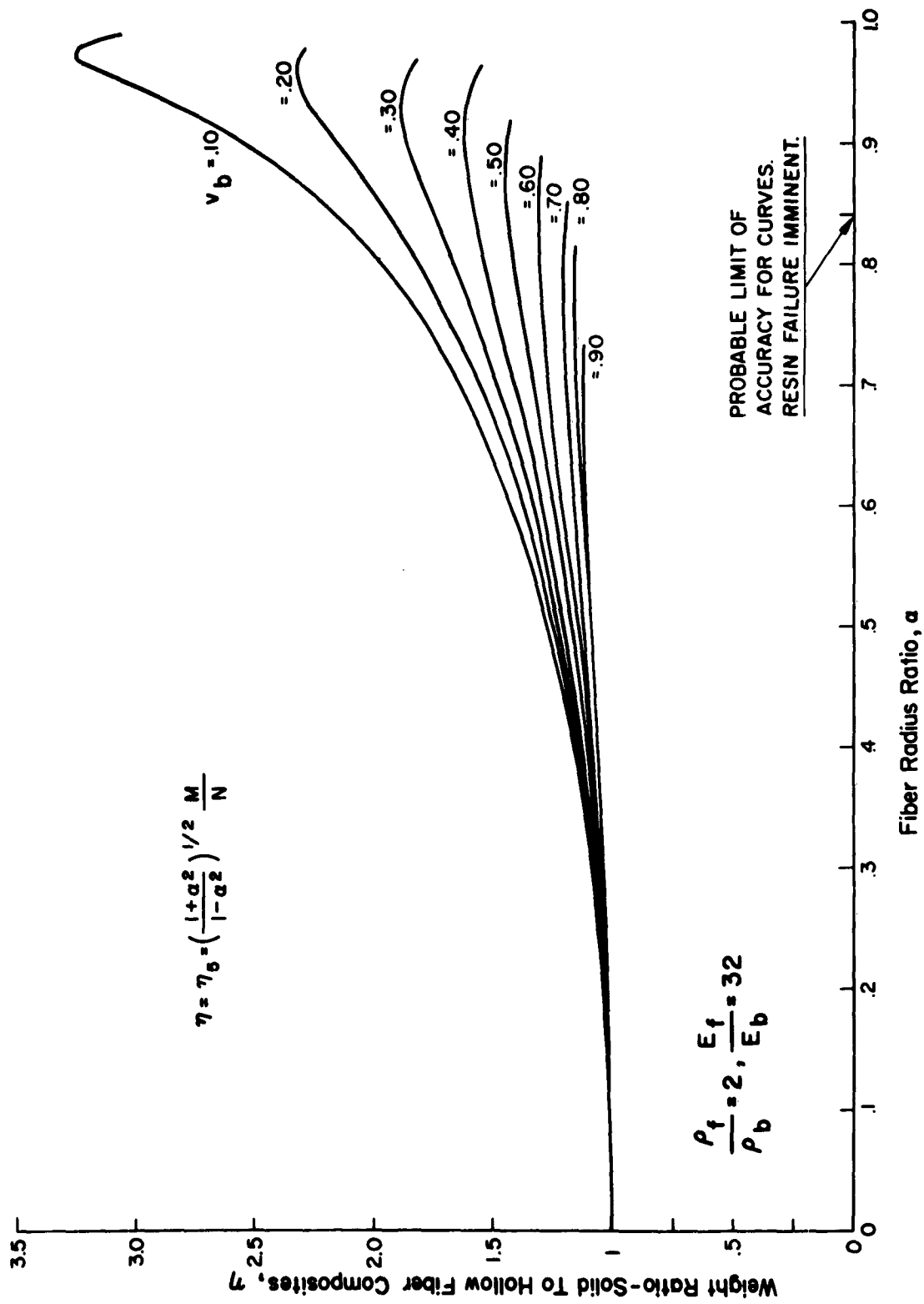


Fig. IV-10 e. Structural Criterion is Compressive Strength.

where

$$\frac{r_o}{r_f} \sim 1$$

Eq. (64) can be written as

$$\sigma_{f,cr} = \frac{2 E_f (1-\alpha)}{(1+\alpha) \sqrt{3(1-\nu_f^2)}} \quad (65)$$

This equation is also plotted in Fig. IV-11 and it is seen that this failure mode is not critical. A maximum glass stress is also indicated and the desirable operating envelope is thus qualitatively pictured.

2. Stability analysis - biaxial stiffening

The structural efficiency analyses described above indicate the potential of hollow glass fiber composites. Most applications, however, will require the use of biaxially stiffened composites and consideration of a typical structural environment is necessary to assess the effect of the biaxial stiffening geometry upon structural weight.

The criterion selected is the buckling strength of a simply supported, long, orthotropic plate subjected to uniaxial in-plane compressive load. The buckling stress, σ_{cr} , for such a plate is given by ref. 7 (pg. 382) as (in the nomenclature of this paper)

$$\sigma_{cr} = \frac{\pi^2}{2a^2h} \left(\sqrt{D_{xx} D_{yy}} + D_{xy} \right) \quad (66)$$

where

$$\begin{aligned} D_{xx} &= \frac{h^3}{12} \left(\frac{E_x}{1-\nu_{xy}\nu_{yx}} \right) \\ D_{yy} &= \frac{h^3}{12} \left(\frac{E_y}{1-\nu_{xy}\nu_{yx}} \right) \\ D_{xy} &= \frac{h^3}{24} \left(\frac{\nu_{xy} E_x}{1-\nu_{xy}\nu_{yx}} + \frac{\nu_{yx} E_y}{1-\nu_{xy}\nu_{yx}} + 4G_{xy} \right) \end{aligned} \quad (67)$$

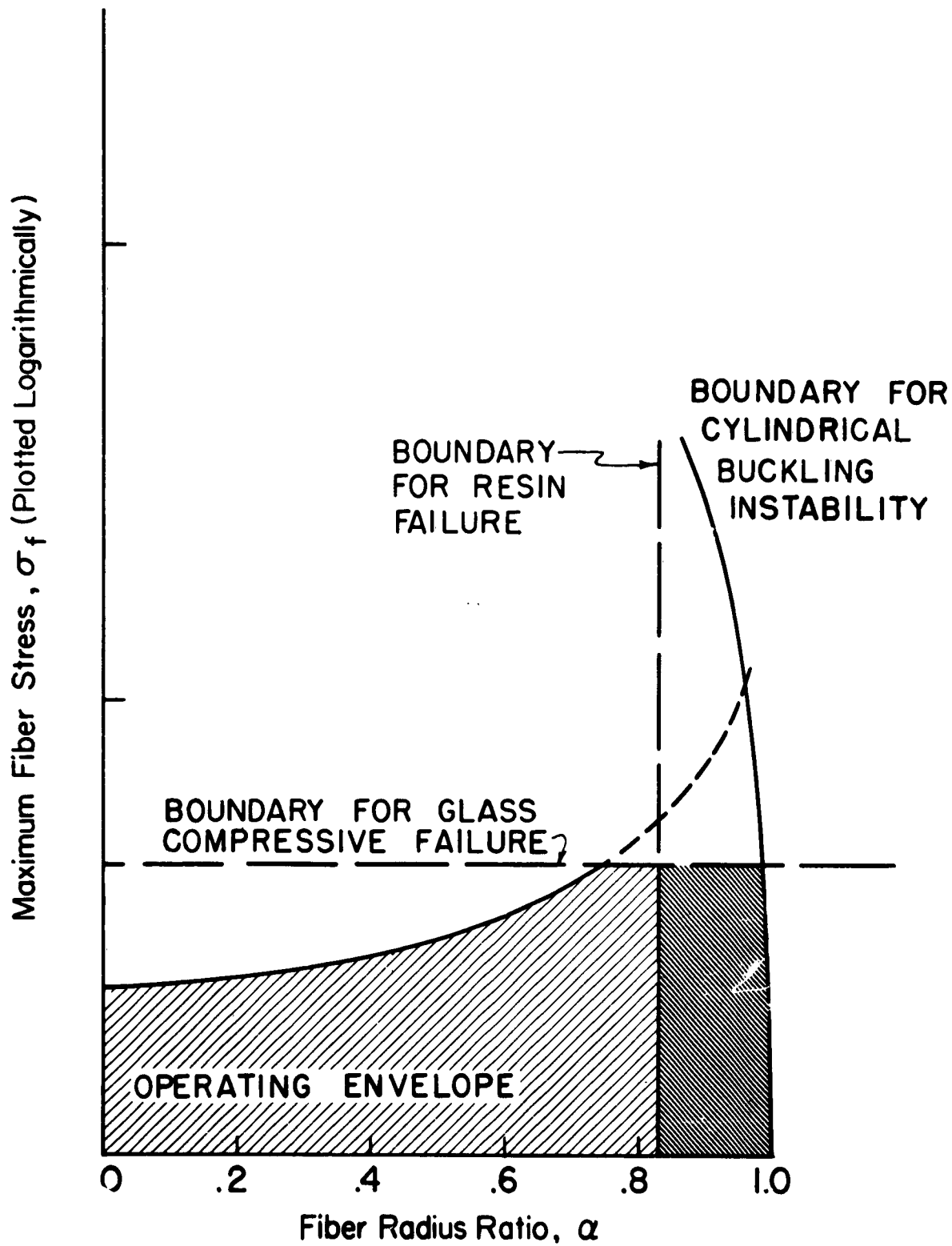


Fig. IV-11 Failure Mode Envelope for Hollow Reinforcing Fiber in a Composite Compression Structure.

a = plate width
h = plate thickness

Substituting eqs. (67) into eq. (66) and noting that:

$$\frac{\nu_{xy}}{E_y} = \frac{\nu_{yx}}{E_x}$$

yields:

$$\sigma_{cr} = \frac{\pi^2 E_y}{24(1-\nu_{xy}\nu_{yx})} \left(\frac{h}{a}\right)^2 \left[\left(\frac{E_x}{E_y}\right)^{1/2} + \nu_{yx} + \frac{2G_{xy}}{E_y}(1-\nu_{xy}\nu_{yx}) \right] \quad (68)$$

The buckling stress of an isotropic plate with properties E_y and ν_{xy} is:

$$\sigma_{cr_i} = \frac{\pi^2 E_y}{12(1-\nu_{xy}^2)} \left(\frac{h}{a}\right)^2 \quad (69)$$

The plate buckling stress ratio for orthotropic plates normalized with respect to an isotropic plate with equal longitudinal properties is given by:

$$\frac{\sigma_{cr_o}}{\sigma_{cr_i}} = \frac{(1-\nu_{xy}^2)}{2(1-\nu_{xy}\nu_{yx})} \left[\left(\frac{E_x}{E_y}\right)^{1/2} + \nu_{yx} + \frac{2G_{xy}}{E_y}(1-\nu_{xy}\nu_{yx}) \right] \quad (70)$$

Eq. (70) was evaluated and the results obtained are presented in Figs. IV-12 and IV-13. Fig. IV-13 presents the critical stress ratio as a function of the lamina orientation angle. Note that maximum stress is achieved at $\theta = 45^\circ$. Further, at this orientation, the critical stress is independent of the shear moduli. The variation in stress associated with change in lamina orientation for a given shear modulus is not large and the variation in weight is even smaller. This latter is because the weight is inversely proportional to a fractional power of an effective plate stiffness, while the stress varies linearly with the effective plate stiffness.

For two limiting lamina orientation angles, the variation in critical stress ratio with elastic constants is shown in Fig. IV-13. The significant effect of E_2 for both θ values and of G_{12} for $\theta = 0$ is apparent.

The indications of the work are that proper selection of geometry can produce significant improvements in performance. When better estimates of G_{12} become available, the selection of binder and matrix geometry for

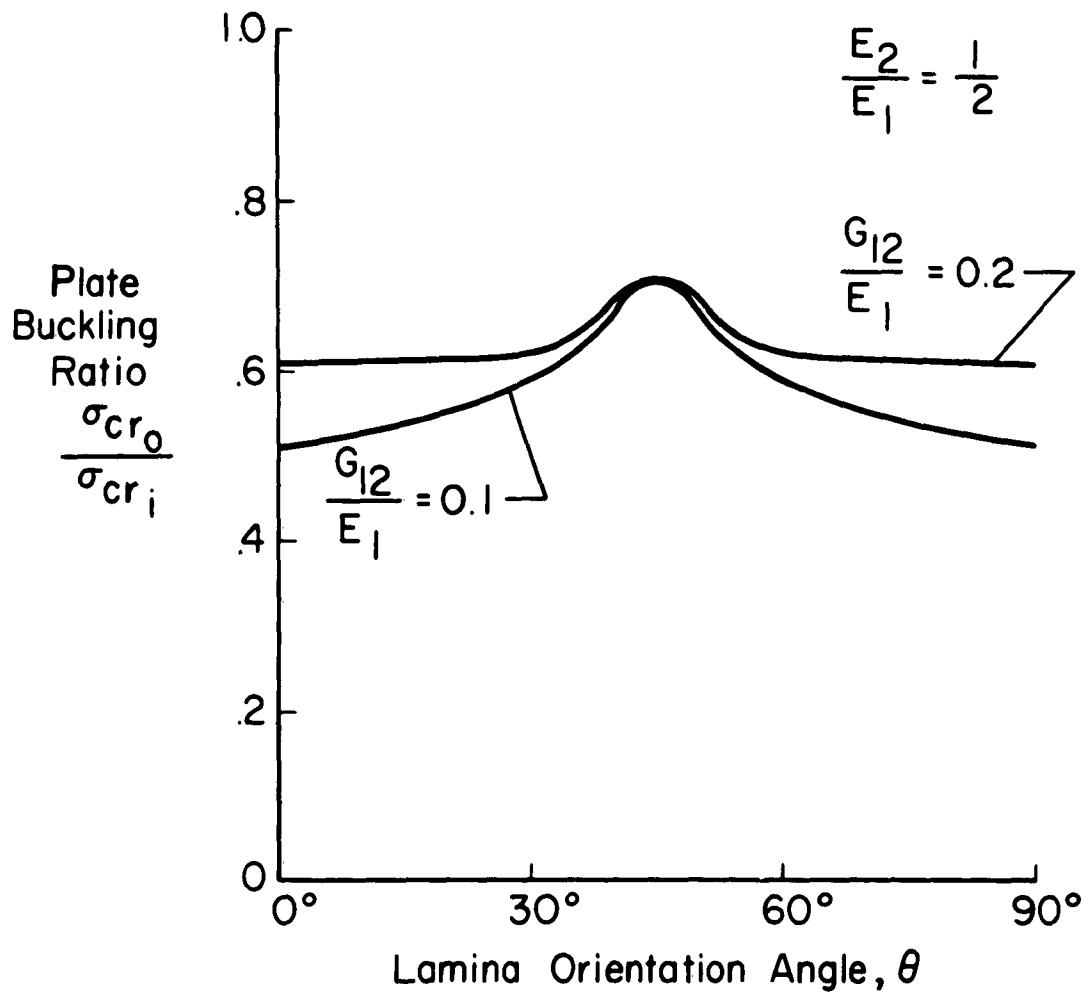


Fig. IV-12 Buckling Stress of Orthotropic Laminates

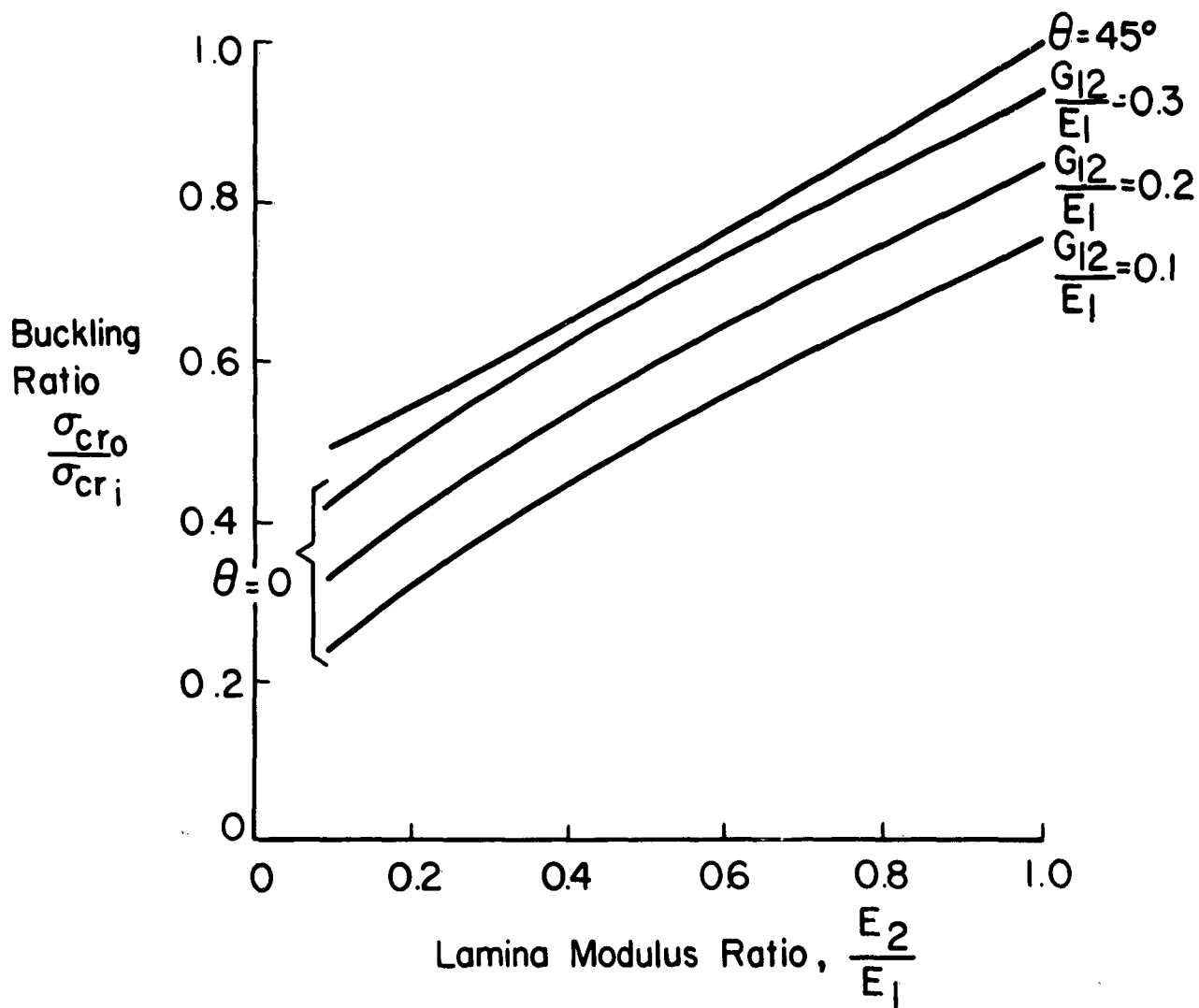


Fig. IV-13 Effect of Lamina Properties on Laminate Buckling Stress.

biaxially stiffened material should be feasible, as a function of the loading environment.

C. Acoustic behavior of hollow-fiber composites

1. Acoustic parameters

The basic properties governing the response of hollow fiber composites subjected to an acoustic disturbance are the characteristic impedance and the propagation constant of the material. The first parameter defines the amount of acoustic energy being reflected at the bounding surface and the latter specifies the degree of attenuation of the pulse inside of the material. Since the wave length of the ordinary acoustic perturbations is large compared to the transverse dimension of the fiber, the behavior of the composite is analyzed by using the ordinary tools of geometrical optics.

2. Velocity of sound in composites

The following analysis, characteristic for an infinite transversely isotropic medium, gives the speed of sound for any direction of propagation of the acoustic disturbance.

Let Σ be the surface bounding that portion of the material which is disturbed by the perturbation at time t . If $l, m,$ and n are the direction cosines of the normal ν to Σ at any of its points having the same orientation of the propagation of the disturbance, and $l', m',$ and n' are the direction cosines of any tangent τ to Σ at the same point, the orthogonality condition is expressed by:

$$ll' + mm' + nn' = 0 \quad (71)$$

The displacement $u = (u_1, u_2, u_3)$ must vanish at Σ ; hence for all directions satisfying eq. (71) it must be

$$\frac{\partial u_1}{\partial \tau} = \frac{\partial u_1}{\partial x_1} l' + \frac{\partial u_1}{\partial x_2} m' + \frac{\partial u_1}{\partial x_3} n' = 0$$

Therefore, for every point of Σ ,

$$l = k \frac{\partial u_1}{\partial x_1}$$

$$m = k \frac{\partial u_1}{\partial x_2}$$

$$n = k \frac{\partial u_1}{\partial x_3}$$

or

$$\frac{1}{l} \frac{\partial u_1}{\partial x_1} = \frac{1}{m} \frac{\partial u_1}{\partial x_2} = \frac{1}{n} \frac{\partial u_1}{\partial x_3} \equiv \frac{\partial u_1}{\partial v} \quad (72)$$

The same boundary conditions for the displacement must hold when the moving surface Σ reaches a new position after the time δt . At this time the coordinates of a point of Σ are :

$$x_1 + c l \delta t$$

$$x_2 + c m \delta t$$

$$x_3 + c n \delta t$$

where c is the velocity of the acoustic disturbance. Hence :

$$c \left\{ l \frac{\partial u_1}{\partial x_1} + m \frac{\partial u_1}{\partial x_2} + n \frac{\partial u_1}{\partial x_3} \right\} + \frac{\partial u_1}{\partial t} \equiv 0$$

From eq. (72) :

$$\frac{\partial u_1}{\partial x_1} = l \frac{\partial u_1}{\partial v}$$

and the analogous ones, so

$$c \frac{\partial u_1}{\partial v} + \frac{\partial u_1}{\partial t} = 0$$

Finally

$$\frac{\partial u_1}{\partial x_1} = \varepsilon_1 = -\frac{l}{c} \dot{u}_1$$

and

$$\begin{aligned} \varepsilon_2 &= -\frac{m}{c} \dot{u}_2 \\ \varepsilon_3 &= -\frac{n}{c} \dot{u}_3 \\ \varepsilon_4 &= -\frac{1}{c} (m \dot{u}_3 + n \dot{u}_2) \\ \varepsilon_5 &= -\frac{1}{c} (n \dot{u}_1 + l \dot{u}_3) \\ \varepsilon_6 &= -\frac{1}{c} (l \dot{u}_2 + m \dot{u}_1) \end{aligned} \tag{73}$$

The above are the kinematic conditions at Σ . The dynamic conditions are given by the equations of momentum:

$$\rho c \dot{u}_1 = X_1^{(\nu)}; \quad \rho c \dot{u}_2 = X_2^{(\nu)}; \quad \rho c \dot{u}_3 = X_3^{(\nu)} \tag{74}$$

where $X_1^{(\nu)}, X_2^{(\nu)}, X_3^{(\nu)}$ are the components of the force per unit area acting across Σ in direction ν .

Introducing the strain energy function W , eq. (74) may be rewritten as :

$$\begin{aligned}
-\rho c \dot{u}_1 &= \sigma_1 l + \sigma_6 m + \sigma_5 n = l \frac{\partial W}{\partial \epsilon_1} + m \frac{\partial W}{\partial \epsilon_6} + n \frac{\partial W}{\partial \epsilon_5} \\
-\rho c \dot{u}_2 &= l \frac{\partial W}{\partial \epsilon_2} + m \frac{\partial W}{\partial \epsilon_2} + n \frac{\partial W}{\partial \epsilon_4} \\
-\rho c \dot{u}_3 &= l \frac{\partial W}{\partial \epsilon_5} + m \frac{\partial W}{\partial \epsilon_4} + n \frac{\partial W}{\partial \epsilon_3}
\end{aligned} \tag{75}$$

The strain energy function for transversely isotropic media may be written as :

$$\begin{aligned}
2W &= C_{11} \epsilon_1^2 + C_{22} (\epsilon_2^2 + \epsilon_3^2) + 2C_{12} (\epsilon_2 \epsilon_1 + \epsilon_3 \epsilon_1) \\
&+ 2C_{23} \epsilon_2 \epsilon_3 + C_{66} (\epsilon_6^2 + \epsilon_5^2) + C_{44} \epsilon_4^2
\end{aligned} \tag{76}$$

If the components of the strain are replaced by the time derivative of the components of the displacement according to eq. (73), the strain energy function is written as :

$$\begin{aligned}
2Wc^2 &= C_{11} l^2 \dot{u}_1^2 + C_{22} (m^2 \dot{u}_2^2 + n^2 \dot{u}_3^2) \\
&+ 2C_{12} (lm \dot{u}_1 \dot{u}_2 + nl \dot{u}_3 \dot{u}_1) + 2C_{23} mn \dot{u}_2 \dot{u}_3 \\
&+ C_{66} [(l \dot{u}_2 + m \dot{u}_1)^2 + (n \dot{u}_1 + l \dot{u}_3)^2] + C_{44} (m \dot{u}_3 + n \dot{u}_2)^2
\end{aligned} \tag{77}$$

Accordingly, the strain energy is a homogeneous quadratic function of $\dot{u}_1, \dot{u}_2, \dot{u}_3$:

$$W = \frac{1}{2c^2} \left[\alpha_{11} \dot{u}_1^2 + \alpha_{22} \dot{u}_2^2 + \alpha_{33} \dot{u}_3^2 + 2\alpha_{23} \dot{u}_2 \dot{u}_3 + 2\alpha_{31} \dot{u}_3 \dot{u}_1 + 2\alpha_{12} \dot{u}_1 \dot{u}_2 \right] \tag{78}$$

where :

$$\alpha_{11} = c_{11} l^2 + c_{66} m^2 + c_{66} n^2$$

$$\alpha_{22} = c_{66} l^2 + c_{22} m^2 + c_{44} n^2$$

$$\alpha_{33} = c_{66} l^2 + c_{44} m^2 + c_{22} n^2$$

$$\alpha_{23} = (c_{23} + c_{44}) m n$$

(79)

$$\alpha_{31} = (c_{12} + c_{66}) n l$$

$$\alpha_{12} = (c_{12} + c_{66}) l m$$

Therefore, using eqs. (77), (73) and (76) one gets :

$$\begin{aligned} c^2 \frac{\partial W}{\partial \dot{u}_1} &= c_{11} l^2 \dot{u}_1 + c_{12} (l m \dot{u}_2 + n l \dot{u}_3) + \\ & c_{66} m (l \dot{u}_2 + m \dot{u}_1) + c_{66} n (n \dot{u}_1 + l \dot{u}_3) = \\ &= -c \left[l (c_{11} \varepsilon_1 + c_{12} \varepsilon_2 + c_{12} \varepsilon_3) + \right. \\ & \left. m c_{66} \varepsilon_6 + n c_{66} \varepsilon_5 \right] \end{aligned} \quad (80)$$

Consequently, by means of eq. (75) :

and the analogous

$$\frac{\partial W}{\partial \dot{u}_1} = \rho \dot{u}_1$$

$$\frac{\partial W}{\partial \dot{u}_2} = \rho \dot{u}_2$$

$$\frac{\partial W}{\partial \dot{u}_3} = \rho \dot{u}_3$$

In terms of the coefficients of the quadratic form (78) the above system of equations may be rewritten as

$$\begin{aligned} (\alpha_{11} - \rho c^2) \dot{u}_1 + \alpha_{12} \dot{u}_2 + \alpha_{31} \dot{u}_3 &= 0 \\ \alpha_{12} \dot{u}_1 + (\alpha_{22} - \rho c^2) \dot{u}_2 + \alpha_{23} \dot{u}_3 &= 0 \\ \alpha_{31} \dot{u}_1 + \alpha_{23} \dot{u}_2 + (\alpha_{33} - \rho c^2) \dot{u}_3 &= 0 \end{aligned} \quad (81)$$

Hence the determinantal equation,

$$\begin{vmatrix} \alpha_{11} - \rho c^2 & \alpha_{12} & \alpha_{31} \\ \alpha_{12} & \alpha_{22} - \rho c^2 & \alpha_{23} \\ \alpha_{31} & \alpha_{23} & \alpha_{33} - \rho c^2 \end{vmatrix} = 0 \quad (82)$$

is bicubic in c . The three pairs of roots represent the velocities of advancing and receding families of waves, one dilatational and two transverse polarized in planes parallel and perpendicular to the fibers orientation, depending upon the direction of the acoustic disturbance.

The velocity of sound, in the direction parallel and perpendicular to the orientation of the fibers, is calculated for a typical composite containing 30% plastic by volume. The elastic properties appearing in this section were thoroughly described in section IV-A of this report.

If α is the inner to outer diameter ratio of the fiber, the following table gives the elastic constants pertaining to various values of α :

α	K^* , psi	ν_{21}	E_1 , psi	G_{23}^* , psi	ρ , $\frac{\# \text{ sec}^2}{\text{in}^4}$
0	1.88×10^6	.238	7.47×10^6	0.677×10^6	2.025×10^{-4}
.2	1.82×10^6	.238	7.18×10^6	0.677×10^6	1.958×10^{-4}
.5	1.49×10^6	.238	5.63×10^6	0.652×10^6	1.608×10^{-4}
.75	0.94×10^6	.240	3.34×10^6	0.544×10^6	1.083×10^{-4}
.9	0.47×10^6	.244	1.52×10^6	0.356×10^6	0.673×10^{-4}
.9999	0.074×10^6	.350	0.120×10^6	0.0115×10^6	0.361×10^{-4}

A satisfactory analytical model which gives G_{12}^* has not been found yet. Therefore, in the following section the numerical results relative to the velocity of the acoustic disturbance across the material have been obtained for values of G_{12}^* corresponding to the following estimate of the upper bound: (Note that the dilatational wave velocity is independent of G_{12}^*)

$$G_{12}^* \leq \frac{E_1}{2(1+\nu_{21})}$$

The above parameters have been related to those strain energy coefficients, c_{ij} , which are of interest in the current analysis.

a. Sound velocity in the direction parallel to the fiber orientation

Eqs. (79) give the values of the coefficients, α_{ij} , corresponding to the direction of the acoustic disturbance, $l = 1$, $m = 0$, and $n = 0$. They are the following:

$$\alpha_{11} = C_{11}$$

$$\alpha_{22} = C_{66}$$

$$\alpha_{32} = C_{66}$$

$$\alpha_{23} = 0$$

$$\alpha_{31} = 0$$

$$\alpha_{12} = 0$$

Hence the determinantal eq. (82) gives

$$(C_{11} - \rho c^2) (C_{66} - \rho c^2)^2 = 0$$

Without considering the case

$$(C_{66} - \rho c^2)^2 = 0$$

corresponding to the transverse disturbances, Fig. IV-14 shows the velocity of the dilatational wave vs. the parameter α .

b. Sound velocity in the direction perpendicular to the fiber orientation

The values of α_{ij} corresponding to the disturbance traveling in the direction $l = 0, m = 1, n = 0$ are the following:

$$\alpha_{11} = C_{66}$$

$$\alpha_{22} = C_{22}$$

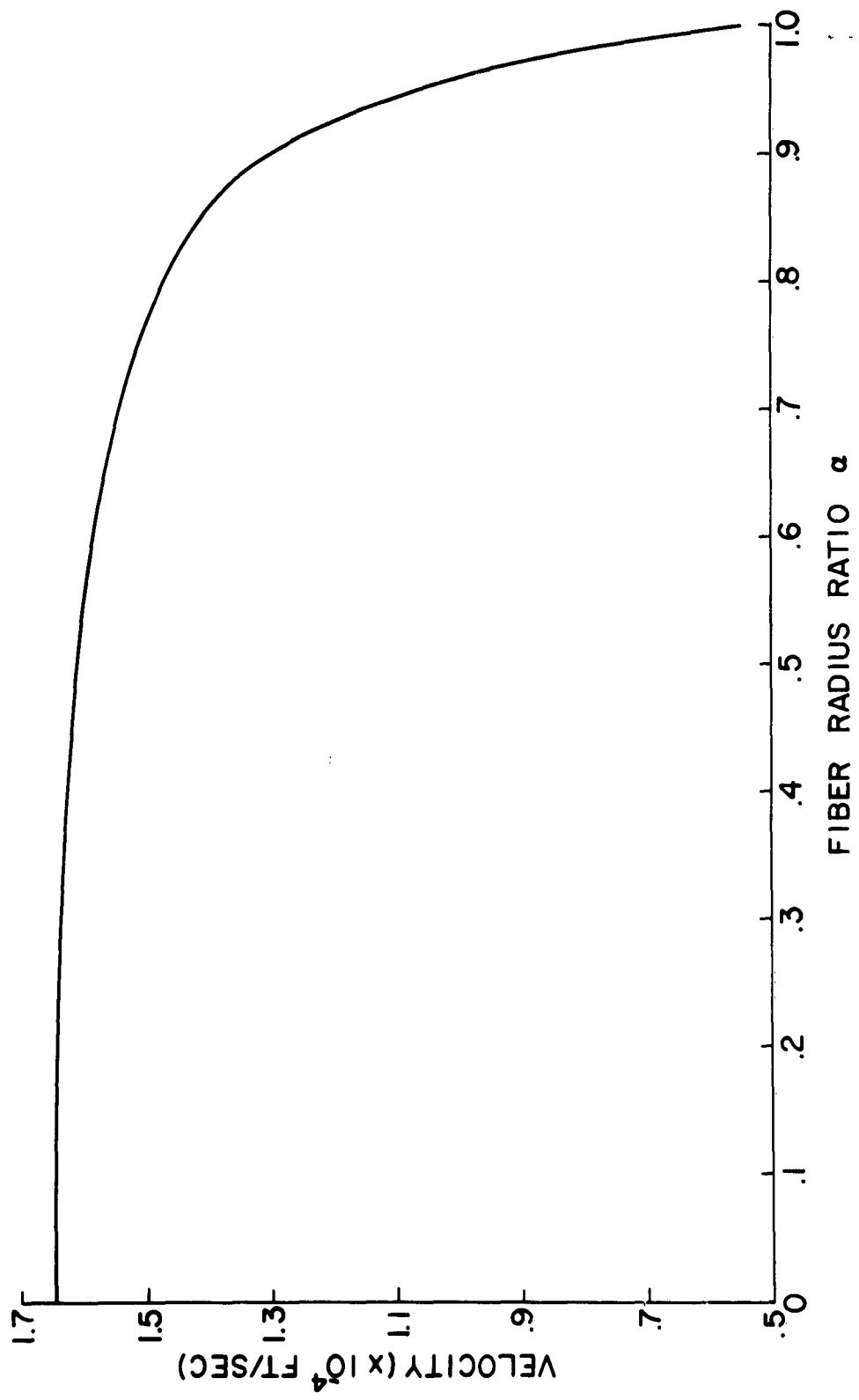


Fig. IV-14 Velocity of Sound in Direction Parallel to Fibers.

$$\alpha_{33} = C_{44}$$

$$\alpha_{23} = 0$$

$$\alpha_{3i} = 0$$

$$\alpha_{12} = 0$$

A plot of the acoustic velocity vs. the parameter α corresponding to this propagation is shown in Fig. IV-15.

It is seen that the velocity of sound increases with α up to $\alpha = 0.75$ at which $c = 9750$ ft/sec. Beyond this value of α the velocity rapidly decreases, until at $\alpha = 1$ the velocity is $c = 4090$ ft/sec. This is the velocity of sound for the plastic matrix containing the holes previously occupied by the fibers. This behavior of the velocity curve may be explained by considering that the glass fibers stiffen the plastic matrix in the transverse direction by virtue of their radial rigidity. As α increases in the region $0 \leq \alpha \leq 0.75$ the ratio of the radial stiffness to the density of the fiber increases because the material at the center of the fiber contributes less to its radial stiffness than does the material at the outer region.

Consequently the speed of sound increases within this range of α .

3. Acoustic impedance

The impedance for anisotropic media varies according to the direction of the acoustic wave, and it is defined as the product of the density by the sound velocity.

A plot of the impedance vs. the inner to outer diameter ratio of the fiber is shown in Fig. IV-16.

As before, the composite contains 30% binder by volume.

The impedance has been calculated in the direction perpendicular to the fibers orientation. The curve decreases regularly from the maximum $z = 22.72$ lb·sec/in³ corresponding to $\alpha = 0$ to the minimum $z = 1.77$ lb·sec/in³ for $\alpha = 1$, that is for the plastic matrix alone with the holes, but without the fibers.

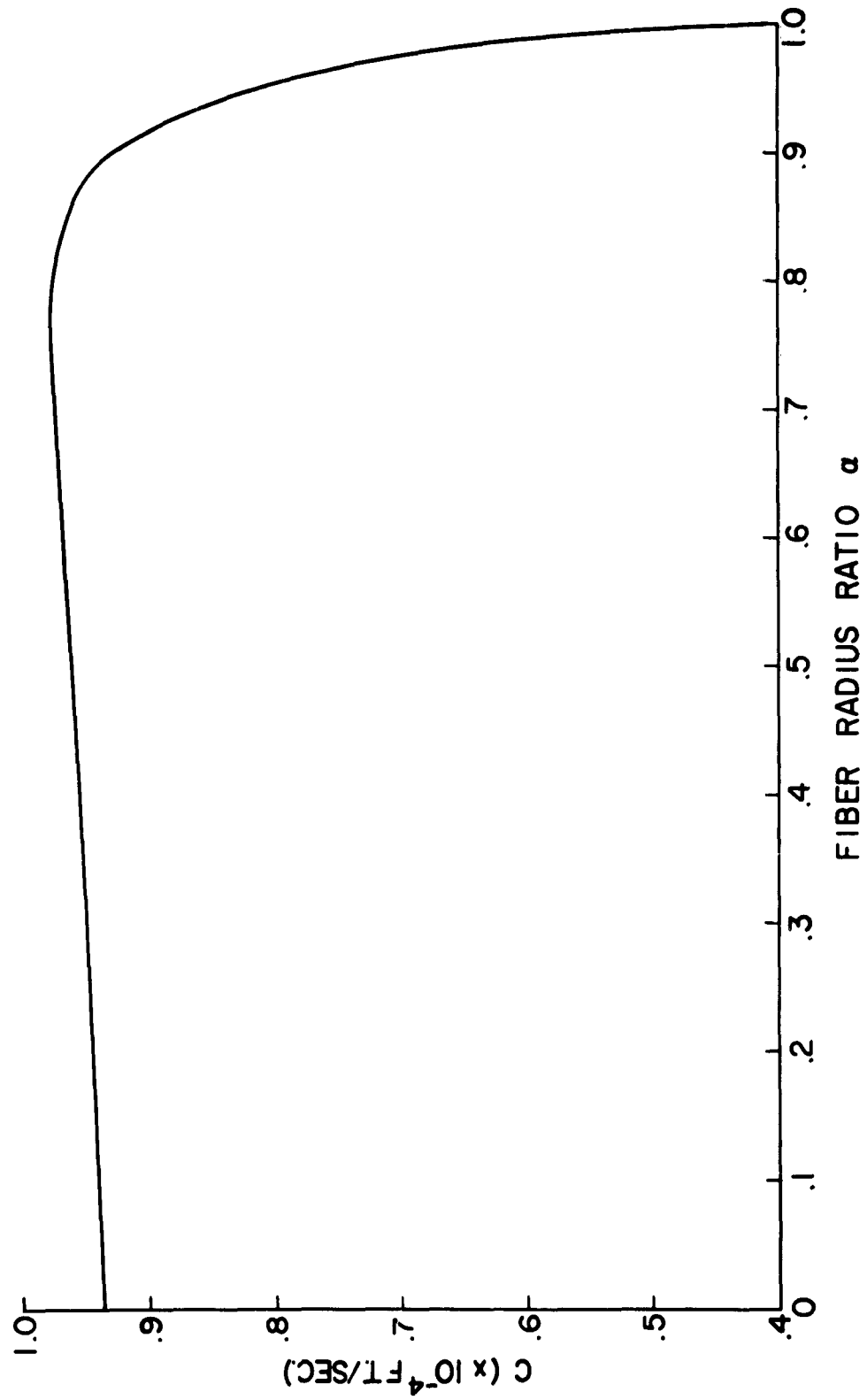


Fig. IV-15 Velocity of Sound in Direction Perpendicular to Fibers.

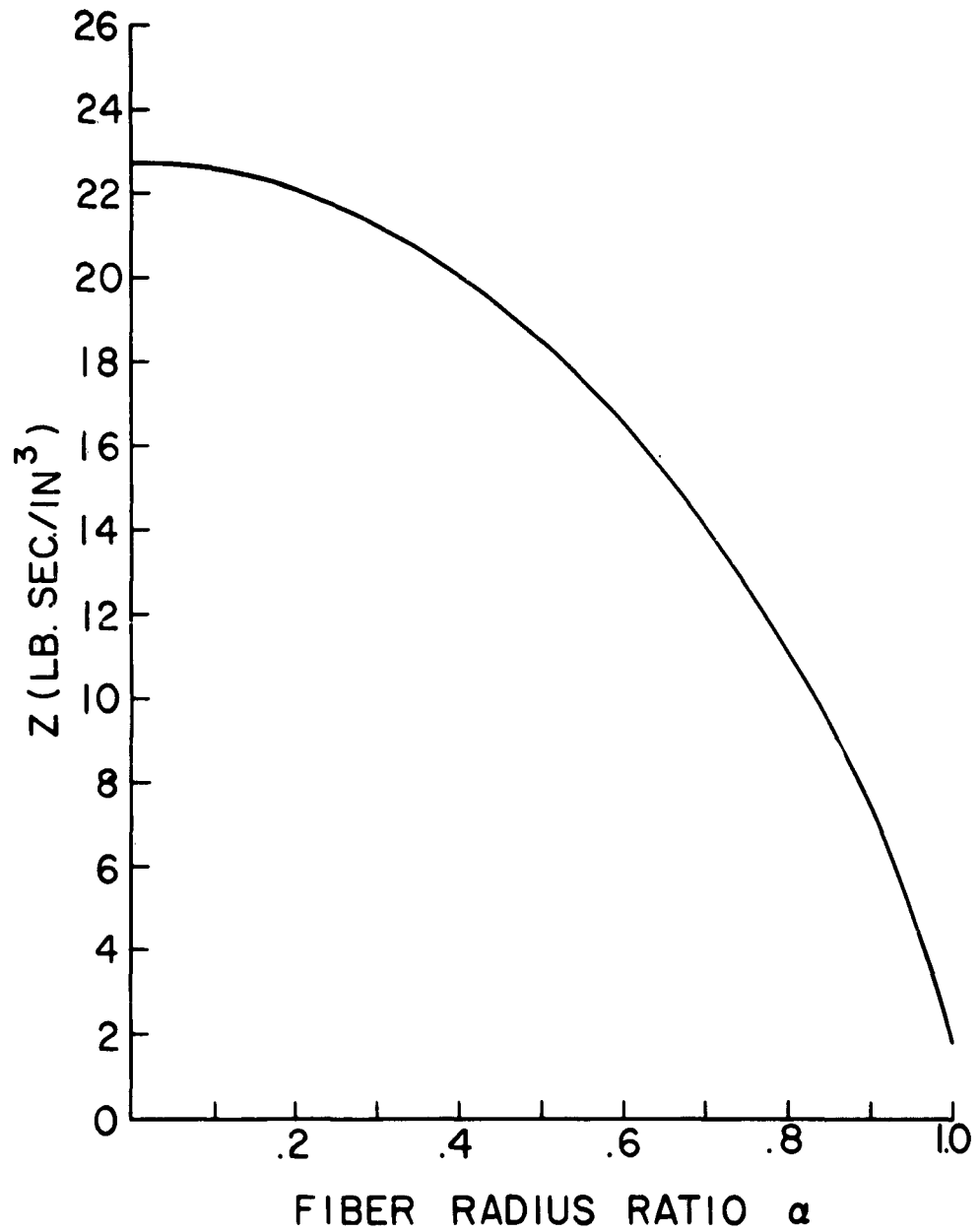


Fig. IV-16 Impedance in Direction Perpendicular to the Fibers.

Appendix A

TRANSVERSE ELASTIC MODULI OF TUBE REINFORCED MATERIALS

by Z. Hashin

1. Introduction

In the following, the problem of the prediction of the transverse elastic moduli of an elastic matrix reinforced by parallel tube shaped fibers, of another elastic material, will be considered.

Since the fibers are all circular and their cross sections are randomly distributed in any transverse plane normal to the fiber generators, it will be assumed that the material is isotropic and homogeneous in this plane. Accordingly, the transverse moduli are completely specified by an effective transverse bulk modulus and shear modulus.

The transverse plane will in the following be chosen as the x_2x_3 plane. The bulk and shear modulus are denoted by K^* and G^*_{23} . For reasons of simplicity, the effective shear modulus will, during the following treatment, be written as G^* .

The actual reinforced material will be treated by means of a simplified model. A cylindrical specimen of the composite (Fig. A-1) will be considered whose generators are parallel to the fiber axes. It will be assumed that the fibers extend from base to base of the specimen. Since the fiber diameters are very small compared to their lengths, it can be assumed that the cylinder will be in plane strain when tractions parallel to the transverse planes which do not vary with generator direction (x_1) are distributed on the cylindrical surface.

The transverse effective moduli can then be regarded as the plane strain moduli of the specimen and the problem is to determine these in terms of the elastic moduli and volume fractions of binder and fiber materials.

The method adopted here is analogous to one used for treatment of a related three dimensional problem of prediction of effective elastic moduli of composite materials (ref. 13)

2. General Method

In the following, a cylinder of composite material of unit thickness (Fig. A-2) will be considered. (+) Points in the transverse plane, normal to

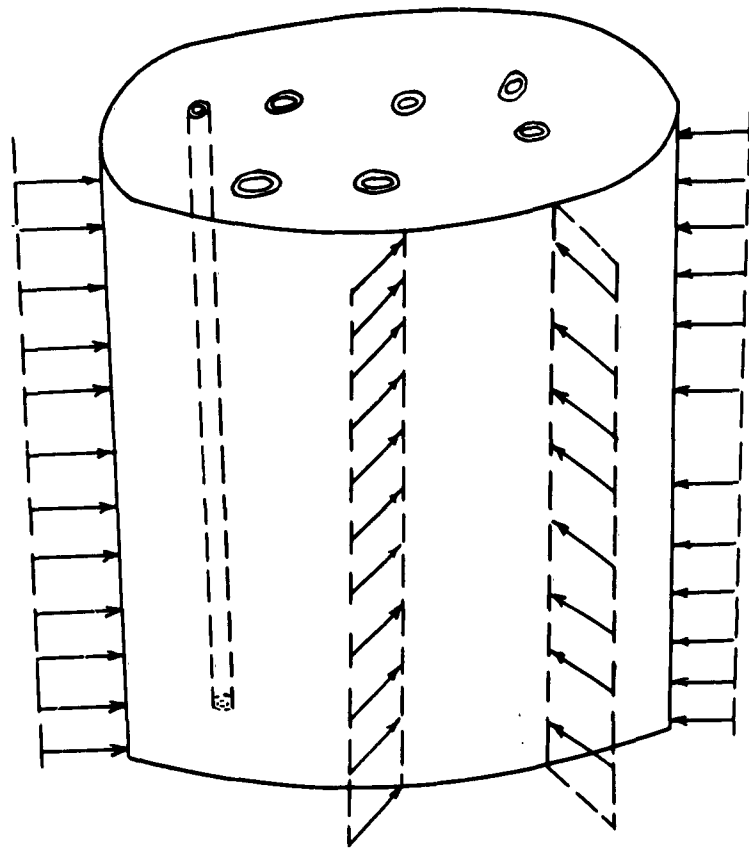


Fig. A-1 Model of Hollow Fiber Reinforced Matrix.

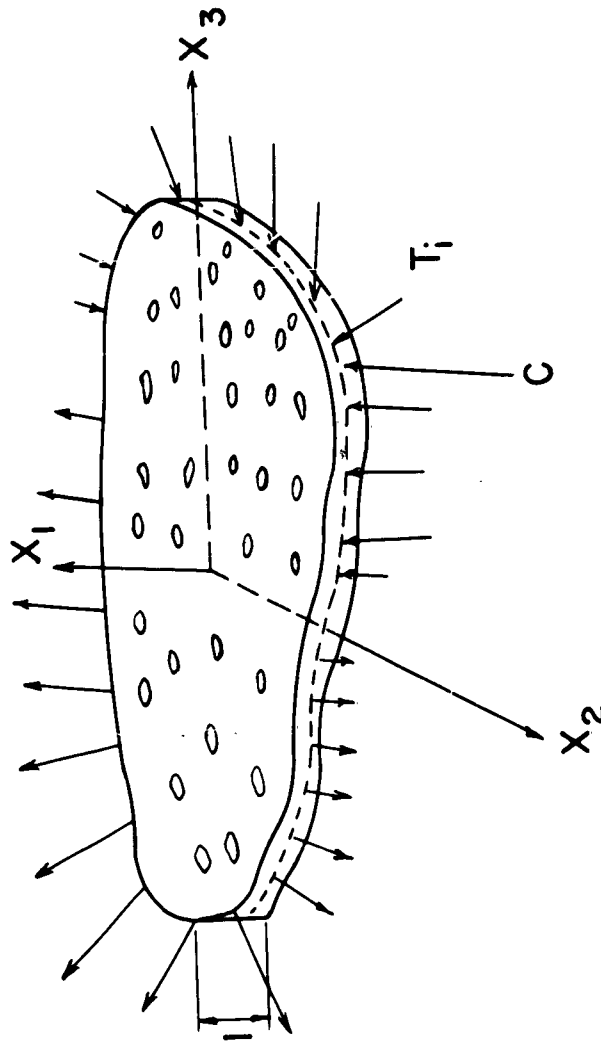


Fig. A-2 Composite Cylinder of Unit Thickness.

tube generators, will be related to an x_2, x_3 system of coordinates.

Assume that the cylinder of composite material has a cross section which is very large in comparison to the tube sections and denote the contour of this section by $C^{(++)}$ and the cylinder volume by V . Let C be loaded by tractions in the x_2, x_3 plane, which are independent of x_1 and are given by

$$T_i^0(C) \sigma_{ij}^0 n_j \quad (2.1)$$

where σ_{ij}^0 are constant stresses, n_j are the components of the outward normal to C and the range of the subscripts i, j is 2, 3. It can be proved that the mean stresses in V are then given by σ_{ij}^0 .

Now let it be assumed that plane displacements on C are prescribed which are of the form

$$u_i^0(C) = \epsilon_{ij}^0 x_j \quad (2.2)$$

where the ϵ_{ij}^0 are constant strains. It can then be proved that the mean strains in V are ϵ_{ij}^0 .

The assumed quasi-homogeneity of the composite will now be defined in the following way. Let a cylindrical element, whose bases coincide with those of the large cylinder be chosen. Let the base area of the large cylinder, contained in C , be denoted by A , that of the cylindrical element by A' and the area of a tube section by A'' . Let these areas be such that

$$A \gg A' \gg A'' \quad (2.3)$$

Then quasi-homogeneity implies that mean values of stresses and strains are the same in A and A' and moreover, that this holds independently of the location of the A' element.

The area A' is now chosen as unit area, then the A' element becomes one of unit volume and will, in the following, be referred to as the unit element.

-
- (+) Plane strain assumptions apply in the case of a very long, cylindrical body. The cylinder of unit thickness considered here may be regarded as a typical element of such a long cylinder.
- (++) Since the curved cylinder surface is of constant unit height. It is completely defined by the curve C and thus will be denoted by C in the following.

By the assumption of homogeneity and isotropy in the x_2, x_3 plane, the strain energy stored in the unit element, which is accordingly the strain energy density for the composite, will be assumed to be representable in the forms

$$W^*(\sigma) = \frac{\sigma^o{}^2}{2\bar{K}^*} + \frac{s^o{}_{ij} s^o{}_{ij}}{4G^*} \quad (2.4)$$

$$W^*(\epsilon) = 2\bar{K}^* \epsilon^o{}^2 + G^* e^o{}_{ij} e^o{}_{ij} \quad (2.5)$$

Here the stresses and strains have been split into isotropic and deviatoric parts as follows

$$\sigma^o{}_{ij} = \sigma^o \delta_{ij} + s^o{}_{ij} \quad (2.6)$$

$$\epsilon^o{}_{ij} = \epsilon^o \delta_{ij} + e^o{}_{ij} \quad (2.7)$$

where

$$\sigma^o = \frac{1}{2} \sigma^o{}_{kk} \quad (2.8)$$

$$\epsilon^o = \frac{1}{2} \epsilon^o{}_{kk} \quad (2.9)$$

It should be recalled that the range of the subscripts is 2, 3. A repeated subscript denotes summation and δ_{ij} are the Kronecker delta. The quantities \bar{K}^* and G^* are the effective bulk and shear moduli, respectively, of the composite. The bulk modulus \bar{K}^* for the present plane strain situation is given by

$$\bar{K}^* = \lambda^* + G^* \quad (2.10)$$

where λ^* is the Lamé modulus. (ref. 14)

It follows from the preceding that if the strain energy density of the composite can be computed by some means, in terms of the elastic moduli and volume fractions of tubes and matrix, then the effective elastic moduli can be determined from (2.4) and (2.5). However, calculation of the strain energy would require a detailed solution for the stresses or displacements in the composite under prescribed surface tractions or displacements, which seems to be an intractable problem.

In the present approach, this problem will be avoided and instead, bounds for the strain energy density, and thus for the effective elastic moduli, will be derived by use of the variational principles of the theory of elasticity.

Consider an elastic body of volume V and surface $S^{(+)}$ with prescribed

surface tractions $u_i^0(S)$ and let U^* be the actual strain energy stored in this body. Consider any displacement field u_i which satisfies the boundary conditions and necessary continuity requirements (2.2). Such a displacement usually called admissible. The "energy" $U(\epsilon)$ is defined by:

$$\tilde{U}(\epsilon) = \int_{(V)} (2\bar{K} \tilde{\epsilon}^2 + G \tilde{\epsilon}_{ij} \tilde{\epsilon}_{ij}) dV \quad (2.11)$$

where the strains $\tilde{\epsilon}_{ij}$ are derived from the u_i by

$$\tilde{\epsilon}_{ij} = \frac{1}{2} (\tilde{u}_{i,j} + \tilde{u}_{j,i}) \quad (2.12)$$

and have been split into isotropic and deviatoric parts (compare 2.7) when used in (2.11). \bar{K} and G are the elastic moduli of the body, which need not be constant in space.

The principle of minimum potential energy can, in the present case, be expressed by the inequality

$$U^* \leq \tilde{U}(\epsilon) \quad (2.13)$$

where the equality sign would hold if, and only if, \tilde{u}_i is the actual displacement field, satisfying also equilibrium.

For minimum complementary energy, consider an elastic body with prescribed surface tractions. Define an admissible stress system as one which satisfies the boundary and equilibrium conditions. Let such a stress system be denoted by $\tilde{\sigma}_{ij}$ and the "energy" $\tilde{U}(\sigma)$ be defined by

$$\tilde{U}(\sigma) = \int_{(V)} \left(\frac{\tilde{\sigma}^2}{2\bar{K}} + \frac{\tilde{s}_{ij} \tilde{s}_{ij}}{4G} \right) dV \quad (2.14)$$

where, again, isotropic and deviatoric components of the $\tilde{\sigma}_{ij}$ have been used and the elastic constants may be variable in space. The principle of minimum complementary energy can then be written in the form

$$U^* \leq \tilde{U}(\sigma) \quad (2.15)$$

where U^* is again the actual strain energy and equality holds if, and only if, the $\tilde{\sigma}_{ij}$ also satisfy necessary compatibility conditions.

(+) For present application, the body is a cylinder in plane strain. The surface S is the curved cylinder surface C . As long as plane strain conditions are satisfied, the cylinder bases A need not be incorporated in S .

The main problem in the application of the variational principles is the suitable choice of admissible stress and displacement fields. These will be chosen in the following way.

Let it be assumed, for example, that a plane traction system of form (2.1) parallel to the x_2, x_3 plane, is applied to the surface of a cylinder of composite material. Let this cylinder be subdivided into composite cylinders each of which contains one tube (Fig. A-3). Furthermore, the ratio of fiber volume to binder volume is the same in all composite tubes. Such a subdivision into composite tubes can be carried out in an infinity of ways and it will here be assumed that this has been done so that the transverse sections approach circles as nearly as possible.

Assume that a set of boundary displacements of the form (2.2) is applied to all the surfaces of the composite cylinders and thus also to the outer surface C of the large cylinder since this surface consists of parts of composite cylinder surfaces. If the displacement fields in all composite cylinders are found, subject to these boundary conditions, then all these fields will constitute an admissible displacement field for the whole composite body. (+)

In order to find an admissible stress field, assume that tractions of the form (2.1) are applied to all composite cylinder surfaces. If now the stresses in all composite cylinders are found, subject to these boundary conditions, then all these stress fields will satisfy boundary conditions and equilibrium for the whole composite cylindrical body and will thus constitute an admissible field.

Such a solution can obviously not be carried out for arbitrary sections of composite cylinders and it will accordingly be assumed that each composite cylinder can be approximated by a tubular fiber surrounded by a concentric cylindrical shell of binder material so that volumes are preserved. (Fig. A-3)

In order to obtain separate bounds for the bulk and shear modulus of the composite, it will be found convenient to separate stresses and strains in

(+) The total displacement field will thus be made up of different parts in different regions. At region interfaces continuity of the displacement vector will have to be satisfied. It can be shown that the principle of minimum potential energy holds for such a displacement field. Similarly, the principle of minimum complementary energy can be extended to the case of different stress fields in different regions, when the tractions are continuous across the region interfaces.

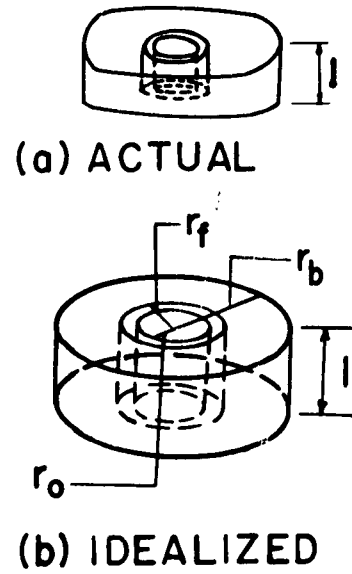


Fig. A-3 Typical Element of Composite Material.

(2.1) and (2.2) into isotropic and deviatoric components and apply the two parts of tractions and displacements thus found separately. This will be done in the following.

It should be borne in mind that because of the idealization of the composite element to circular cylindrical shape, the bounds derived will be of an approximate nature.

3. Effective Transverse Bulk Modulus \bar{K}^*

According to the procedure outlined above, a traction system in the x_2, x_3 plane of the form

$$T_i^o = \sigma^o n_i \quad (3.1)$$

associated with the isotropic stress system

$$\sigma_{ij}^o = \sigma^o \delta_{ij} \quad (3.2)$$

is applied to C and accordingly to all the surfaces of the composite cylinders where it assumes the form

$$\sigma_{rr}^o = \sigma^o \quad (3.3)$$

in cylindrical coordinates.

A radially symmetric plane strain problem for the circular composite cylinder is thus defined. The general solution to such a problem is well known and can be written down in the following form

$$u_r^b = A_b r + \frac{B_b}{r} \quad (3.4)$$

$$\sigma_{rr}^b = 2\bar{K}_b A_b - 2G_b \frac{B_b}{r^2} \quad (3.5)$$

$$u_r^f = A_f r + \frac{B_f}{r} \quad (3.6)$$

$$\sigma_{rr}^f = 2\bar{K}_f A_f - 2G_f \frac{B_f}{r^2} \quad (3.7)$$

Here b refers to binder and f to tubular fiber, u_r and σ_{rr} are radial displacement and radial stress respectively, A_b , B_b , A_f , and B_f are arbitrary constants and the different radii are indicated in Fig. A-3.

The boundary conditions to be satisfied are

$$\sigma_{rr}^b = \sigma^o, \quad r = r_b \quad (3.8)$$

$$u_r^b = u_r^f \quad (3.9)$$

$$\sigma_{rr}^b = \sigma_{rr}^f \quad (3.10)$$

$$\sigma_{rr}^f = 0 \quad r = r_o \quad (3.11)$$

The four boundary conditions expressed in terms of (3.4 - 7) give a set of four linear equations for the arbitrary constants. The solution is thus completely defined.

The strain energy stored in the composite cylinder is then given by

$$U_c^{(\sigma)} = \frac{1}{2} \int_{r=r_b} u_r^b \sigma_{rr}^b r_b d\theta \quad (3.12)$$

which in the present radially symmetric case simplifies to

$$U_c^{(\sigma)} = \pi r_b u_r^b(r_b) \sigma_{rr}^b(r_b) \quad (3.13)$$

From the solution of the boundary value problem, $u_r^b(r_b)$ is found to be

$$u_r^b(r_b) = \frac{\sigma^o r_b}{2K_b} \left\{ 1 - \frac{v_t(1+2v_b) \left[\phi(1-\alpha^2) - \left(1 + \frac{\alpha^2}{2v_t} \right) \right]}{\phi(1-\alpha^2)(1+2v_b \frac{v_t}{\phi}) + 2v_b v_b \left(1 + \frac{\alpha^2}{2v_t} \right)} \right\} \quad (3.14)$$

Here

$$\alpha = \frac{r_o}{r_f} \quad (3.15)$$

$$v_t = \left(\frac{r_f}{r_b} \right)^2 \quad (3.16)$$

$$\phi = \frac{\bar{K}_f}{K_b} \quad (3.17)$$

and ν_f and ν_b are the Poisson's ratios of fiber and binder materials respectively.

Under the present assumptions, the complementary energy for the composite is then given by

$$\tilde{U}(\sigma) = \sum_c U_c(\sigma) \quad (3.18)$$

where the summation extends over all composite cylinders and $u_r^b(r_b)$ and $\sigma_{rr}^{(b)}(r_b)$ in (3.13) are given by (3.14) and (3.8) respectively.

The actual strain energy stored in the composite material, when (3.1) is applied to the boundary, is given, with the use of (2.4) by

$$U^* = \frac{\sigma_0^2}{2\bar{K}^*} V \quad (3.19)$$

where V is the total volume including binder, tubular fibers and their inner voids. Writing (3.18) in the form

$$\tilde{U}(\sigma) = \frac{\sigma_0^2}{2\bar{K}_1^*} V \quad (3.20)$$

and introducing (3.19) and (3.20) into (2.15), \bar{K}_1^* becomes a lower bound for \bar{K}^* and is found to be

$$\bar{K}_1^* = \bar{K}_b \frac{\rho(1-\alpha^2)(1+2\nu_b\nu_f) + (1 + \frac{\alpha^2}{2\nu_f})(2\nu_b\nu_f)}{\rho\nu_b(1-\alpha^2) + (1 + \frac{\alpha^2}{2\nu_f})(2\nu_b + \nu_f)} \quad (3.21)$$

In order to find an upper bound for \bar{K}^* , the composite material is investigated for a surface displacement of the form

$$u_i^0 = \epsilon^0 x_i \quad (3.22)$$

where $\epsilon^0 \delta_{ij}$ is the isotropic part of the strains associated with (2.2). In order to get an admissible displacement system, it is assumed that all composite circular cylinders, defined above, are subjected to a surface displacement of the form (3.22) with respect to a coordinate system x_2, x_3 in the transverse plane, common to all the tubes.

If (3.22) is transformed to a local coordinate system whose origin is at the center of a tubular fiber, it becomes a surface displacement at $r = r_b$, of the form (3.22) and a rigid body displacement which does not contribute to the stresses. Accordingly, only the boundary value problem of a composite cylinder with surface displacement (3.22), with respect to its axis, needs

to be considered.

In polar co-ordinates, (3.22) assumes the form

$$u_r^o(r_b) = \epsilon^o r_b \quad (3.23)$$

The boundary value problem to be solved is now analogous to the one considered above. The only change is replacement of (3.8) by (3.23). The displacement fields in all composite cylinders, resulting from this boundary value problem, form an admissible displacement field for the composite material.

The energy, $U_p^{(\epsilon)}$, stored in a composite cylinder, is again given by (3.13). At present $u_r^b(r_b)$ is given by (3.23) and $\sigma_{rr}^b(r_b)$ is given from the displacement boundary value problem by

$$\sigma_{rr}^b(r_b) = 2\epsilon^o \bar{K}_b \frac{\phi(1-\alpha^2)(1+2\nu_b\nu_t) + (1+\frac{\alpha^2}{2\nu_t})(2\nu_b\nu_b)}{\phi\nu_b(1-\alpha^2) + (1+\frac{\alpha^2}{2\nu_t})(2\nu_b + \nu_t)} \quad (3.24)$$

The energy $\tilde{U}^{(\epsilon)}$ is now computed by

$$\tilde{U}^{(\epsilon)} = \sum_p U_p^{(\epsilon)} \quad (3.25)$$

and is then set equal to

$$\tilde{U}^{(\epsilon)} = 2\bar{K}_2^* \epsilon^{o2} V \quad (3.26)$$

According to (2.5), U^* can be written as

$$U^* = \bar{K}^* \epsilon^{o2} V \quad (3.27)$$

whence introducing (3.26 and (3.27) into (2.13), \bar{K}_2^* becomes an upper bound for \bar{K}^* . Carrying out the calculation it is found that \bar{K}_2^* is also given by (3.21). Hence the lower and upper bounds coincide and the effective bulk modulus is also given by (3.21).

It should be realized that this does not mean that an exact result for the effective bulk modulus has been found because of the replacement of composite cylinders of arbitrary cross sections by circular ones. However, it is to be expected that (3.21) should be a good approximation for \bar{K}^* .

A similar method employed in a three dimensional case (ref. 13) has yielded results which checked well with experimental measurements.

4. Bounds for the Effective Shear Modulus G^*

The method to be used is essentially the same as for the bulk modulus. However, the mathematical difficulties encountered are much more serious and it will not be possible to give results in closed form. Also, the bounds obtained for the shear modulus do not generally coincide.

Let tractions T_i^0 , derived from a pure shear stress in the x_2, x_3 plane, be applied to the surface C of the large cylinder (Fig. A-2). Such a traction system can be given in the form

$$\begin{aligned} T_2^0 &= \tau^0 n_3 \\ T_3^0 &= \tau^0 n_2 \end{aligned} \quad (4.1)$$

where τ^0 is the shear stress and n_2 and n_3 are the components of the unit outward normal to C .

According to the present interpretation of quasi-homogeneity and quasi-isotropy, the strain energy stored in the cylinder can be expressed with the aid of (2.4) in the form

$$U^*(\sigma) = \frac{\tau^{02}}{2G^*} V \quad (4.2)$$

Analogously, a displacement u_i^0 , associated with a pure shear strain $\frac{\gamma^0}{2}$ in the x_2, x_3 plane, is applied to C . Such a displacement has the form

$$\begin{aligned} u_2^0 &= \frac{\gamma^0}{2} x_3 \\ u_3^0 &= -\frac{\gamma^0}{2} x_2 \end{aligned} \quad (4.3)$$

and the strain energy stored in the cylinder can then be given, with the aid of (2.5), in the form,

$$U^*(\epsilon) = \frac{G^* \gamma^{02}}{2} V \quad (4.4)$$

In order to derive a lower bound for the effective shear modulus, the tractions (4.1) are applied to the surfaces of all composite cylinders. The boundary value problem for the composite circular cylinder is then as follows: Solve the plane systems of differential equations of the theory of elasticity.

$$u_{j,ji}^b + (1 - 2\nu_b) \nabla_b^2 u_i^b = 0 \text{ in } R_b \quad (4.5)$$

$$u_{j,ji}^f + (1 - 2\nu_b) \nabla_b^2 u_i^f = 0 \text{ in } R_f \quad (4.6)$$

where u_i^b and u_i^f are the displacement components in binder and fiber respectively, ∇^2 denotes the Laplace operator in the x_2, x_3 plane, R_b is the binder region $r_f \leq r \leq r_b$ and R_f is the fiber region $r_0 \leq r \leq r_f$.

The solution must satisfy the following boundary conditions:

$$T_i^b = T_i^o \quad r = r_b \quad (4.7)$$

$$u_i^b = u_i^f \quad (4.8)$$

$$T_i^b = T_i^f \quad (4.9)$$

$$T_i^f = 0 \quad r = r_0 \quad (4.10)$$

Here T_i^b and T_i^f are the tractions in binder and matrix, respectively, T_i^o is given by (4.1), eqs. (4.8-9) are continuity conditions at binder-fiber interface and (4.10) expresses the fact that the fiber contains an unloaded void. In order to find an upper bound, the displacements (4.3) are applied to the surfaces of the composite cylinders. The boundary value problem for the circular composite cylinder has then to be modified only by replacement of (4.7) by

$$u_i^b = u_i^o \quad (4.11)$$

where u_i^o is given by (4.3).

These two boundary value problems can be solved exactly and in closed form in terms of plane harmonics. The solution is outlined in the following section. Here, only the results which are needed for the establishment of bounds will be given.

Having found the solutions for the circular composite cylinder, the bounds for the effective shear modulus can be found by exactly the same method used for the bulk modulus in Section 3. The strain energy stored in a composite circular cylinder is evaluated for both boundary value problems and is summed over all composite cylinders. These energies are then used in inequalities (2.13) and (2.15) as $\tilde{U}(\sigma)$ and $\tilde{U}(\epsilon)$. The energy U^* is in one case given by (4.2) and in the other by (4.4). Thus, a lower and upper bound are obtained.

These bounds are given in the following form:

$$G_1^* = \frac{G_b}{1 + \frac{2(1-\nu_b)\nu_f A_+^\sigma}{1-2\nu_b}} \quad (4.12)$$

$$G_2^* = G_b \left[1 - \frac{2(1-\nu_b)\nu_f}{1-2\nu_b} A_4^e \right] \quad (4.13)$$

where A_4^σ and A_4^e are defined by systems of equations (20-29) in section (5). The effective shear modulus G^* satisfies the inequality

$$G_1^* \leq G^* \leq G_2^* \quad (4.14)$$

5. Problem of Sheared Composite Cylinder

In order to derive bounds for the shear modulus, it is necessary to solve the boundary value problem given by (4.5-10) and the one where (4.7) is replaced by (4.11).

A general formulation for elastic plane strain problems is provided by the method of complex functions, however, in the present case it is more convenient to use another method of solution, in terms of plane harmonics. Plane harmonic functions are defined as homogeneous polynomials which satisfy the two dimensional Laplace equation. The two dimensional ring problem can be solved in general with the aid of such functions (ref. 8-15). It may be shown that in the present case, the solution for the displacement vector can be given in terms of the plane harmonic $x_2 x_3$ in the following form:

$$\vec{u} = \bar{A}_1 \vec{u}^1 + \bar{A}_2 \vec{u}^2 + \bar{A}_3 \vec{u}^3 + \bar{A}_4 \vec{u}^4 \quad (5.1)$$

where

$$\vec{u}^1 = \text{grad}(x_2 x_3) \quad (5.2)$$

$$\vec{u}^2 = r^2 \text{grad}(x_2 x_3) + \alpha_2 x_2 x_3 \vec{r} \quad (5.3)$$

$$\vec{u}^3 = \text{grad}\left(\frac{x_2 x_3}{r^4}\right) \quad (5.4)$$

$$\vec{u}^4 = r^2 \text{grad}\left(\frac{x_2 x_3}{r^4}\right) + \alpha_{-2} \frac{x_2 x_3}{r^4} \vec{r} \quad (5.5)$$

Here

$$r^2 = x_2^2 + x_3^2 \quad (5.6)$$

$$\alpha_2 = -2 \frac{3-4\nu}{3-2\nu} \quad (5.7)$$

$$\alpha_{-2} = 2 \frac{3-4\nu}{1-2\nu} \quad (5.8)$$

where ν is the Poisson's ratio. The solutions for the binder ring and the fiber ring are obtained by substituting the appropriate Poisson's ratios. The solution for the composite tube thus involves eight arbitrary constants which have to be determined from the boundary conditions of the problem. In order to do this the displacements and tractions have to be given in detail.

The dimensional constants in (1) are first replaced by the nondimensional constants

$$A_1 = \bar{A}_1 \quad (5.9)$$

$$A_2 = \bar{A}_2 r_f^2 \quad (5.10)$$

$$A_3 = \frac{\bar{A}_3}{r_i^4} \quad (5.11)$$

$$A_4 = \frac{\bar{A}_4}{r_f^2} \quad (5.12)$$

A straight forward calculation then yields the following displacements. In the binder

$$\begin{aligned} u_2^b &= (A_1 + \rho^2 A_2 + \rho^{-4} A_3 + \rho^{-2} A_4) x_3 \\ &+ \left(-2 \frac{3 - 4\nu_b}{3 - 2\nu_b} \rho^2 A_2 - 4 \rho^{-4} A_3 + \frac{2}{1 - 2\nu_b} \rho^{-2} A_4\right) \frac{x_2^2 x_3}{r^2} \end{aligned} \quad (5.13)$$

Here ρ is given by

$$\rho = \frac{r}{r_f} \quad (5.14)$$

and the displacement component u_3^b in x_3 direction is simply obtained by interchanging x_2 and x_3 in (13).

The displacements in the fiber are given by:

$$\begin{aligned} u_2^f &= (B_1 + \rho^2 B_2 + \rho^{-4} B_3 + \rho^{-2} B_4) x_3 \\ &+ \left(-2 \frac{3 - 4\nu_f}{3 - 2\nu_f} \rho^2 B_2 - 4 \rho^{-4} B_3 + \frac{2}{1 - 2\nu_f} \rho^{-2} B_4\right) \frac{x_2^2 x_3}{r^2} \end{aligned} \quad (5.15)$$

where, again, u_3^f is defined by co-ordinate interchange.

The strains can now be computed by differentiation of the displacements, whence the stresses can be found from Hooke's law. The tractions on a circle are defined in terms of the stresses by

$$T_i = \sigma_{ij} \frac{x_j}{r} \quad (5.16)$$

where x_j are the co-ordinates of a point on the circle of radius r .

Accordingly, the tractions on a circle in the binder have the form

$$\begin{aligned} T_2^b &= 2G_b \left(A_1 + \frac{3}{3-2\nu_b} \rho^2 A_2 - 3 \rho^{-4} A_3 + \frac{1}{1-2\nu_b} \rho^{-2} A_4 \right) \frac{x_3}{r} \\ &+ 12G_b \left(-\frac{1}{3-2\nu_b} \rho^2 A_2 + 2 \rho^{-4} A_3 - \frac{1}{1-2\nu_b} \rho^{-2} A_4 \right) \frac{x_2 x_3}{r^3} \end{aligned} \quad (5.17)$$

where the other traction component T_3^b is found from (5.17) by co-ordinate interchange. The tractions in the fiber can be written down by replacing G_b and ν_b by G_f and ν_f and the A's by the B's.

In the foregoing solution, each displacement and traction component contains two co-ordinate functions. Thus, fulfillment of a boundary condition on a circle will yield equations for the coefficients of these functions, which involve the unknown constants. It should be realized, from the form of these expressions, that if a boundary condition is satisfied for one component of a displacement or traction, the same condition is automatically satisfied for the other component. Since in each boundary value problem there are four boundary conditions, eight linear equations for the unknown constants will be obtained in each case, which is exactly the required number. These equations will now be given for each boundary value problem. For convenience, the unknown constants are redefined. For the stress boundary value problem define

$$A_i^{(\sigma)}, B_i^{(\sigma)} = \frac{2G_b}{\tau^0} (A_i, B_i) \quad i = 1, 2, 3, 4 \quad (5.18)$$

where τ^0 is defined by (4.1).

For the displacement boundary value problem define

$$A_i^{(\epsilon)}, B_i^{(\epsilon)} = \frac{2}{\gamma^0} (A_i, B_i) \quad i = 1, 2, 3, 4 \quad (5.19)$$

where γ^0 is defined by (4.3).

The A_i , B_i satisfy the following set of equations:

$$A_1^\sigma + \frac{3}{(3-2\nu_b)\nu_b} A_2^\sigma - 3\nu_b^2 A_3^\sigma + \frac{\nu_c}{1-2\nu_b} A_4^\sigma = 1 \quad (5.20)$$

$$-\frac{1}{(3-2\nu_b)\nu_b} A_2^\sigma + 2\nu_b^2 A_3^\sigma - \frac{\nu_c}{1-2\nu_b} A_4^\sigma = 0 \quad (5.21)$$

$$A_1^\sigma + A_2^\sigma + A_3^\sigma + A_4^\sigma - B_1^\sigma - B_2^\sigma - B_3^\sigma - B_4^\sigma = 0 \quad (5.22)$$

$$-\frac{3-4\nu_b}{3-2\nu_b} A_2^\sigma - 2A_3^\sigma + \frac{1}{1-2\nu_b} A_4^\sigma + \frac{3-4\nu_b}{3-2\nu_b} B_2^\sigma + 2B_3^\sigma - \frac{1}{1-2\nu_b} B_4^\sigma = 0 \quad (5.23)$$

$$A_1^\sigma + \frac{3}{3-2\nu_b} A_2^\sigma - 3A_3^\sigma + \frac{1}{1-2\nu_b} A_4^\sigma - \mu B_1^\sigma - \frac{3\mu}{3-2\nu_b} B_2^\sigma + 3\mu B_3^\sigma - \frac{\mu}{1-2\nu_b} B_4^\sigma = 0 \quad (5.24)$$

$$-\frac{1}{3-2\nu_b} A_2^\sigma + 2A_3^\sigma - \frac{1}{1-2\nu_b} A_4^\sigma + \frac{\mu}{3-2\nu_b} B_2^\sigma - 2\mu B_3^\sigma + \frac{\mu}{1-2\nu_b} B_4^\sigma = 0 \quad (5.25)$$

$$B_1^\sigma + \frac{3\alpha^2}{3-2\nu_b} B_2^\sigma - 3\alpha^{-1} B_3^\sigma + \frac{\alpha^{-2}}{1-2\nu_b} B_4^\sigma = 0 \quad (5.26)$$

$$-\frac{\alpha^2}{3-2\nu_b} B_2^\sigma + 2\alpha^{-1} B_3^\sigma - \frac{\alpha^{-2}}{1-2\nu_b} B_4^\sigma = 0 \quad (5.27)$$

where $\mu = \frac{C_f}{C_b}$

Each pair of these equations is derived from one boundary condition and the order of equations corresponds to the order of the boundary conditions (4.7-10).

For the displacement problem, (4.11) is prescribed at $r = r_b$. Consequently, only eqns. (20) and (21) change. They have to be replaced by

$$A_1^{(\epsilon)} + \nu_t^{-1} A_2^{(\epsilon)} + \nu_t^2 A_3^{(\epsilon)} + \nu_t A_4^{(\epsilon)} = 1 \quad (5.28)$$

$$- \frac{(3 - 4\nu_b)}{3 - 2\nu_b} \nu_t^{-1} A_2^{(\epsilon)} - 2 \nu_t^2 A_3^{(\epsilon)} + \frac{1}{1 - 2\nu_b} \nu_t A_4^{(\epsilon)} = 0 \quad (5.29)$$

whereas the coefficients in the other six equations are the same as in (5.22 - 5.27).

The solution for solid fiber inclusions is readily obtained from the above solution. The boundary condition (4.10) is deleted and the associated constants B_3 and B_4 are zero. Consequently, the boundary condition equations 5.26 and 5.27 do not exist. The result is a set of six simultaneous linear equations and again the resulting values of A_4 and A_4 are used in eqs. 4.12 and 4.13 to define G^* .

References

1. Timoshenko, S. and Goodier, J. N., "Theory of Elasticity," McGraw Hill, New York, 1951.
2. Rosen, B. W., "Elastic Constants of Laminates of Orthotropic Plates," Space Mechanics Memo #112, General Electric Co., June 1962.
3. Dow, N. F. and Gruntfest, I. J., "Determination of Most Needed, Potentially Possible Improvements in Materials for Ballistic and Space Vehicles," General Electric Co. TIS Report No. 60SD389, June 1960.
4. "Improvement of Reinforced Plastics," Quarterly Progress Reports, No. 1, October, 1961; No. 2, January 1962; No. 3, April, 1962; No. 4, June, 1962; and No. 5, October 30, 1962; prepared by the General Electric Company, Missile and Space Division, under U. S. Navy, Bureau of Naval Weapons, Contract NOW 61-0613-d.
5. Lorsch, H. G., "Buckling Tests of Plastic Specimens Reinforced by Hollow or Solid Glass Fibers," Final Report, Contract NOTS 60530/4064Y6598-61, General Electric Company, July 1961.
6. Pulos, J. G., and Buhl, J. A., Jr., "Hydrostatic Pressure Tests of an Unstiffened Cylindrical Shell of a Glass Fiber Reinforced Epoxy Resin," David Taylor Model Basin Report No. 1414, April 1960.
7. Timoshenko, S., "Theory of Elastic Stability," McGraw Hill, New York, 1936.
8. Love, A. E. H., "A Treatise on the Mathematical Theory of Elasticity," Dover, New York, 1944.
9. Friedlander, F. G., "Sound Pulse," Cambridge Press.
10. Ewing, W. M., Jardetzky, W. S., and Press, F., "Elastic Waves in Layered Media," McGraw Hill Co.
11. Mason, W. P., "Physical Acoustics and the Properties of Solids," Van Nostrand Co.
12. Morse, P. M., "Vibration and Sound," McGraw Hill Co.

13. Hashin, Z., "The Elastic Moduli of Heterogeneous Materials," Journ. Appl. Mech. Trans., ASME, Vol. 29E, pp. 143-150, (1962).
14. Sokolnikoff, I. S., "Mathematical Theory of Elasticity," McGraw-Hill New York, (1956).
15. Goodier, J. N., "Concentration of Stress Around Spherical Inclusions and Flaws," Journ. Appl. Mech. Trans., ASME, Vol. 55, A-39, (1933).
16. Timoshenko, S., "Strength of Materials," Part II, Van Nostrand, New York (1941).

Key to Nomenclature

A	Area
d	Diameter
E	Young's modulus of elasticity
G	Shear modulus of elasticity
K	Bulk modulus of elasticity
\bar{K}	Bulk modulus of elasticity in plane strain
l	Fiber length
M	Ratio of moduli of hollow fiber to solid fiber composites
N	Ratio of densities of hollow fiber to solid fiber composites
P	Force
r	Radius
r_o	Void radius
r_f	Fiber radius
s	Deviatoric stress
T	Traction
u	Displacement
U	Strain energy
v	Volume fraction of constituent relative to total composite
v_o	Volume fraction of voids
v_b	Volume fraction of binder material
v_f	Volume fraction of fiber material
v_t	Volume fraction of fiber tubes: $v_t = v_f + v_o$
w_b	Weight fraction of binder material
w_f	Weight fraction of fiber material

α	Fiber radius ratio	$\alpha = r_o/r_f$
ϵ	Strain	
ν	Poisson's ratio	
ν_{ij}	Poisson's ratio for anisotropic material, negative of ratio of strain in i direction to strain in j direction for stress in j direction.	
θ	Lamina orientation angle	
η	Ratio of structural efficiencies of hollow to solid fiber reinforced composites	
λ	Angle between principal axis and loading direction	
ρ	Specific weight	
σ	Stress	
ψ	Foundation modulus	
ϕ	Ratio of plane strain bulk moduli of fiber to binder	
μ	Ratio of shear moduli of fiber to binder	

Subscripts

a	air
b	binder
c	composite
cr	critical
f	fiber
g	glass
h	hollow fiber composite
mb	micro-buckling
o	void
s	solid fiber composite

t tension or tube
v void
z axial direction
1 in fiber direction
2 normal to fiber direction
3 normal to 1 and 2 directions

Superscript* indicates effective elastic constants

EXTERNAL DISTRIBUTION LIST

Contract NOW 61-0613-d

- | | |
|--|--|
| <p>1. Picatinny Arsenal
Dover, New Jersey
Attn: Mr. J. Matlack,
Chief Plastics</p> <p>2. National Aeronautics & Space Adm.
Langley Research Center
Langley, Virginia
Attn: Mr. Ross Levine,
Structures Group</p> <p>3. Ordnance Materials Res. Office
Watertown Arsenal
Watertown 72, Mass.
Attn: Mr. Irving Kahn</p> <p>4. Office of Naval Research
T-3 Bldg.
17th & Constitution Ave., N. W.
Washington 25, D. C.
Attn: Dr. Harold Liebowitz</p> <p>5. Boeing Aircraft Company
Box 2976
Seattle, Washington
Attn: Mr. L. J. Workman</p> <p>6. Office, Chief of Ordnance
Department of the Army
Washington 25, D. C.
Attn: ORD'TB Mtls.</p> <p>7-10. Chief, Bureau of Ships
Washington 25, D. C.
Attn: Code 634c (John Alferts)</p> <p>11. Eng. Res. & Development Labs.
Corps of Engineers
U. S. Army
Ft. Belvoir, Virginia</p> <p>12-13. U. S. Naval Ord. Lab.
Silver Springs 19, Maryland
Attn: Dr. A. Lightbody</p> | <p>14. Owens-Corning Fiberglas Corp.
806 Conn. Ave., N. W.
Washington 6, D. C.
Attn: Mr. R. J. Weaver</p> <p>15. U. S. Naval Res. Lab.
Washington 25, D. C.
Attn: Code 6210 (Mr. Jos. Kies)</p> <p>16-17. Chief, Bur. of Naval Weapons
Washington 25, D. C.
Attn: Code RRMA-35
Via: Inspector of Naval Material
Philadelphia, Pa.</p> <p>18. Wright Air Develop. Div. (WCLTEM)
Wright-Patterson Air Force Base
Dayton, Ohio</p> <p>19. Aeronautical Systems Division
Wright-Patterson Air Force Base,
Ohio Attn: WWRCWC-1</p> <p>20. Aeronautical Systems Division
Wright-Patterson Air Force Base,
Ohio Attn: WCLTEC</p> <p>21-22. Chief, Bur. of Naval Weap. (12 copies)
Washington 25, D. C.
Attn: DLI-311 (For file & release
to ASTIA)</p> <p>33. Commander
Aeronautical Systems Division
Air Material Command
Wright-Patterson Air Force Base,
Ohio Attn: LMMC</p> <p>34-35. Plastic Technical Eval. Center
Army Ordnance Corps
Picatinny Arsenal
Dover, New Jersey
Attn: Mr. Harry E. Peibly, Jr.</p> |
|--|--|

External Distribution List**Contract NOW 61-0613-d**

36. Forest Products Laboratory
Madison 5, Wisconsin
Attn: Dr. Don Brouse
37. Norair, Div. of Northrup Corp.
1001 E. Broadway
Hawthorne, California
Attn: Mr. A. P. Binsacca, Supv.
Mtls. & Process Eng.
38. Ferro Corporation
4150 East 56th St.
Cleveland 5, Ohio
Attn: Mr. B. A. McDermoty
39. Natl. Aeronautics & Space Adm.
Lewis Research Center
21000 Brookpark Road
Cleveland 35, Ohio
Attn: Library
40. Commander
U. S. Naval Ordnance Test Stat.
China Lake, California
Attn: Mr. S. H. Herzog, Code 5557
41. Hdqtrs., Air Force Systems Command
Aeronautical Systems Division
Wright-Patterson Air Force Base,
Ohio Attn: ASRCM-2
(Mr. T. J. Reinhart)
42. Electric Boat
Division of General Dynamics Corp.
Groton, Conn.
Attn: Robinson Research Library
43. Pittsburgh Plate Glass Company
Glass Research Center
Box 11472
Pittsburgh 38, Pa.
Attn: R. M. Watterson, Librarian
44. Bureau of Naval Weapons
Special Projects Division
Attn: Mr. Harold Bernstein
- 45-48. Aerospace Industries Assn.
Shoreham Bldg.
Washington, D. C.
Attn: Mr. J. P. Reese
49. Aerojet-General Corp.
Azusa, California
Attn: Mr. Ed Rucks
50. U. S. Rubber Research Center
Wayne, N. J.
Attn: E. J. Joss
51. Commander
Naval Ordnance Test Station
China Lake, California
Attn: Code 4064 (Mr. Charles Jenkins)

GE DISTRIBUTION LIST

Contract NOw 61-0613-d

<u>Valley Forge</u>	<u>Room</u>
F. Wendt (2)	M7023H
J. H. Wood (3+tissue)	U1240
J. B. Butler	U3206
H. G. Lorsch (2)	M3217
N. F. Dow	Bldg. #5
A. E. Ketler (5)	M3217
L. McCreight	M9531
C. Wilson (2)	M9151
E. A. Blum (2+tissue)	M3041
B. W. Rosen (5)	M7047G
R. F. Koenig	U4229
L. Chasen	L1345
W. H. Sutton	M9124
G. DiLeonardo	M7023D
H. T. McLean	U4223
J. D. Dunbar	U4223
K. R. Stadthaus	U3210
C. LaCombe (6)	U1240

Chestnut Street

A. Garber	5423
O. Klima	5101
I. J. Gruntfest	5206
J. D. Stewart	5501A

C. C. & F. #6

R. J. Kirby	6305
R. F. Peck	6246

MSD - Burlington, Vermont

W. Aswad
C. Schultz
O. Reimer